AN ABSTRACT OF THE DISSERTATION OF

Kristen D.M. Splinter for the degree of Doctor of Philosophy in Oceanography presented on May 1, 2009.

Title:

Development of 2D Models to Estimate Nearshore Bathymetry and Sediment Transport

Abstract approved:

Robert A. Holman

We examine the interactions and feedbacks between bathymetry, waves, currents, and sediment transport. The first two projects focus on the use of remote sensing techniques to expand our knowledge of the nearshore. Due to the plethora of snap-shot data that is available from satellites and their distribution via Google Earth, having a method that can determine bathymetry from spatial wave patterns would be very valuable. Utilizing remotely-sensed wave refraction patterns of nearshore waves, we estimate bathymetry gradients in the nearshore through the 2D irrotationality of the wave number equation. The model, discussed in Chapter 2, uses an augmented form of the refraction equation that relates gradients in bathymetry to gradients in wavenumber and wave angle through the chain rule. The equations are cast in a form that is independent of wave period, so can be solved using wavenumber and direction data from a single snapshot rather than the normally-required time series of images. Synthetic testing of the model using monochromatic waves on three bathymetries of increasing complexity, showed that the model accurately estimated 2D bathymetry gradients, hence bathymetry, with a mean bias of 0.01 m and mean root mean square error over the three beaches of 0.17 m for

depths less than 5 m. While the model is not useful for cases of complex seas or small refraction signals, the simplified data requirement of only a single snapshot is attractive. The model is perhaps best suited for shorter period swell conditions (wave periods of 8-10 seconds), for example, where strong refraction patterns are visible and wave number, k, and wave angle, θ, are easily extracted from a single frame image.

Secondly, remotely sensed images of wave breaking over complex bathymetry are used to study the nonlinear feedbacks between two-dimensional (horizontal), 2DH, morphology and cross-shore migration rates of the alongshore averaged bar. We first test a linear model on a subset of 4 years of data at Palm Beach, Australia. The results are discussed in Chapter 3. The model requires eight free parameters, solved for using linear regression of the data to model the relationship between alongshore averaged bar position, x, alongshore sinuosity of the bar, a, and wave forcing, $F = H_o^2$. The linear model suggests that 2DH bathymetry is linked to cross-shore bar migration rates. Nevertheless, the primary limitation is that variations in bar position and variability are required to be temporally uncorrelated with forcing in order to achieve meaningful results. For large storms, this is indeed the case. However, many smaller storms seen at Palm Beach show that changes in bar position and variability are correlated with forcing and bar interaction dynamics are not separable from bar - forcing dynamics.

In Chapter 4 a nonlinear model is subsequently developed and tested on the same data set. Initial equations for cross-shore sediment transport are formulated from commonly accepted theory using energetics-type equations. Cross-shore transport is based on the deviations around an equilibrium amount of roller contribution with the nonlinearity of the model forcing sediment transport to zero in the absence of wave breaking. The extension to 2DH is based on parameterizations of bar variability and the associated 2DH circulation. The model has five free parameters used to describe the relation between alongshore averaged bar position, x, 2DH bar variability, a, and wave characteristics (wave height, H, wave period, T, and wave angle, θ). The model is able to span multiple storms, accurately predicting bar migration for both onshore and offshore events. The

longest individual data set tested is approximately 6 months. Using manually determined values for the coefficients, bar position is predicted with an R^2 value of 0.42 over this time period. The effect of including a 2D dependency both increased rates of onshore migration and prevented highly 2D systems from migrating offshore under moderate wave heights. The model is also compared against a 1DH version by setting the 2D dependency term to unity and using the same values for the five free parameters. The 1DH model showed limited skill at predicting onshore migration rates, suggesting again that the inclusion of 2DH terms is important.

The last project (Chapter 5) explored the utilization of changes in bathymetry, $\Delta h/\Delta t$, to gain further understanding of the feedbacks between 2D sediment transport patterns, Q_x and Q_y, with respect to existing bathymetry in the nearshore. The model is based on the 2D continuity equation that relates changes in bathymetry to gradients in the cross-shore, $\partial Q_x/\partial x$, and the alongshore, $\partial Q_y/\partial y$, directions. The problem is under-determined, having two unknowns (Q_y and Q_x) and only one known ($\Delta h/\Delta t$) such that a series of constraints must be applied in order to solve for transport. We assume that that the cross-shore integral of Q_x is closed, such that no sand enters or exits the system in this direction. By conservation of mass, this requires changes in volume of the cross-shore transect to be due to longshore gradients in Q_y. We test six rules for distributing Q_y: three rules describing the initial longshore transport (Q_y^r) and three describing the cross-shore distribution of the excess volume component (Q_y^e). Initial results suggest that requiring sediment to travel down slope ($Q_y^r = f(\beta_y)$) is an intuitive choice for describing transport of distinct perturbations. However, in one example field test this method did not perform well and the approach may need further refinements. Alternatively, having Q_x^r and Q_y^r depend on spatial correlation lags between two surveys showed good results for identifying transport associated with alongshore migrating features. This method, however, did not do well under strict onshore migration of 2D features, where alongshore transport was not predicted. A hybrid approach, using both the down-slope constraint and spatial correlation lags may provide more robust predic-

tions of sediment transport patterns in complex environments. Due to the lack of closed boundaries in the alongshore, knowledge of $Q_y(x, y_0)$ is required to obtain sensible net sediment transport patterns. Alternatively, spatial patterns of the transport gradients ($\partial Q_y/\partial y$, $\partial Q_x/\partial x$), which ultimately determine bar migrations provide useful insight into the system behavior without requiring $Q_y(x, y_0)$.

Development of 2D Models to Estimate Nearshore Bathymetry and Sediment Transport

by

Kristen D.M. Splinter

A DISSERTATION

submitted to

Oregon State University

in partial fulfillment of
the requirements for the
degree of

Doctor of Philosophy

Presented May 1, 2009

Commencement June 2009

Doctor of Philosophy dissertation of Kristen D.M. Splinter

presented on May 1, 2009

APPROVED:

Major Professor, representing Oceanography

Dean of the College of Oceanic and Atmospheric Sciences

Dean of the Graduate School

I understand that my dissertation will become part of the permanent collection of the Oregon State University libraries. My signature below authorizes release of my dissertation to any reader upon request

---

Kristen D.M. Splinter, Author

ACKNOWLEDGEMENTS

First off, I would like to thank my family back home for putting up with a girl that gets horribly homesick yet moves further away with each degree. I'm on a secret mission to live on every continent. I miss you and love you dearly. Thank goodness for internet and Skpe. Without your support I could never have reached such heights. To my Corvallis family: the friends, professors and co-workers that have made living so far away from home an enjoyable experience. I feel that I have grown roots and it will be hard to leave. You have all been so wonderful. It has been such a blessing to get to know so many wonderful faces. With laughter and tears, I feel I have life-long friends all over the world. I wish I could take you all with me on my next adventure. Specifically, I must thank four friends who have been my support system: Maribeth; my ever-patient roomate and co-owner of our first house for 4 years. I wish you and Scott all the best. Your friendship has meant the world to me. Thank you for always being there. To my other roommates - you are awesome too. Thanks for all the laughs, tears, rants, walks and glasses of wine around the table. To Surly (Joe) and Rocky (Meg); my two office mates who have been with me from start to finish. It has been great to have you next to me: putting up with my rants, my lounge wear, questions, and always offering good advice and a laugh. I can't forget John; the CIL is lucky to have you. I will miss your antics, your computer savvy and the eternally full candy jar. Who's my friend? You are:) PK - thanks for making the end so amazing.

To think at 16 I wanted to study dolphins and live on tropical islands (like every 16 year old girl did of course). Coming from Canada, this was a bit of long shot, so I opted for a more traditional route and headed back to the place I was born, Queen's University on the advice of my parents. At 19 I was obsessed with coral reefs, 20 it was sand and water. Yup, I'm an Aquarius to the bone or should I say gill?? To Dr. Kevin Hall and the "F'ing Shields Curve" in my coastal engineering class that convinced me this is

what I want to do. By 21 I had stepped into the world of research thanks to NSERC and Dr. Bruce Anderson. I was helping to develop engineered wetlands for wastewater treatment. By 24 I was floundering around in German sewer systems hoping that sound of cavitation down the pipe wasn't coming from the one right by my head. There was definitely some 'shitty' years. I cleaned up my act and headed south, where I became part of the Gator Nation. Thanks to Dr. Don Slinn, I learned that computers don't just revolve around Microsoft and you can do some pretty complex stuff with the right amount of is and js. To Dr. Bob Dean for spending as much time in the office as I did on Sunday mornings and all our wonderful conversations. I was craving more hands on knowledge, which led me to 6 degrees of knowing everyone in this world: Rob Holman, who's sister worked with my dad it turned out. Here I was introduced to the wonderful world of MATLAB and remote-sensing: You CAN study the beach from the comfort of your desk. Who knew? I have experienced so much here: the blue smurf cast from spray-painting in North Carolina, blue-bottle stings in Australia, broken down cars in Spain, and food poisoning in Italy. It has been a blast. Kathy; thanks for always looking out for all the CILers.

To the folks at Dixon, ORC, OSU TriClub, OSU Cycling Club, my crazy outdoor friends, and the MindSpa. Thank you for getting my mind off work and out to experience this gorgeous place. I should have done it more. Oregon is such a beautiful area. I will miss the flowers, mountains, veggies, the long sunny summers, and everything being so big and so green. I won't miss the rain. For those that got me out on the rivers, on back country road rides, hiking, snow shoeing, camping, and to the coast: thank you.

To Murphy's Law: if it can happen, it will, and to me... It's a miracle that I'm making it out of here intact. To the American medical system who provided me with care during my various injuries and illnesses that required textbooks to diagnose. These are stories to tell my grandkids when I'm old and gray (provided I make it that far). To my PTs; thanks for pushing me harder than I'd push myself. It's been a long road to recovery, but I'm so glad to be back. To my cross-fit crew: keep kicking ass and taking

names. What are we training for? Life.

To the economy: for tanking the year I graduated. You provided me with the opportunity to move to Australia as my next adventure, a journey I wouldn't have taken otherwise. I should be careful, they have a lot of deadly creatures there.

To all my committee: for pushing me to think about the big picture and understand the science. The challenge has been daunting, but rewarding nonetheless. Tuba, in case I never told you, thanks for convincing me to come here. Our phone conversation with kids playing in the background made me realize that you could have a career and be an awesome mom. It was great to have that role model here. You did scare the crap out of me when I had to do my Nearshore exam orally though. Nothing is more intimidating than having you sit there and say, "so, what should I write here?". Finally, and by no means the last, I need to thank my advisor, Rob. You have put up with so much: your patience is unending. To think I started this adventure the morning of my 25th birthday. I don't know how I convinced you to take a chance on me, but thank you. You have groomed me into a confident scientist. I've come a long way from 'precious'. I am forever indebted. I owe you a scotch and a hug.

I was generously funded for 4 years by ONR SECNAV/CNO Chair of Oceanography (N00014-03-1-0973) and the Coastal Geosciences Program (N00014-07-1-0490). Thanks to Tom Drake for extending my funding for an extra term, Rob for helping with tuition and the Chipman-Downs Memorial Fund for getting me through the home stretch.

CONTRIBUTION OF AUTHORS

The preliminary work on refraction based bathymetry estimation was presented at the International Conference in Coastal Engineering (ICCE) 2006 in Sand Diego, CA (*Splinter and Holman*, 2006). Chapter 2 has been accepted for publication to IEEE Transactions on Geoscience and Remote Sensing. Dr. Nathaniel Plant contributed to the work in Chapters 2 through 4. The linear model used in Chapter 3 was based on *Plant et al.* (2006). Chapter 3 was presented in poster form at the American Geophysical Union (AGU) Annual Meeting in December 2006. The nonlinear bar dynamics model presented in Chapter 4 will be submitted for publication in the Journal of Geophysical Research. The work on 2DH sediment transport patterns and feedbacks based on bathymetric inversions has been presented in preliminary form at AGU Ocean Sciences Meeting 2008 in Orlando, FL. The completed version is expected to be submitted for publication at a later date.

TABLE OF CONTENTS

TABLE OF CONTENTS (Continued)

TABLE OF CONTENTS (Continued)

TABLE OF CONTENTS (Continued)

LIST OF FIGURES

LIST OF FIGURES (Continued)

LIST OF FIGURES (Continued)

LIST OF FIGURES (Continued)

LIST OF TABLES

DEVELOPMENT OF 2D MODELS TO ESTIMATE BATHYMETRY AND SEDIMENT TRANSPORT IN THE NEARSHORE

1. INTRODUCTION

1.1 The Nearshore Environment

1.1.1 Definition of the Nearshore

The nearshore region is a highly dynamic system where waves, currents, and bathymetry interact through complex feedback mechanisms in response to changing wave climates and sediment budgets. While few sandy beaches exhibit a featureless cross-shore structure, most contain features, such as sand bars (e.g. *Keulegan* (1948); *Davis and Fox* (1972); *Plant et al.* (1999); *Wijnberg and Kroon* (2002); *Ruessink et al.* (2003); *Alexander and Holman* (2004)). Observations show the morphology can rarely be considered alongshore uniform (e.g. *Zenkovich* (1967); *Sonu* (1973); *Wright and Short* (1984); *Lippmann and Holman* (1990); *Alexander and Holman* (2004); *van Enckevort et al.* (2004)), such that a full description of the bathymetry ($h(x, y, t)$) requires specification of cross-shore (x), alongshore (y), and temporal (t) dependencies:

$$h(x, y, t) = \bar{h}(x, y) + \tilde{h}(x, y, t), \tag{1.1}$$

where $\bar{h}(x, y)$ and $\tilde{h}(x, y, t)$ represent a background (long term mean) and a time-varying profile, respectively.

Several works, including *Wright and Short* (1984) and *Lippmann and Holman* (1990), formed detailed classification schemes to describe the morphology of sand bars. The classification scheme is summarized in Table 1.1.1 and Fig. 1.1. The varying states can be separated by a non-dimensional fall velocity term, $\Omega = H_b/TW$, (e.g. *Shepard*

(1950); *Bascom* (1954); *Dean* (1973); *Wright and Short* (1984)) where H_b is the breaking wave height, T is wave period, and W is the fall velocity, that relates beach response to varying wave conditions. Reflective conditions ($\Omega < 2$) exist under very mild waves, where sand bars, if present, are very close to shore or form low-tide terraces (e.g. Fig. 1.1 (b)). Intermediate wave conditions ($2 < \Omega < 5$) coincide with the development of more complex bathymetry, such as 2DH sand bars or transverse bar and rip systems (e.g. Fig. 1.1 (c-f)). Under energetic wave conditions ($\Omega > 5$), the most common morphological state is a longshore linear sand bar (e.g. Fig. 1.1 (g)).

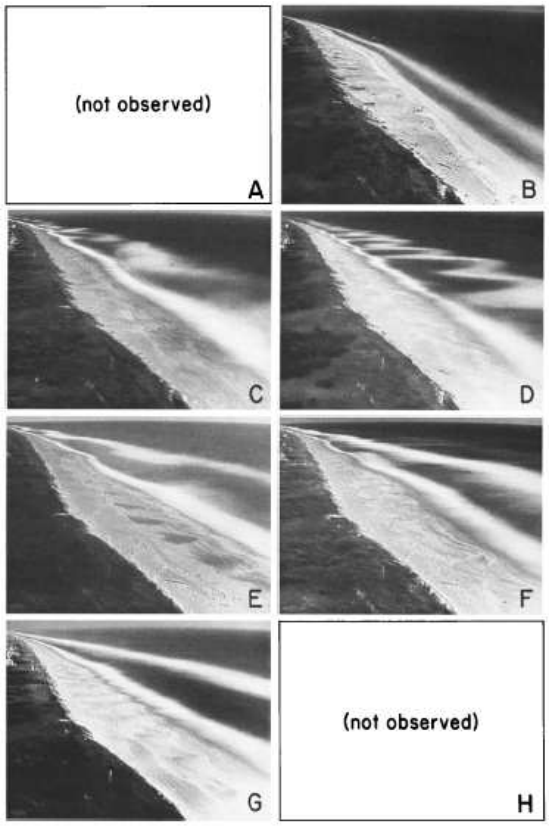

Fig. 1.1: Example images of the morphological state classification scheme proposed by *Lippmann and Holman* (1990). All images from Duck, NC. (a) Bar Type A; not observed, (b) Bar Type B; August 9, 1987, (c) Bar Type C; January 10, 1988, (d) Bar Type D; October 17, 1987, (e) Bar Type E; January 25, 1987, (f) Bar Type F; March 6, 1987, (g) Bar Type G; December 25, 1996, (h) Bar Type H; not observed. Figure originally published in *Lippmann and Holman* (1990).

Wright and Short (1984)	Lippmann and Holman (1990)
Beach State 6 DISSIPATIVE (unbarred; flat beach face)	Bar Type H DISSIPATIVE (unbarred; infragravity scaled surf zone)
Beach State 5 LONGSHORE BAR AND TROUGH (quasi-straight bar; may have some longshore variability)	Bar Type G INFRAGRAVITY SCALED 2-D BAR (no longshore variability; infragravity scaling)
	Bar Type F NON-RHYTHMIC, 3-D BAR (longshore variable, non-rhythmic; continuous trough; infragravity scaled)
Beach State 4 RHYTHMIC BAR AND BEACH (crescentic; normal or skewed)	Bar Type E OFFSHORE RHYTHMIC BAR (longshore rhythmicity; continuous trough; infragravity scaling)
Beach State 3 TRANSVERSE BAR AND RIP (attached; may be rhythmic; normal or skewed)	Bar Type D ATTACHED RHYTHMIC BAR (longshore rhythmicity, discontinuous trough; infragravity scaling)
	Bar Type C NON-RHYTHMIC, ATTACHED BAR (no coherent longshore rhythmicity; discontinuous trough; infragravity scaling)
Beach State 2 RIDGE-RUNNEL/LOW TIDE TERRACE (may be attached)	Bar Type B INCIDENT SCALED BAR (little or no alongshore variability; maybe attached; incident scaling)
Beach State 1 REFLECTIVE (unbarred; steep beach face)	Bar Type A REFLECTIVE (unbarred; incident scaled surfzone)

Table 1.1: Comparison of Morphological Beach State Classification Scheme by *Wright and Short* (1984) (*left*) and *Lippmann and Holman* (1990) (*right*).

For the purposes of this dissertation, we will limit our definition of the nearshore region to the sub-aqueous part; spanning from the shoreline to a depth (h) of roughly 10 m. However, this seaward boundary is dependent on the wave climate, such that relative depths (h/L), where L is the wave length of the incident waves, is a more robust definition of the seaward limit. We will define the seaward boundary of the nearshore at $h/L = 0.5$. In relative water depths less than 0.5, waves begin to feel the presence of the bottom and undergo transformations such as shoaling and refraction as they approach the beach. At some point, the relative wave height ($\gamma = H/h$) exceeds a stable limit and we observe depth-limited wave breaking. Because the waves react to changes in depth, this also indicates that they influence the bottom in such a way that this region is also characterized by active sediment transport.

1.1.2 Properties of Nearshore Wave Propagation

As waves enter the nearshore, they begin to feel the presence of the bottom and react to changes in depth by shoaling and refracting. The first principle we must introduce is the linear dispersion relationship (*Dean and Dalrymple*, 1991) that relates changes in wave frequency to changes in wave length and depth. If we assume currents to be negligible, then the linear dispersion relationship can be written as

$$\sigma^2 = gk \tanh kh, \tag{1.2}$$

where $\sigma = 2\pi/T$ is the radial frequency, related to the wave period (T), g is the acceleration due to gravity, and $k = 2\pi/L$ is the wave number. If we assume σ is constant for a single wave, then by equation (1.2), changes in depth correspond to changes in wave length. Since wave celerity ($C = L/T$) is a function of wave length, as waves enter shallower water, they both reduce their length and slow down based on equation (1.2).

Prior to wave breaking, energy flux ($\mathcal{F} = EC_g$) is conserved between two points,

$$(EC_g)_1 \cos\theta_1 = (EC_g)_2 \cos\theta_2, \tag{1.3}$$

where $E = 1/8\rho g H^2$ is the wave energy, ρ is the density of water, H is the wave height, and C_g is the group velocity. Since a wave slows down as it enters shallower water, the ratio $C_{g_1}/C_{g_2} > 1$. Therefore, according to equation (1.3), wave height must increase through the process known as linear shoaling:

$$H_2 = \sqrt{H_1^2 \frac{C_{g_1}}{C_{g_2}} \frac{\cos\theta_1}{\cos\theta_2}}. \tag{1.4}$$

The refraction of waves is also related to wave celerity. If a wave is traveling at some angle to depth contours there exists a celerity differentiation along the wave crest, where the portion of the wave in deeper water is traveling faster and the wave appears to bend towards the shallower water as it propagates. This is explained through the irrotationality of wave number:

$$\begin{aligned} \nabla \times \vec{k} &= 0, \\ \frac{\partial k_y}{\partial x} - \frac{\partial k_x}{\partial y} &= 0. \end{aligned} \tag{1.5}$$

where directional components of wave number are

$$k_x = k\cos\theta, \tag{1.6}$$

$$k_y = k\sin\theta, \tag{1.7}$$

and θ is the local wave angle with respect to shore normal. For a simplified case of straight and parallel contours, $\partial()/\partial y = 0$, therefore equation (1.5) reduces to

$$\frac{\partial k\sin\theta}{\partial x} = 0, \tag{1.8}$$

$$k\sin\theta = \text{constant}. \tag{1.9}$$

Dividing through by σ, we are left with the relationship known as Snell's law that describes the refraction of waves between two points due to variations in depth:

$$\frac{\sin\theta_2}{C_2} = \frac{\sin\theta_1}{C_1}. \tag{1.10}$$

1.1.3 Feedback Systems

Both refraction and shoaling of waves due to changes in bathymetry cause convergences and divergences of wave energy. As the wave shoals, the wave height increases until the relative wave height ($\gamma = H/h$) exceeds the stable limit and the wave breaks, transferring its momentum into the water column and driving nearshore flows. *Thornton and Guza* (1982) suggest $H_{rms} < 0.42h$ as the region for stable waves. Strong feedbacks exist between the location and patterns of wave breaking and the resulting mean flows and sediment transport (e.g. *Stive and Battjes* (1984); *Roelvink and Stive* (1989); *Thornton et al.* (1996); *Gallagher et al.* (1998); *Hoefel and Elgar* (2003)). One well-known example is the breakpoint model (e.g. *King and Williams* (1949); *Greenwood and Davidson-Arnott* (1979); *Roelvink and Stive* (1989); *Marino-Tapia et al.* (2007)) that suggests sand bars exist at the location of wave breaking due to convergences in flow and sediment transport. Once a bar begins to develop, this reinforces the location of wave breaking by providing a local reduction in water depth and a locally unstable relative wave height, γ, due to the decreased water depth at the bar. Nearshore morphodynamics are dominated by sand bar migration (e.g. *Birkemeier* (1985); *Thornton et al.* (1996); *Gallagher et al.* (1998); *Plant et al.* (1999, 2001); *Ruessink et al.* (2003)), suggesting strong feedbacks between existing morphology, sediment transport and wave breaking also exist.

Instability models are another example of feedback systems. Small perturbations to an initially longshore uniform shoreline or sand bar may excite the fluid forcing at a variety of length scales. The fastest growing of these modes produces rhythmic bathymetry through positive feedback mechanisms between morphology and the fluid forcing (e.g. *Deigaard et al.* (1999); *Falques et al.* (1999); *Coco et al.* (2000); *Falques et al.* (2000);

Caballeria et al. (2002); *Calvete et al.* (2005); *Garnier et al.* (2006)). The simpler, linear models explain the initial formations of these features, while the fully nonlinear models (e.g. *Reniers et al.* (2004); *Dronen and Deigaard* (2007)) can be run to finite amplitude, giving a more complete description of the instability. These models describe the evolution of the nearshore morphology with time and the feedbacks that drive the fluids and sediments.

1.2 Motivation and Goals of Work

One of the driving motivations of this work is the increasing interaction between human populations and the nearshore system. Gaining a greater understanding of the complexities between waves, currents, bathymetry, and sediment transport, will help with navigational efforts (e.g. Mouth of the Columbia River), understanding coastal ecology (e.g. *McLachlan et al.* (1993)), pollutant fate (e.g. *Feddersen* (2007)), and user safety (e.g. The United States Lifesaving Association reported 32,428 rescues and 36 deaths due to rip currents and surf for 2008). Chaos seemingly abounds around us, but can it be explained by simple patterns or rules based on observations, such that the system is ultimately predictable. The following quote inspired me several years ago when I started looking at feedback systems between sand bars and the resulting sediment transport. I thought it timely as I stared at a seemingly chaotic movie of beach morphology.

> By the law of periodical repetition, everything which has happened once must happen again, and again, and again - and not just capriciously, but at regular periods, and each thing in its own period, not another's, and each obeying it's own law ... The same nature which delights in periodical repetition in the skies is the nature which orders the affairs of the Earth. Let us not underrate the value of that hint. $\sim$ Mark Twain

The goal of this work is to gain a greater understanding of the complex world in which we live through the use of simple models.

1.2.1 Bathymetry Estimation from Refraction Patterns of Surface Waves

Accurate and quick estimation of bathymetry from remotely sensed images has two main motivations: navigation of unfamiliar waters and as required input of the bottom boundary condition for numerical modeling of the full wave-current system. Existing methods for determining bathymetry from remotely-sensed images of nearshore waves exploit only information on the magnitude of wave number, $k = 2\pi/L$, ignoring spatial changes in wave direction, θ, that can provide information about bathymetry gradients in the nearshore. These methods also require wave period information, so are limited to periods when time series data are available. Based on the irrotationality of the wavenumber condition (equation 1.5) and the dispersion relationship (equation 1.2), surface patterns of refracting waves are mathematically related to the underlying 2D bathymetry. The first goal is to develop a method for determining bathymetry gradients in the nearshore from spatial patterns of refracting waves based on irrotationality of wave number such that time series data is not required.

1.2.2 Feedbacks between 2DH Morphology and Cross-shore Sand Bar Migration

Understanding the influence of 2DH circulation on cross-shore sand bar migration has two main consequences: increased accuracy in modeling sand bar migration rates and increasing our predictive capability for the potential threats to beach users in response to changing wave conditions (Table 1.1.1). Observations show that 2DH morphology is quite common (e.g. *Wright and Short* (1984); *Lippmann and Holman* (1990); *Ranasinghe et al.* (2004)), especially during onshore bar migration periods. For example, *Lippmann and Holman* (1990) found that the most common morphological state observed at Duck, North Carolina was longshore-periodic bars (Fig. 1.1(e)) (68% of the data), while *Ranasinghe et al.* (2004) found that the transverse-bar-rip system (Fig. 1.1(c-d)) was the most common state (55% of the data) at Palm Beach, Australia. Both of these beach states are associated with rip-current systems and can pose threats to swimmers.

Continuous, long term predictions of nearshore morphology are currently unavailable. The majority of sand bar migration models assume that 2DH circulation is a negligible contributor such that a 1DH approach is sufficient. However, these models have limited accuracy in predicting both onshore and offshore transport under a variety of wave conditions (e.g. *Gallagher et al.* (1998); *Henderson et al.* (2004); *van Maanen et al.* (2008)). Recently, *Plant et al.* (2006) proposed that the presence of 2DH morphology (and thus 2DH currents) could be dynamically linked to sand bar migration. This linear model had limited skill when tested on a variety of wave conditions, such that a nonlinear version is required to predict the cross-shore migration - morphology feedbacks in complex systems. The second goal is to develop a nonlinear dynamic model that includes 2DH processes in order to increase our understanding of the driving forces of cross-shore sand bar migration and the feedbacks between existing morphology and sediment transport. This will ultimately lead to models that are capable of predicting long-term sand bar evolution patterns based on external forcing.

1.2.3 Feedbacks between 2DH Morphology and 2D Sediment Transport Patterns

This work was motivated by the effect of 2DH morphology on cross-shore sand bar migration and by previous 1DH work by *Plant et al.* (2001). Using a parametric form, *Plant et al.* (2001) modeled the beach profile using a sum of Gaussian curves and mean slope. Requiring conservation of mass, they showed that the resulting sediment transport patterns due to sand bar migration were similar in form to the existing bedform profile. Sediment transport patterns associated with migrations of the alongshore-averaged bar were separated into two components: one describing the migration of a constant Gaussian-shaped bed form whose amplitude was fixed and the other describing the transport associated with the growth or decay of the Gaussian bed form. These strong feedbacks between the bar profile and sediment transport patterns in 1DH likely exist when we consider 2D sediment transport as well. Both *Lippmann and Holman* (1990) and *Ranasinghe et al.*

(2004) found that down-state transitions (i.e. progression from energetic wave conditions (e.g. Fig. 1.1(d)) to more mild conditions (e.g. Fig. 1.1(c)) were based on the previous morphological state, suggesting a positive feedback system in which 2DH processes influence the time-varying response of sand bars to changing wave conditions. The third goal is to gain a greater understanding of 2DH sediment transport patterns through the use of bathymetry inversions. In 1D, cross-shore integration of the changes in bathymetry led to sediment transport patterns that resembled the underlying bathymetry. We assume the same can be said for 2D systems, but understanding how to uniquely constrain the 2D problem is unknown.

1.3 Approach

The variability of any system is daunting when you search for patterns, but ultimately, patterns do exist in their own specific form. First, we identify certain rules or patterns that can help describe the nearshore using simple models. Second, we expand our thinking to include 2DH processes, such as directional wave information and bar variability. Much of the work presented here has been based on similar 1DH approaches, and the expansion into 2DH is not trivial. The inclusion of 2DH morphology affects how waves propagate towards shore, their spatial breaking patterns, the resulting fluid forcing and currents, and ultimately sediment transport.

This dissertation is separated into 4 research projects encompassing nearshore systems. Chapter 2 introduces a refraction-based method for determining bathymetry gradients in the nearshore. Chapter 3 and 4 look at the use of parametric dynamical models to study feedbacks between 2DH morphology and sand bar migration. Chapter 3 details the linear model initially used, while Chapter 4 details the development of a new nonlinear model. Chapter 5 discusses preliminary work on 2DH sediment transport patterns in relation to existing bathymetry. Chapter 6 summarizes the general conclusions of the research presented.

2. BATHYMETRY ESTIMATION FROM SINGLE FRAME IMAGES OF NEARSHORE WAVES

2.1 Abstract

Existing methods for determining bathymetry from remotely-sensed images of nearshore waves exploit only information on the magnitude of wavenumber, $k = 2\pi/L$, ignoring spatial changes in wave direction, θ, that can provide information about bathymetry gradients. These methods also require wave period information, so they can only be used when time series imagery is available. We present an algorithm where changes in direction of refracting waves are used to determine underlying bathymetry gradients based on the irrotationality of wavenumber condition. Depth dependencies are explicitly introduced through the linear dispersion relationship. The final form of the model is independent of wave period so that all necessary input measurements can be derived from a single aerial snapshot taken from a plane, UAV, or satellite.

Three different methods were tested for extracting wavenumber and angle from images, two based on spatial gradients of wave phase and one based on integrated travel times between sample locations (a tomographic approach). Synthetic testing using monochromatic and bi-chromatic waves, with and without noise, showed that while all three methods work well under ideal wave conditions, gradient methods were overly sensitive to data imperfections. The tomographic approach yielded robust wave measurements and provided confidence limits to objectively identify unusable areas. Further tests of this method using monochromatic waves on three synthetic bathymetries of increasing complexity showed a mean bathymetry bias of 0.01 m and a mean root mean square (rms) error of 0.17 m. While not always applicable, the model provides an alternative form of bathymetry estimation when celerity information is not available.

2.2 Introduction

The nearshore region is a highly dynamic system where waves, currents, and bathymetry interact through complex feedback mechanisms. For most practical applications, these physical processes must be represented by numerical models that yield predictions of nearshore hydrodynamics when provided with input wave forcing conditions and bathymetry. Typically, wave forcing can be estimated using a number of approaches, but bathymetry, the bottom boundary condition for the models, is more difficult to obtain and changes rapidly in response to waves and storms. Thus, predictive capability is often limited by poor knowledge of bathymetry rather than of physics.

The most accurate nearshore bathymetries are collected using traditional survey techniques in which land and water based vehicles drive along a suite of survey lines while their position is measured either using optical methods or, more recently, high resolution kinematic global positioning system (GPS) equipment (e.g. *Birkemeier and Mason* (1984); *MacMahan* (2001)). Although these methods provide an accurate (error O(cm)) and dense data set (O(cm-m) resolution in the cross-shore and O(25 m) in the alongshore), they are typically very costly and time consuming and are usually restricted to fair weather conditions. They are obviously impractical for denied-access beaches of potential military interest (e.g. *Williams* (1946); *Seiwell* (1947)).

Alternatively, remote sensing techniques can cover large areas and time spans at a much-reduced cost over traditional beach surveys. Light Detection And Ranging (LiDAR) is an active laser-based pulsed sensor that derives depth estimates from time-of-flight data of the optical bottom echo (e.g. *Hickman and Hogg* (1969); *Guenther* (1985); *Irish and Lillycrop* (1999)). Current Airborne LiDAR Bathymetry (ALB) techniques can provide accurate and dense datasets with penetration depths reaching 2-3 times the Secchi Disk depth. New techniques using the red-channel waveforms produce accurate bathymetry measurements in the extreme nearshore (< 2 m) *Pe'eri and Philpot* (2007). However, ALB still has only limited use in many areas, particularly in mid-latitudes, due to turbidity or surf zone bubbles, and the majority of LiDAR data for the US Coastline

have been limited to the sub-aerial beach on sandy coastlines. In all cases, the use of ALB requires short standoff ranges and is still not sufficiently covert for most military applications.

Hyper-spectral imaging techniques exploit the wavelength dependence of optical attenuation in water to infer water depth from the color content of light reflected from the bottom (e.g. *Sandidge and Holyer* (1998); *Adler-Golden et al.* (2005)). This method is also limited by water clarity (seeing the bottom) and by variability in the optical properties of both the water column and the reflecting bottom material (e.g. *Adler-Golden et al.* (2005)).

Because optical penetration to the bottom is often so limiting, a series of methods have been developed that exploit observable characteristics of the sea surface to derive depth data. *Plant and Holman* (1997) developed a shoreline finding algorithm based on the wave dissipation maximum at the shorebreak measured from time-exposure images of wave breaking patterns. With knowledge of the tide level and local wave conditions the intertidal beach is mapped by defining shoreline contours as the tide level changes, creating a three-dimensional map of the intertidal area. Within the surf zone, *Aarninkhof and Ruessink* (2004) found a direct relationship between modeled wave dissipation patterns and pixel intensity patterns seen in time-exposure optical images. Using this proxy, model - data assimilation techniques are used to update the model bathymetry until modeled dissipation and observed dissipation proxies match within a specified range of acceptance.

Of direct relevance to this manuscript are a series of papers that exploit the relationship between wave frequency, σ, wavelength, $L = 2\pi/k$, where k is the magnitude of the wavenumber, and depth, h, represented by the linear dispersion relationship:

$$\sigma = \sqrt{gk \tanh kh} + \vec{k} \cdot U, \tag{2.1}$$

where g is the acceleration due to gravity, $\vec{k}$ are the vector components of the wavenumber, and U is the local current vector (which we will assume to be negligible outside the

surf zone). Wave propagation is visible in many sensors (visible, infrared, radar) so that time-space remote sensing observations can be used to measure frequency and wavenumber content for a small patch of the nearshore ocean. Depth is then estimated using equation (2.1) and a spatial map of bathymetry is built up (e.g. *Williams* (1946); *Bell* (1999); *Stockdon and Holman* (2000); *Dugan et al.* (2001); *Piotrowski and Dugan* (2002); *Misra et al.* (2003); *Senet et al.* (2008)). Linear dispersion-based methods of bathymetry estimation are moderately accurate, with rms errors $O(10^{-1}$ - 10^{0} m) (e.g. *Stockdon and Holman* (2000); *Senet et al.* (2008); *Flampouris et al.* (2008)) and work best outside the surf zone where linear wave theory is valid (e.g. *Stockdon and Holman* (2000); *Holland* (2001); *Senet et al.* (2008); *Flampouris et al.* (2008)).

While celerity- or linear dispersion-based remote sensing methods can provide bathymetric measurements of reasonable accuracy, they suffer from two problems. First, they require time series data of sea-surface elevations or a proxy thereof. While snapshot data are commonly available (e.g. publicly available Google Earth Images), time series in a format amenable to analysis are much more rare. Second, the linear dispersion relationship (2.1) exploits only the magnitude of wavenumber, not the directional variations of the vector wavenumber. Under certain conditions, wave curvature can be a very strong visual signal that can, in principle, be exploited (e.g. *Williams* (1946); *Munk and Traylor* (1947); *Seiwell* (1947)) . So instead of relying on the changes in just the magnitude of the wavenumber ($k = |\vec{k}|$), to invert for depth, in this paper we wish to test the hypothesis that gradients in directional wave information k_x, k_y can be used to determine gradients in local bathymetry in the absence of significant current shear, where x and y are the cross-shore and alongshore axes. k_x and k_y are defined as:

$$\begin{aligned} k_x &= k\cos\theta, \\ k_y &= k\sin\theta, \end{aligned} \tag{2.2}$$

and θ is the local wave angle measured with respect to the cross-shore axis. Of special

interest, we investigate whether refractive turning can yield bathymetry estimates based simply on a single snapshot without requiring time series imagery.

The remainder of the paper is organized as follows. Section 2 outlines the theory and numerical implementation of the algorithm, including tests based on idealized wavenumber and wave direction data. Model sensitivity to noisy data is also discussed. Section 3 describes and tests three candidate methods for estimating wavenumber and wave direction data from synthetic images and further discusses algorithm sensitivity to errors in these estimates. Section 4 discusses the wave period dependence of the model. Section 5 points out some of the complications of using real world imagery. Finally, there are discussion and conclusion sections.

2.3 Estimating Depth Gradients from Directional Wave Information

2.3.1 Model Formulation

The algorithm is based on the wave refraction equation (2.3) (*Dean and Dalrymple*, 1991) that relates gradients in wavenumber k and wave curvature to depth:

$$\nabla \times \vec{k} = 0, \tag{2.3}$$
$$\frac{\partial k_y}{\partial x} - \frac{\partial k_x}{\partial y} = 0.$$

Expanding (2.3) using (2.2) yields:

$$k\cos\theta\frac{\partial\theta}{\partial x} + k\sin\theta\frac{\partial\theta}{\partial y} = \cos\theta\frac{\partial k}{\partial y} - \sin\theta\frac{\partial k}{\partial x}. \tag{2.4}$$

Depth dependence is only implicitly part of this relationship and can be made explicit by using the chain rule to substitute for spatial gradients of wavenumber:

$$\frac{\partial k}{\partial x} = \frac{\partial k}{\partial h}\frac{\partial h}{\partial x}, \qquad \frac{\partial k}{\partial y} = \frac{\partial k}{\partial h}\frac{\partial h}{\partial y}, \tag{2.5}$$

so that the depth-dependent refraction equation becomes:

$$k\cos\theta\frac{\partial \theta}{\partial x} + k\sin\theta\frac{\partial \theta}{\partial y} = \cos\theta\frac{\partial k}{\partial h}\frac{\partial h}{\partial y} - \sin\theta\frac{\partial k}{\partial h}\frac{\partial h}{\partial x}. \tag{2.6}$$

Equation (2.6) is rearranged so that the unknown bathymetry gradients ($\partial h/\partial x$ and $\partial h/\partial y$) are a function of wave curvature (the curl of the directional component of wavenumber) and wavenumber:

$$\frac{\partial h}{\partial x}\sin\theta - \frac{\partial h}{\partial y}\cos\theta = -\kappa\left(\frac{\partial \sin\theta}{\partial x} - \frac{\partial \cos\theta}{\partial y}\right), \tag{2.7}$$

where

$$\kappa = \frac{k}{\partial k/\partial h}. \tag{2.8}$$

With the exception of κ, all terms in (2.7) are directly observable from a single image. However, the term $\partial k/\partial h$ would seem to depend on wave period T so requires temporal sampling or alternate estimation means. In the following, the performance of the algorithm will be examined based on the assumption that wave period information is available. However, in section 2.5, it will be demonstrated that a universal form for κ can be found that is independent of wave period. Thus, bathymetry can be estimated from snapshot images, albeit by solving a much more complex form of the equation.

Equation (2.7) was originally implemented in finite difference form as a tri-diagonal matrix and inverted to estimate depth on a row-by-row basis since there were still two unknowns. Knowing the wave period, κ was approximated numerically using a first-order finite difference implementation of the linear dispersion relationship (2.1) based on the

variations in depth h for small deviations (+/- ϵ) of k. Several limitations were found with using (2.7). The first was that an initial depth was required at some offshore location in order to use the finite difference technique. As well, under locally normal ($\theta = 0$) wave incidence, the inversion was poorly conditioned and solutions were unstable. The first of these problems was inherent to the differential equation. To remedy the second problem, the model was rearranged, using (2.5) to replace $\partial h/\partial y$ with:

$$\frac{\partial h}{\partial y} = \left(\frac{\partial k/\partial y}{\partial k/\partial x}\right)\frac{\partial h}{\partial x}. \tag{2.9}$$

Solving for cross-shore gradients in depth independently as a function of local gradients in directional wave information:

$$\beta_x = \frac{\partial h}{\partial x} = \frac{\kappa(\frac{\partial cos\theta}{\partial y} - \frac{\partial sin\theta}{\partial x})}{sin\theta - cos\theta\frac{\partial k}{\partial y}/\frac{\partial k}{\partial x}}. \tag{2.10}$$

This form of the model is numerically more stable for low wave angles provided the denominator is nonzero. Another advantage of (2.10) is that the solutions at different alongshore locations are independent of each other and the calculated cross-shore gradients can be filtered using a 3σ median filter to remove anomalies, discussed further below. Depths are then estimated by integrating (2.10) in the cross-shore from a location of known depth, such as the shoreline. We chose to integrate depths from an interior point to minimize errors associated with end points. Since integration proceeds away from an initial value, any error early in the integral is carried throughout the domain and total errors will be large. Thus, different choices of initial values (offshore or onshore) could yield completely different error estimates. Nevertheless, comparisons are included since bathymetry is the ultimate desired product and since error maps provide insight into the nature of the errors. The remainder of the paper will focus on the performance of the algorithm based on (2.10).

2.3.2 Algorithm Performance for Idealized Data

We first tested the accuracy of the model using idealized directional wave information. Tests were carried out on three synthetic bathymetries: a planar beach; a planar beach with a superimposed Gaussian shoal to add 2D variable bathymetry; and a pocket beach with headlands at either end, (See Figs. 2.7 and 2.8 for reference). Beach parameters are summarized in Table 2.1.

Table 2.1: Summary of synthetic beach parameters used in testing the refraction-based bathymetry estimation model.

Case	Grid size [nx,ny]	dx, dy (m)	β_x	Period) (s)	θ_0 degrees
Planar	250 x 250	2	1:100	8	30
Shoal	250 x 250	2	1:100	8	30
Pocket	250 x 500	2	1:100	8	0

Wavenumbers for each domain were determined from the linear dispersion relationship (2.1) based on known bathymetry. Wave angle was solved for using (2.4) by stepping shoreward from the known offshore wave angle, θ_0, using the spatial changes in wavenumber to determine changes in wave angle. The resulting data were then used in (2.10) and the process inverted to solve for bathymetry gradients, β_x, and, by integration, the estimated bathymetry, h. Model performance is summarized in Table 2.2. Since the solution was just the inverse of the equations used to generate the idealized data, it was not surprising that the model performed exceptionally well for all cases tested. rms errors in β_x were $< 1\%$ of the true gradients and rms errors in bathymetry were typically a few millimeters.

Table 2.2: rms error of β_x and h for idealized data.

	Beach		
	Planar	Shoal	Pocket
β_x	8.8×10^{-6}	8.8×10^{-6}	9.6×10^{-5}
$h(m)$	2.9×10^{-3}	1.4×10^{-3}	3.7×10^{-3}

2.3.3 Algorithm Performance for Noisy Data

We performed two different tests using the planar beach case in which Gaussian white noise was added to k and θ in order to test the model's sensitivity to data errors. To start, true k and true θ were calculated as described in Section 2.3.2. In test 1, we tested the model's sensitivity to errors in θ or wave curvature with ideal wavenumber data by applying Gaussian white noise of 1% of the median θ value to the true θ. True k values were used with the noisy θ estimates to solve for β_x. In test 2, we tested the model sensitivity to errors in k, thus testing that if our estimates in wavenumber were off but curvature could be measured more robustly, could the model still converge to the correct solution. This was done by applying Gaussian white noise of 1% of the median k value to true k and using the noisy k values with true θ values in (2.10) to solve for β_x. Algorithm performance is summarized in Table 2.3.

Table 2.3: rms error of k, θ, β_x, and h for noise sensitivity tests.

Test #	$k(\mathrm{m}^{-1})$	θ (°)	β_x	h (m)
1	N/A	0.2	0.02	0.15
2	0.002	N/A	0.03	2.0

Examination of the sensitivity results leads to several conclusions. First, results in Table 2.3 show a high sensitivity to even this low level of noise. The primary reason for this is that noise introduced in the data (k, θ) affect the algorithm through their spatial gradients ($\partial k/\partial x$, etc), so that for the 2 m grid spacing of the tests, even the small rms noise levels used produced gradients that were of order 200% (k) and 150% (θ) the true gradient signals. Second, the model sensitivity to gradients implies that the method eventually selected for estimating these input variables from images will need to be spatially smooth, either through an explicit smoothing or implicitly due to the method. Third, even extreme noise in the beach slope estimates (rms error in $\beta_x >$ true β_x) yielded substantially smaller errors in bathymetry since the slope gradient errors were Gaussian and were partially averaged out by integration.

2.4 Bathymetry Estimation From Synthetic Images

Results in the previous section were based on idealized k, θ information that were given a priori. Typically these variables will have to be estimated from images of shoaling and refracting waves. In this section we describe and test three candidate methods using synthetic idealized data.

2.4.1 Methods for Extracting Directional Wave Information from Images

In general, a wave field, $\eta(x, y)$, can be represented in terms of spatially-variable amplitude and phase functions, $A(x, y)$ and $\phi(x, y)$, respectively as:

$$\eta(x, y) = \Re(A(x, y)e^{i\phi(x,y)}) \tag{2.11}$$

where the enclosed function is called the analytical signal and $\Re()$ represents the real-valued component thereof. The phase function $\phi(x, y)$ is related to the components of wavenumber, (k_x, k_y) by:

$$\phi(x, y) = \int_0^x k_x dx + \int_0^y k_y dy. \tag{2.12}$$

If the spatial map of phase is given or can be found from image data, this relationship can be inverted to find k_x and k_y as the x and y spatial derivatives of phase.

Sea surface elevations (Fig. 2.1), or proxies such as changes in image intensity caused by sloping wave surfaces are real valued, and the phase function cannot be directly extracted from the signal. Instead, phase function estimates are found by taking the Hilbert transforms in the cross-shore direction of the observed data to get the analytic signal, $\hat{\eta}$, (*Bendat and Piersol*, 1986; *Havlicek et al.*, 1997). To reduce spectral leakage, the input data is windowed using a 20% cosine taper with the tapered points removed from later analysis. The phase function $\phi(x, y)$ is then determined by:

$$\phi(x, y) = \tan^{-1}\left(\frac{\Im(\hat{\eta}(x, y))}{\Re(\hat{\eta}(x, y))}\right), \tag{2.13}$$

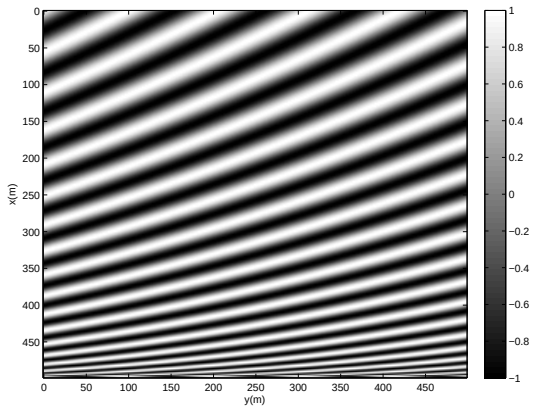

Fig. 2.1: Example shoaling wave field for a planar bathymetry. Cross-shore distance is along the vertical axis and the shoreline is at the bottom. Wave period and offshore wave angle were 8 seconds and 30 degrees, respectively. Surface elevation measured in meters.

where $\Im()$ and $\Re()$ indicate the imaginary and real components, respectively, and the phase function $\phi(x, y)$ is measured in radians. The resulting two-dimensional phase map has values between $-\pi$ and π (Fig. 2.2(left)), with discontinuities each time phase jumps from $+\pi$ to $-\pi$. By unwrapping the phase function in both directions, a global phase map $\phi_G(x, y)$ (Fig. 2.2(right)) is produced in which simple gradient methods can be directly applied to estimate the two wavenumber components.

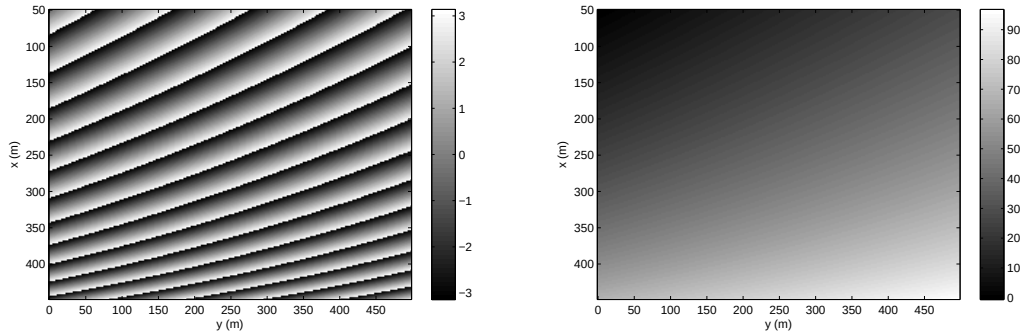

Fig. 2.2: 2D spatial maps of phase estimates for monochromatic waves. (*left*) Phase estimate (radians) of the input wave field (Fig. 2.1). (*right*) Unwrapped phase (radians) starting at the top left corner of the image and integrating in both directions.

Gradient methods for determining directional wave information

Two different methods for determining wavenumber through phase gradients are tested. Eventually both are abandoned in favor of a method that implicitly smoothes estimates across the domain. Discussion is nevertheless included, both for completeness and to illustrate the importance of smooth input data. In the first method, wavenumber components are computed by taking the spatial gradients of the globally unwrapped phase $\phi_G(x, y)$ (Fig. 2.2(right)) through finite differencing:

$$[k_x, k_y] = \nabla \phi_G(x, y). \tag{2.14}$$

For the case of a monochromatic wave field (Fig. 2.1), gradients of the globally - unwrapped phase provide accurate directional wavenumber information (Table 2.4).

For more complicated seas, however, the performance of the global gradient method degrades substantially. Fig. 2.3 illustrates the group structure of waves due to a bichromatic wave field. The wrapped phase (Fig. 2.4(left)) includes anomalies at the nodal points that cause two problems. First, attempts to unwrap the phase in two dimensions (Fig. 2.4(right)) are non-unique and include jumps in phase that cause anomalies in estimated wavenumber. Second, since waves on either side of nodal points are in anti-phase, the wavelength of the waves that are split across the group nodes are correspondingly split and appear as short waves (Fig. 2.4(left)).

The former problem can be solved by removing the requirement for phase unwrapping. Therefore, the second method we test is a local gradient method that computes gradients in the complex domain space of the analytic signal (*Havlicek et al.*, 1996, 1998):

$$[k_x, k_y] = \nabla \phi(x, y) = \Re \left[\frac{\nabla \hat{\eta}(x, y)}{i \hat{\eta}(x, y)} \right]. \tag{2.15}$$

This method produces accurate estimates of k for most of the image. In areas of wave group nodes, wavenumber components are higher than expected due to the extra phase shift of π. Wavenumbers that lie outside 3σ from the mean k are replaced with the local

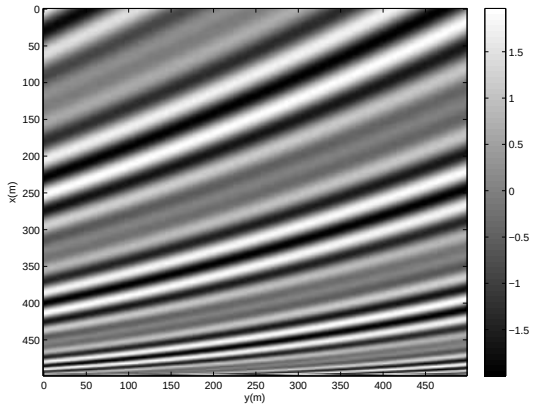

Fig. 2.3: Example of a narrow-banded wave field, with two waves, $T_1 = 8$ seconds, $T_2 = 10$ seconds. Offshore wave angle is 30 degrees for both cases. Surface elevation measured in meters.

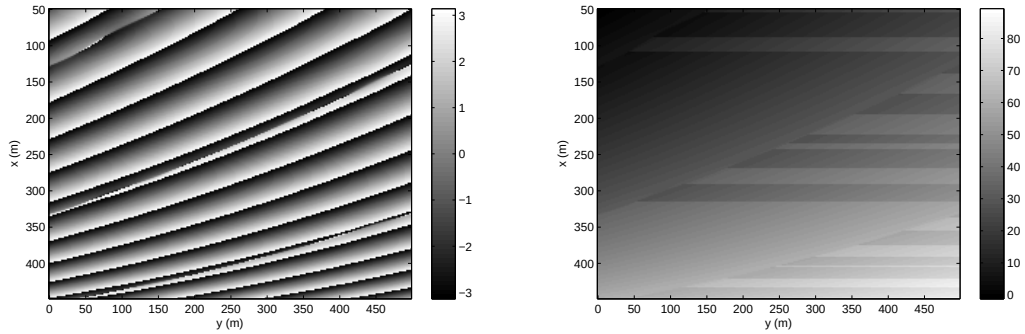

Fig. 2.4: 2D phase maps of narrow-banded wave field. (*left*) Phase estimate (radians) of the finite-bandwidth wave field. (*right*) 2D unwrapped phase (radians) starting from the top left of the image. Jumps in phase that are less than 2π are not unwrapped and cause the streaks in the unwrapped phase image.

mean wavenumber. Estimating k from local gradients is an improvement over the global phase unwrapping technique when applied to finite-bandwidth waves because it isolates the areas (wave group nodes) where wavenumber estimates are not consistent with the expected values.

From the wavenumber estimates, wave angle is calculated from the arctangent of the directional wave components:

$$\theta = \tan^{-1}\left(\frac{k_y}{k_x}\right). \tag{2.16}$$

Nonlinear Inversion Technique

A third technique for estimating k, θ from images uses a nonlinear inversion method *Plant et al.* (2008), hereafter referred to as PHH08. The method, essentially a tomographic approach based on wave propagation time delays across many spatial lags, uses a nonlinear search to find the single values of wavenumber and direction that best explain the complex analytical signal, found by Hilbert transform of the imagery, over each of a suite of sub-regions of the domain. Because time delays for all possible pixel pairs (close and widely-spaced) in each sub-region are incorporated in the estimate, extreme contamination by short gradient noise is avoided. The shortest resolvable features that can be estimated from variations in k are equal to about 10 times the local water depth (*Plant et al.*, 2008), so the spatial resolution of the model domain is such that it will not attempt to estimate variations in k and θ shorter than these scales. For the cases tested, estimates for wavenumber and wave angle are done on a coarse tomographic domain with spatial resolution of 30 m, utilizing input data $\pm$ 60 m in the cross-shore and $\pm$ 100 m in the alongshore direction to estimate k and θ. The data are then interpolated onto a finer grid with spatial resolution of 2 m. This both speeds up the inversion technique and removes high-frequency noise that may be in the initial data signal. The coarse domain, however, is not well suited to the extreme nearshore where rapid variations in wavenumber and angle may occur that are unresolved by the spatial scale of the tile. Note also that since the resulting data will be used in gradient calculations, linear interpolation will yield step-wise changes in gradients, hence patchy bathymetry gradients, so higher-order interpolations must be used. The reader is referred to *Plant et al.* (2008) for a detailed description of the method.

2.4.2 Synthetic Test Results

Comparison of Data-Extraction Techniques

The three methods of data extraction were tested using synthetic waves approaching the planar beach. Three tests were carried out: a monochromatic case (M) of 8 second waves

approaching with a 30 degree offshore angle of incidence (Figs. 2.1, 2.2), a noiseless bi-chromatic sea (B) with 8 and 10 second waves approaching from 30 degrees, (Figs. 2.3, 2.4), and a noisy case (N) of the same waves with superimposed Gaussian white noise with standard deviation equal to 10 % of the maximum wave height (Figs. 2.5, 2.6). For each case, maps of k, θ, β_x, and h were computed by each of the three data extraction methods and compared to known values through both mean and rms statistics. Results are summarized in Table 2.4.

Table 2.4: Mean (rms) error of k, θ, β_x, and h estimation for monochromatic (M), noise sensitivity (N), and bi-chromatic (B) wave conditions, using the three data extraction techniques. While wavenumber varies across the domain, a representative magnitude for comparison is 0.1 - 0.4 m^{-1}. True β_x is 0.01.

Case		k (m^{-1})	θ(°)	β_x	h (m)
M	$\nabla\phi_G(x,y)$	5.1×10^{-4}	-0.03	5.6×10^{-6}	0.03
		(1.3×10^{-3})	(0.2)	(3.5×10^{-3})	(0.06)
	$\nabla\phi(x,y)$	-3.8×10^{-3}	0.3	8.7×10^{-5}	0.03
		(5.9×10^{-3})	(0.3)	(4.4×10^{-3})	(0.06)
	PHH08	4.3×10^{-4}	-0.1	6.0×10^{-4}	-0.02
		(5.0×10^{-3})	(0.2)	(1.7×10^{-3})	(0.10)
N	$\nabla\phi_G(x,y)$	3.9×10^{-3}	-0.3	3.5×10^{-3}	1.33
		(3.4×10^{-2})	(12.2)	(1.64)	(26.02)
	$\nabla\phi(x,y)$	-2.2×10^{-4}	-0.3	6.2×10^{-4}	-0.66
		(2.3×10^{-2})	(11.8)	(2.33)	(41.23)
	PHH08	2.8×10^{-4}	-0.1	5.5×10^{-4}	-0.01
		(5.4×10^{-3})	(0.2)	(1.3×10^{-3})	(0.06)
B	$\nabla\phi_G(x,y)$	4.1×10^{-1}	6.9	4.1×10^{-3}	-0.30
		(4.3×10^{-1})	(40)	(0.44)	(4.37)
	$\nabla\phi(x,y)$	-4.8×10^{-4}	0.3	2.1×10^{-3}	-0.03
		(1.3×10^{-2})	(0.7)	(0.01)	(0.48)
	PHH08	2.5×10^{-3}	-0.1	6.0×10^{-4}	-0.09
		(4.6×10^{-3})	(0.2)	(0.01)	(0.49)

All methods performed very well for the monochromatic wave field. The Hilbert transform introduced slight ringing into the analytic signal that carried through into the phase estimates. The gradient methods for determining k, θ emphasized this ringing, with rms errors in k on the order of a few percent. β_x oscillated around the true mean, causing larger rms errors in β_x for the gradient methods, but reasonable estimates for integrated bathymetry, h (Fig. 2.7 (left)). However, performance of the gradient methods

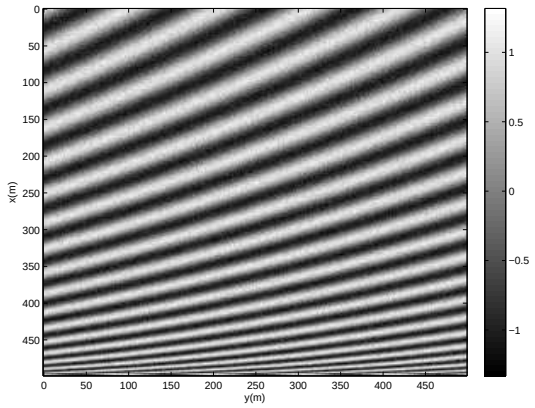

Fig. 2.5: Example of a monochromatic wave field with 10% noise superimposed. $T = 8$ seconds. Offshore wave angle is 30 degrees. Surface elevation measured in meters.

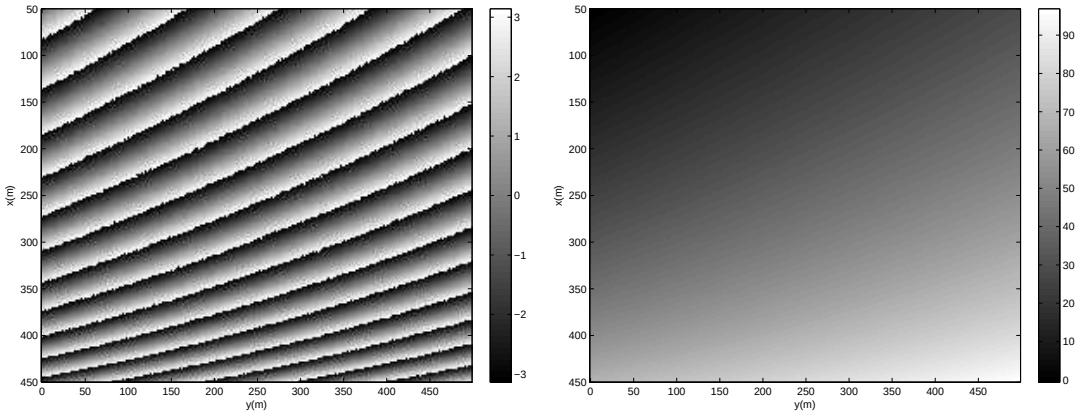

Fig. 2.6: 2D phase estimates for noisy wave field. (*left*) Phase estimate (radians) of the noisy wave field. (*right*) 2D unwrapped phase (radians) starting from the top left of the image.

declined rapidly with data imperfections. Phase jumps in the bi-chromatic case yielded unacceptable results of k, θ for the global phase unwrapping method, although they were better handled by the local gradient method. rms errors in h were at least an order of magnitude greater in the bi-chromatic case using the gradient methods. As expected, the addition of white noise to the data led to performance statistics for the gradient methods that were completely unusable. Early attempts at spatial filtering improved results somewhat, but a general robust methodology was never found. Thus, gradient methods are not recommended for the purpose of wave characteristic estimation.

The PHH08 approach performed well for all three tests. Since this method uses a constant depth assumption over each analysis sub-array, slight biases in k, θ on the order of 1% were expected for the bathymetry and model domain used. For the monochromatic case, the PHH08 approach had error results similar to the gradient methods, with rms errors in k of a few percent. rms error in β_x was on the order of 1% and rms errors in integrated bathymetry of 10 cm (Fig. 2.7(right)). The small amount of ringing associated with computing the Hilbert transform that led to oscillations in β_x estimates using gradient methods was smoothed over with the PHH08 approach. Errors using this method were concentrated near the shoreline, where rapid changes in k were likely not well resolved on the coarse tomographic domain, and at the lateral boundaries, where a reduced number of points used in the estimation led to less accurate results. The latter issue can be resolved by over-lapping images in the alongshore and/or removing the edge points.

In contrast to gradient methods, the performance of the PHH08 method was robust to noise, as expected, with rms statistics for all parameters similar to those of the monochromatic case. For the bi-chromatic case, the method was still troubled at the wave node locations, but since this approach provided a skill estimate, values with skill < 0.5 were objectively identified, removed and interpolated over for a more accurate solution. No such skill estimate was available for the gradient methods. rms errors in β_x for the bi-chromatic case were on the order of the true beach slope, producing larger errors in integrated bathymetry (rms error in $h \sim 0.5$ m). As a whole, the PHH08 method produced the most consistent results, with skill estimates to objectively identify areas of concern. Thus, the PHH08 method is preferred for k, θ extraction and will be used for the remainder of the paper and for recommended future work.

Complex Bathymetry Results

The PHH08 method was utilized to extract k, θ data for monochromatic wave conditions on more complex bathymetry. The results are summarized in Table 2.5. For the planar

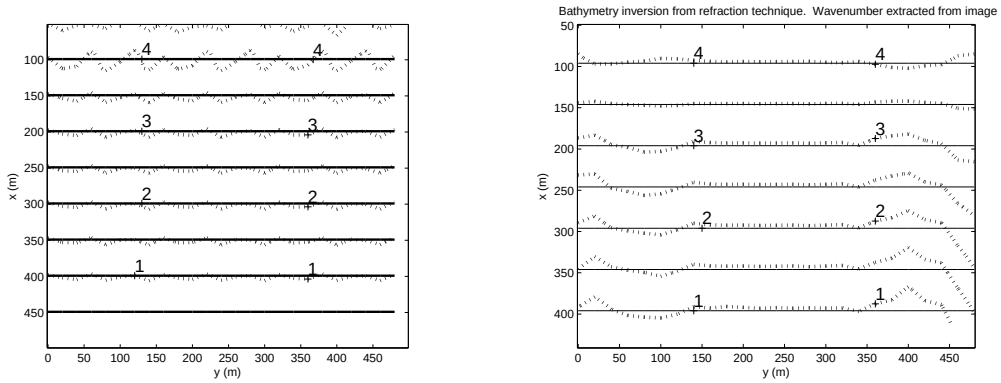

Fig. 2.7: Comparison of bathymetry estimated from global phase and non-linear least squares extraction of data. True bathymetry (*solid*) and estimated bathymetry (*dash*) measured in m. (*left*) k, θ extracted from image using global phase unwrap methods. Mean error in estimated bathymetry was 3 cm. (*right*) k, θ extracted from image using PHH08 techniques. Mean error in estimated bathymetry was -2 cm.

beach with a Gaussian shoal, bathymetry gradients over the shoal were well-predicted (Fig. 2.8(a)) with mean (rms) errors in bathymetry of order 1 cm (10 cm). For the pocket beach, normal wave incidence, combined with $\partial k/\partial y = 0$ produced an unstable solution for β_x at some locations in the cross-shore around $y = 500$ m. Since this is a known limitation of the refraction model, a standard deviation filter was applied to remove anomalies and smooth over these areas. Integrated bathymetry had slight offsets at the center of the image and close to shore where changes in wavenumber and angle were not well resolved due to the tiling method of the PHH08 model (Fig. 2.8(b)). Even with these known limitations, mean (rms) errors in bathymetry were of order 1 cm (30 cm). Overall, the results were very encouraging that the proposed model could predict complex bathymetry based on refraction signatures.

Table 2.5: Mean (rms) error for the PHH08 method over complex bathymetry.

Case	k (m^{-1})	θ (°)	β_x	h (m)
Shoal	3.6×10^{-4}	-0.13	6.55×10^{-4}	-0.01
	(5.3×10^{-3})	(0.43)	(2.0×10^{-3})	(0.13)
Pocket	3.2×10^{-4}	-0.01	6.5×10^{-4}	-0.01
	(8.9×10^{-3})	(0.06)	(8.6×10^{-3})	(0.28)

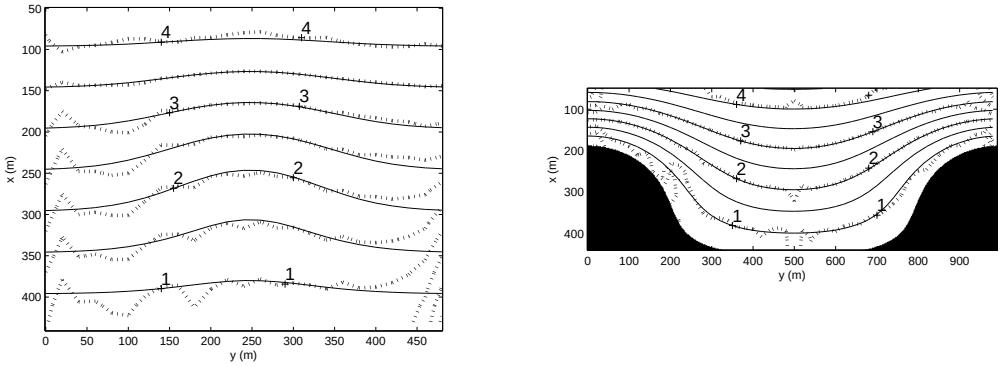

Fig. 2.8: Bathymetry estimates for complex bathymetry using PHH08 method. True bathymetry (*solid*) and estimated bathymetry (*dash*) using (2.10). (*left*) Beach with shoal: mean error in bathymetry was -0.01 m. (*right*) Pocket beach: mean error in estimated bathymetry of -0.01 m.

2.5 Wave Period Dependence

The above analysis was based on the use of equation (2.10). All terms in this equation are directly observable from a single image with the exception of κ. Wave period cannot be estimated from a snapshot unless it spans into deep water, where $T = \sqrt{2\pi L_o/g}$. It would appear that motion imagery (a sequence of images) is required and that single snapshots are not helpful. In fact, κ is independent of wave period. For example, in the shallow water limit ($kh < \pi/10$), κ simplifies to eliminate the wave period dependence as follows:

$$\begin{aligned} k &= \frac{\sigma}{\sqrt{gh}}, \\ \frac{\partial k}{\partial h} &= -\frac{\sigma}{\sqrt{gh}}\frac{1}{2h}, \\ \kappa = \frac{k}{\partial k/\partial h} &= -2h. \end{aligned} \tag{2.17}$$

Fig. 2.9 shows the deviation from $\kappa = -2h$ as a function of non-dimensional depth (kh). At the small kh values associated with shallow water, the value of $-\kappa/2h$ is just 1.0, as expected above. But even for larger values of kh the curve is independent of wave period

so the algorithm can be applied to a single snapshot.

The form of the curve in Fig. 2.9 can be well approximated by a polynomial, such that:

$$\kappa = -2h\left[0.55(kh)^3 - 0.61(kh)^2 + 0.55(kh) + 0.91\right]. \tag{2.18}$$

Substituting (2.18) in (2.10) yields a somewhat complicated form that must be solved numerically, but is based solely on wavenumber and wave angle estimates that can be extracted from a single snapshot.

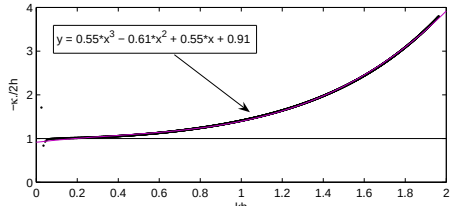

Fig. 2.9: Expected error associated with the assumption of shallow water $\kappa = -2h$ vs. non-dimensional depth (kh).

2.6 Application to Field Data

This research was motivated by the need for remote sensing methods to measure bathymetry, and the common availability of remotely-sensed snapshots in which strong wave refraction signals must be related to underlying bathymetry gradients. While our eyes are good at picking out the desired pattern, a variety of problems complicate the computer automation of this process.

Optically, images contain contamination at many scales. At low wavenumber, lighting varies both in the skydome and due to the general variation of water surface reflectivity with vertical viewing angle. There are also complications in the region between non-breaking and breaking waves where the optical signature of a wave crest shifts from being dark (non-breaking) to light (breaking). Since the optical signature of a wave depends on its local wave steepness (*Walker*, 1994), short but steep features, such as

wind chop, are exaggerated compared to the slowly varying swell.

Filtering techniques, such as weighted standard deviation and band-pass filters, can be used to isolate and enhance the swell band to a reasonable degree (*Splinter and Holman*, 2006). Better yet, the PHH08 method does a good job estimating a dominant k, θ over a user-selected analysis window, averaging out both short and long-scale contamination and smoothing through anomalies. The PHH08 model also returns skill estimates for each k, θ estimate, so questionable results are easily identified and possibly eliminated. But it should be recognized that the refraction-based algorithm proposed in this paper is useful only in cases of narrow-banded swell with strong refraction patterns.

2.7 Discussion

The motivations for this work were to develop a bathymetry estimation technique that could be based on single-image snapshots rather than time series imagery and that also exploited both the magnitude and varying directions of wavenumber. Thus, it was rewarding to see that the equations could be formulated without reference to wave period. However, the method does not work under all conditions. For example, the solution blows up under the joint circumstances of normal incidence, relative to bathymetry contours, and no longshore gradients in wavenumber, when the denominator of equation (2.10) approaches zero. In this case there is simply no refractive signal to exploit.

The method is also based on an underlying assumption of a monochromatic or very narrow-banded wave field that can be represented adequately by a single wavenumber and direction. For time series imagery data, more complicated seas could be handled spectrally by isolating individual coherent components of the wave field both by frequency and direction. However, for single snapshots such a partitioning is not possible and the method will yield noisy results. Fortunately, the PHH08 method flags the quality of results through a skill statistic that can be used to objectively identify where bathymetry estimates can and cannot be trusted.

The primary products of the refraction method are estimates of bathymetry gradi-

ents, in contrast to linear dispersion-based methods that directly estimate depth. Consequently, depth estimates must be found by integration from some known value, for example the shoreline. In some parts of the region of interest, bathymetry gradient estimates may be poor, perhaps due to locally low wave contrast or the above-mentioned problem of normal incidence with no alongshore gradients. Cross-shore integration cannot continue through regions such as this that are flagged as bad, so knowledge of the full profile can be limited. However, these regions are usually spatially patchy and can be bypassed using surrounding information. The details of such an algorithm are beyond the scope of this paper.

The effect of currents on the dispersion relation has been neglected in the current model. The implications of this simplification are discussed here. Uniform currents that are perpendicular to the direction of wave propagation have no effect on the frequency and wave number estimates determined from equation (2.1). Alternatively, currents which are parallel or at an angle to the direction of wave propagation will affect the estimated wave phase speed, c, and frequency, σ, as seen by a stationary observer, but have no effect on the estimated wavenumber provided the current can be considered uniform over the area in question (*Svendsen*, 2006). Thus, it is the spatial variation (shear) in the current that can contaminate the bathymetric refraction patterns of incident waves. The magnitude of this error can be found by considering the simplified case of a wave propagating in the x-direction against an opposing current in shallow water. The equation governing wave angle (*Dean and Dalrymple* (1991), p.106) can be written as:

$$\frac{\partial \theta}{\partial x} = \frac{-1}{c_a}\frac{\partial c_a}{\partial y}, \tag{2.19}$$

where:

$$c_a = \sqrt{gh} - U. \tag{2.20}$$

Therefore, changes in wave angle are related to the combined contributions of bathymetric

changes and currents:

$$\frac{\partial\theta}{\partial x} = \frac{-1}{\sqrt{gh} - U}\left(\frac{1}{2}\left(\frac{g}{h}\right)^{1/2}\frac{\partial h}{\partial y} - \frac{\partial U}{\partial y}\right) \tag{2.21}$$

For an example of a 1 m/s rip current with a half-width of 50 m in 1 m of water ($\partial U/\partial y = -1/50$), the terms on the right hand side become:

$$\frac{-1}{\sqrt{gh} - U} = \frac{-1}{\sqrt{9.81} - 1} \tag{2.22}$$

$$\frac{1}{2}\left(\frac{g}{h}\right)^{1/2}\frac{\partial h}{\partial y} - \frac{\partial U}{\partial y} = \frac{\sqrt{g}}{2}\frac{\partial h}{\partial y} - \frac{1}{50} \tag{2.23}$$

The first term suggests strong opposing currents reduce $\partial\theta/\partial x$ by 30%, while the second term suggests that the shears of a strong rip current can produce refractive turning that is equivalent to bathymetry gradients of $\sim 1/80$. The sense of the error would be to reduce estimated depths in a rip channel.

In the nearshore, the currents with the strongest shears are either longshore currents or rip currents. In the former case, the direction of flow will be nearly orthogonal to the usual near-normal angles of wave approach, so contamination will be minimal. As shown above, rip currents can cause a refractive turning that is equivalent to a $\sim 1/80$ slope, but the error will be predominantly in longshore slope, smoothing out rip channels as opposed to cross-shore beach slope. Areas of strong shear around tidal inlets should, of course, be avoided with this method.

With the assumption that all changes in wavenumber are due to bathymetric variation, the presence of a current, such as a rip current or flow from an inlet, will change the wavenumber and wave angle characteristics and yield errors in bathymetry gradient estimates. In the most extreme cases, such as strong rip currents exiting the surf zone in a rip channel, the proposed method will predict a shoal in the location of the current, while the bathymetry is most likely a trench. Since this method is most applicable outside the surf zone, these situations should be limited. In tidally influenced areas, images

taken at the peaks of the tidal cycle (high tide/low tide) when tidal currents are reduced should be used to limit error in bathymetry gradient estimation.

Initial tests of the refractive method were based on gradient approaches for estimating the required wavenumber and direction inputs. While successful for perfect (synthetic) data, they were sensitive to noise, especially the high wavenumber noise due to short, wind-blown chop that is typical of real world images. Extensive filtering was required to produce stable results. Thus, it was not until the introduction of the tomographic method of PHH08 that smooth and reliable values of wave quantities could be derived for imperfect data. Because time delays for all possible pixel pairs (close and widely-spaced) in the sub-region are incorporated in the estimate, extreme contamination by short gradient noise is avoided. Areas of known wave anomalies such as the edge of the surf zone where the optical signatures of wave fronts change from dark to white breakers can be reasonably smoothed through. For waves with a finite bandwidth spectrum, a single best-fit set of wave characteristics can be found. A requirement of this approach is computation of a corresponding confidence interval or skill for the solution. For some cases, waves will simply be too broad-banded for representation by a single direction and wavelength. These can be identified objectively by low skill values and the data disregarded.

As with other remote sensing methods of determining bathymetry, the refraction-based method has limitations in its application. Most importantly, the model requires there to be measurable gradients in both wavenumber and angle. Although longer waves feel the bottom at greater depth, (kh for any given depth is always less for longer waves), shorter period waves have their advantage in the nearshore because they undergo rapid changes in wave angle and wavenumber at shallower depths (e.g. *Dean and Dalrymple* (1991) p.108). This suggests the method is best suited for shorter period swell conditions in intermediate ($\pi/10 < kh < \pi$) water depths.

2.8 Conclusions

An algorithm has been developed to estimate nearshore bathymetry based on the changing directions of refracting waves. The model uses an augmented form of the refraction equation that relates gradients in bathymetry to gradients in k, θ through the chain rule. The equations can be cast in a form that is independent of wave period, so can be solved using wavenumber and direction data from a single snapshot rather than the normally-required time series of images.

Three methods for extracting k, θ data from images were tested. Under monochromatic conditions, all methods performed well. However, for cases with high-frequency noise or a non-ideal wave field, the two gradient methods for determining k, θ were found to be unusable. The tomographic approach of the PHH08 method was robust to these complications and had the added advantage of providing skill estimates that allowed objective identification of unacceptable results. Synthetic testing of the model using monochromatic waves on three bathymetries of increasing complexity, showed that the model accurately estimated 2D bathymetry gradients, hence bathymetry, with a mean bias of 0.01 m and mean rms error over the three beaches of 0.17 m. While the model is not useful for cases of complex seas or small refraction signals, the simplified data requirement of only a single snapshot is attractive. The model is perhaps best suited for shorter period swell conditions, for example from a semi-enclosed sea, where strong refraction patterns are visible and k, θ easily extracted from a single frame image.

3. A LINEAR MODEL TO PREDICT BAR DYNAMICS

3.1 Abstract

Nearshore systems are highly dynamic in both space and time. The majority of this variability can be attributed to the migration and morphological evolution of sandbars. Models of bar dynamics typically involve moments of the cross-shore flow, with offshore movement associated with the strong offshore directed undertow and onshore migration related to wave asymmetry and skewness (e.g. *Gallagher et al.* (1998); *Hoefel and Elgar* (2003)). Based on these hypotheses, models and laboratory studies have used the alongshore-mean bar position and alongshore-uniform wave conditions (a 1DH approach) to study bar response to varying wave conditions. Commonly, cases of offshore migration were reproduced with reasonable accuracy, but predictions of onshore migration were less successful. However, examination of time-exposure images of waves show that during periods of offshore migration, bars tend to be alongshore uniform and move rapidly offshore, but during onshore migration, sand bars are rarely straight, instead becoming very sinuous, violating the 1DH approach. We hypothesize that under milder wave conditions, the 2DH circulation associated with this alongshore-variable morphology is responsible for increased onshore net sand transport and the resulting onshore bar movement.

We extend the work of *Plant et al.* (2006) that relates bar position, sinuosity, and wave forcing within a linear dynamical feedback model. The model consists of coupled differential equations that govern the rates of change of cross-shore position and horizontal sinuosity as a function of the current cross-shore position and sinuosity and a proxy for wave forcing. We apply this model, relating bar position, sinuosity, and incident wave conditions, over a four-year period of time-exposure images of Palm Beach, Australia. The resulting analysis produces clear links between bar sinuosity and the rate of change of mean bar position, suggesting a 2DH approach should be used when modeling cross-

shore sand bar migration. However, limitations for the use of a linear model to study complex systems are also apparent, suggesting a more detailed model is required to study the role of sinuosity on highly dynamic beaches.

3.2 Introduction

The nearshore environment, which we will define as the ocean environment that is visible from the shoreline, is highly dynamic in both space and time (e.g. *Keulegan* (1948); *Davis and Fox* (1972); *Wright and Short* (1984); *Plant et al.* (1999); *Ruessink et al.* (2003); *Alexander and Holman* (2004)). As waves break, they transfer their momentum into the water column, generating nearshore currents and moving sand around. One of the most visible signatures related to changing wave conditions is the evolution of sand bars that often develop at, or migrate towards, the location of wave breaking (e.g. *King and Williams* (1949); *Greenwood and Davidson-Arnott* (1979); *Roelvink and Stive* (1989); *Plant et al.* (1999)). Examination of time-exposure images of waves have shown that during periods of high waves, sand bar evolution is rapid as the bar moves offshore and becomes alongshore uniform (e.g. *Wright and Short* (1984); *Lippmann and Holman* (1990) (Fig. 3.1 (May 8, 1996)). This is in stark contrast to sand bar evolution during milder wave conditions, which is marked by slower onshore migration and development of 2DH morphology (e.g. *Wright and Short* (1984); *Lippmann and Holman* (1990)) (Fig. 3.1).

Many of the processed-based models describing sediment transport related to sand bar migration utilize an energetics approach (e.g. *Bagnold* (1963); *Bowen* (1980); *Bailard* (1981)) (referred to herein as BBB) and assume cross-shore processes, such as undertow and velocity skewness, dominate the forcing terms (e.g. *Gallagher et al.* (1998)). Offshore migrations are well predicted, but the models fail to accurately predict the proper rates of onshore sand bar migration during more quiescent times. Model predictions improved with the inclusion of pressure gradients and the related wave acceleration skewness (e.g. *Drake and Calantoni* (2001); *Hoefel and Elgar* (2003)), and various boundary layer ef-

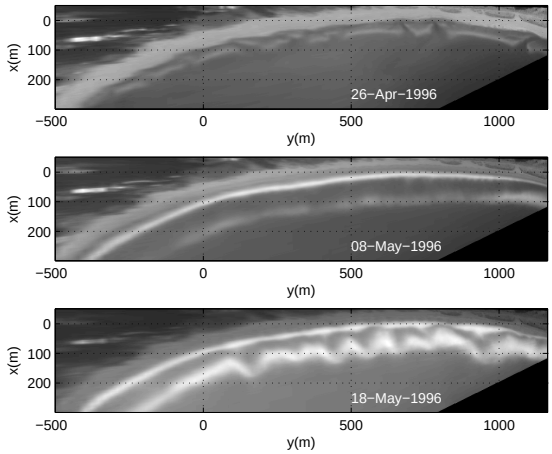

Fig. 3.1: Storm sequence at Palm Beach, AU depicting various stages of morphological evolution. (*top*) April 26, 1996 shows a transverse bar/terrace and rip system; (*middle*) May 8, 1996 shows an offshore linear bar system just after a storm; (*bottom*) May 18, 1996 shows the development of 2DH variability of the bar as it migrates onshore.

fects (*Henderson et al.*, 2004). However, sand bars can rarely be considered alongshore uniform (e.g. *Zenkovich* (1967); *Sonu* (1973); *Wright and Short* (1984); *Lippmann and Holman* (1990); *Alexander and Holman* (2004)), thus suggesting other processes, such as 2DH currents, also influence the time-varying response of sand bars to changing wave conditions. We hypothesize that under milder wave conditions, the 2DH circulation associated with this alongshore-variable morphology is largely responsible for increased onshore net sand transport and cannot be neglected in sediment transport models.

A recent paper by *Plant et al.* (2006) showed that for an onshore sand bar migration period following Hurricane Bonnie, mean sand bar position and bar sinuosity were dynamically linked through a simple linear model. This was the first attempt at quantifying the influence of 2DH morphology with respect to the onshore migration of the alongshore-averaged sand bar, showing rates of sand bar change and bar sinuosity were strongly coupled. We extend the work of *Plant et al.* (2006) to a second beach under a variety of wave conditions to test if such a model can link bar sinuosity to onshore migration events in more complex systems.

3.3 Model

The model uses a linear approach, with alongshore mean sand bar migration rates, $\dot{x}$, related to the alongshore mean sand bar position, x, bar sinuosity, a, and the forcing, F, which is chosen as the square of the offshore root mean square (rms) wave height, H^2. The dynamical equations relating mean sand bar position, x, and sinuosity, a, are:

$$\begin{bmatrix} \dot{x} \\ \dot{a} \end{bmatrix} = A \begin{bmatrix} x \\ a \end{bmatrix} + B \begin{bmatrix} 1 \\ F \end{bmatrix}, \tag{3.1}$$

where A and B are [2 x 2] matrices solved for by linear regression. The nature of the system is determined by the values obtained for A and B. A is the internal interaction matrix, where the diagonal terms represent self-interaction (e.g. how x influences $\dot{x}$). The sign of these terms indicate the stability of the system, where negative values indicate a stabilizing tendency. The off-diagonal terms of A represent cross-interaction (e.g. how a influences $\dot{x}$). These terms do not affect the systems stability if they are oppositely signed and the diagonal terms are negative. The B matrix describes how external parameters influence $\dot{x}$ and $\dot{a}$. The first column in B accounts for non-zero mean values in the absence of coupling. The second column describes the effect of varying wave height on bar response.

3.4 Study site

Palm Beach, Australia is a nearly east facing, 2-km long pocket beach located about 30 km north of Sydney (Fig. 4.1). Wave forcing is swell dominated, propagating from the SSE, with some energy from the E and NE (*Short and Trenaman*, 1992). The nearshore bed slope is 0.03 and has a median grain size of 0.30 mm (*Wright et al.*, 1980). The mean significant offshore wave height is 1.5 m with no significant seasonal variability in the wave conditions (*Short and Trenaman*, 1992). The beach morphology is highly variable, experiencing bar reset events (return to an offshore linear bar form) during higher wave forcing, followed by onshore bar migration and transverse bar rip development during

milder waves (*Holman et al.*, 2006). Bar position is significantly correlated to offshore wave height for timescales less than 8 days (*Alexander and Holman*, 2004). State changes occur quite rapidly, with rhythmic sandbars and rip channels developing usually within a week of a major storm. The most observed state is the transverse bar rip (TBR), occurring roughly 55% of the time (*Ranasinghe et al.*, 2004). Although no preferential rip locations were found in a study by *Holman et al.* (2006), *Alexander and Holman* (2004) found a significant correlation between offshore significant wave height and inverse rip spacing at short lags ($\sim$ day) indicating that morphology responds very rapidly to changing wave conditions.

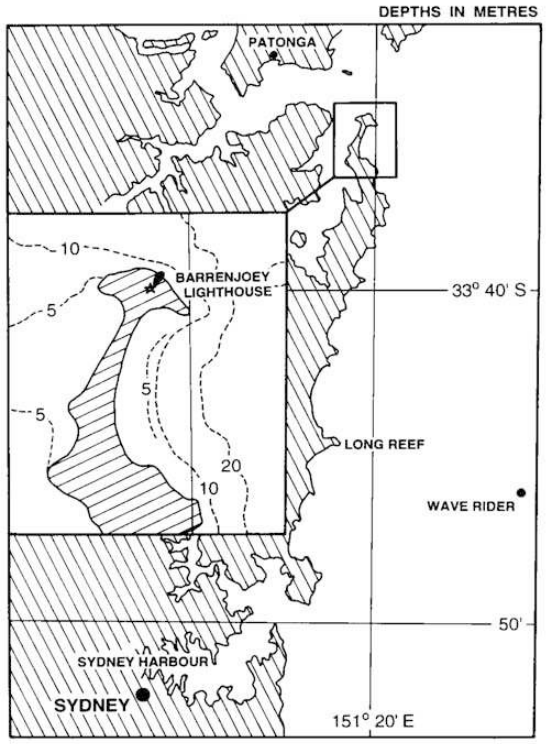

Fig. 3.2: Map of the Sydney area, Australia with a close up of Palm Beach, Australia. Offshore wave data is collect at the wave rider offshore of Long Reef (south of Palm Beach). Tide information is collected at Patonga (north of Palm Beach).

3.5 Data

In January 1996, a 2-camera Argus video-imaging station (*Holman et al.*, 1993) was installed in Barranjoey lighthouse, 115 m above sea level. The oblique images from camera C1 are rectified according to *Holland et al.* (1997) using known ground control point (GCP) and world camera locations (Fig. 3.3 (top)). The curved beach is then straightened using a circular best fit to the shoreline (*Alexander and Holman*, 2004)(Fig. 3.3 (bottom)) in order to improve our estimates of the alongshore-averaged bar position with respect to the shoreline.

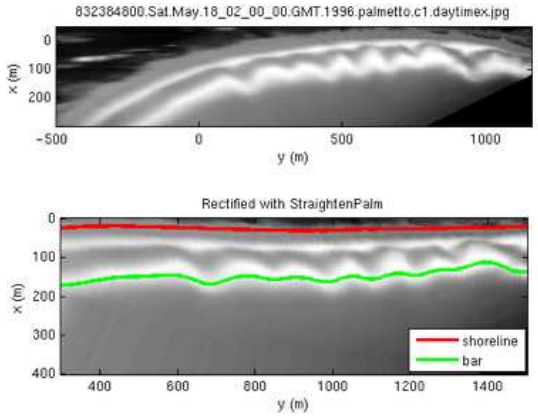

Fig. 3.3: Rectification of Images and Bar Identification. (*top*) Rectified image for Palm Beach, AU. (*bottom*) Straightened image with shoreline and bar position identified.

Bar locations are estimated by fitting the cross-shore intensity to a series of Gaussian curves. Bar position, $x_b(y)$, is defined as the center of the best-fit Gaussian curve depicting the inner-most sandbar (*Alexander and Holman*, 2004). Bar locations are identified at 5 m intervals in the alongshore at low and high tide and then linearly transformed to mean sea level. Bar positions are then interpolated in space to remove variations smaller than 50 m. Shoreline positions, $x_s(y)$, are identified using the maximum in intensity difference between the low and high tide images (*Alexander and Holman*, 2004). The mean daily bar position, x, is then calculated as the alongshore mean of the bar position, $x_b(y)$, minus the shoreline, $x_s(y)$. Sinuosity, a, is defined as the root mean variance in

the band 100 m $< L <$ 400 m, obtained from an alongshore Fourier decomposition of the bar position. Forcing for the model is given as $F = H^2$. Due to the orientation of the beach with respect to the dominant wave direction, daily significant wave heights, H_s, from an offshore wave rider (Fig. 4.1) are shoaled in to 10 m contour using the HISWA wave refraction model described by *Holthuijsen et al.* (1989). Wave data is then interpolated in time to 0.5 day intervals and low pass filtered using a 3 - day Hanning window to smooth the data and fill in missing data points.

3.6 Results

Four years of bar position data (1996 - 2000) were collected by *Alexander and Holman* (2004) as part of a multi-beach study. Sub-data sets spanning 1-2 months surrounding storm events (*Holman et al.*, 2006) were used to test the model and examine the relationship between bar position and sinuosity. Two of the data sets are presented here for discussion. The first data set (April - May, 1996) (Fig. 3.4) shows a clear example of a large storm passing, resulting in a linear bar beach state, followed by a slow and gradual onshore migration of the bar as sinuosity grows (Fig. 3.4). The data set spans $\sim$ 40 days before the wave gauge went offline, limiting the amount of onshore migration we are able to model. The second data set (March - April, 1998) (Fig. 3.5), also $\sim$ 40 days, contains two sequential minor storms with bar position, variability and forcing all varying on similar time scales (Fig. 3.5). One observation to note for this data set is that a actually decreases as the bar gets very close to shore, possibly suggesting a threshold relationship between bar position and sinuosity, similar to the evolution of rhythmic (or non-rhythmic) shore-attached bars into low-tide terraces under mild waves (e.g. *Wright and Short* (1984); *Lippmann and Holman* (1990)).

The predictive capability of the model is tested by initializing the model with the initial values of $x(t = 0)$ and $a(t = 0)$ and then driving the model with the given forcing (H^2) (Figs. 3.4, 3.5). For both data sets, the model skill is significant at the 95% level, predicting both onshore and offshore bar migration rates in the presence of variable

forcing and sinuoisty.

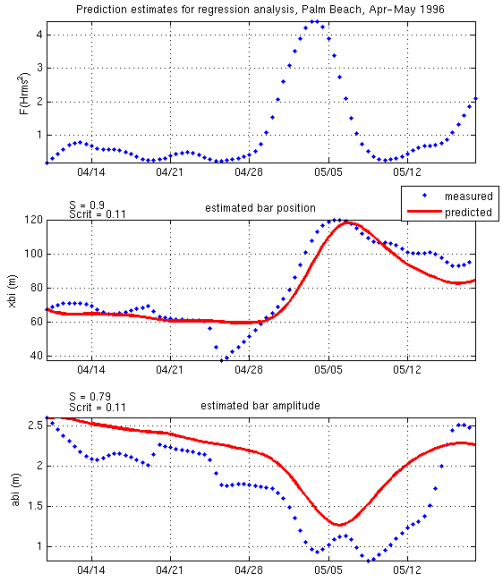

Fig. 3.4: Results for April - May 1996. Blue dots are measured data and red lines are predicted values based on forward prediction using regression results. (*top*) Wave forcing. (*middle*) Bar position. (*bottom*) Sinuosity.

3.6.1 Interaction Matrices

The interaction matrices (A, B) are determined using linear regression of equation (3.1) from known bar position, sinuosity, forcing, and the respective derivatives. We also supply the 95% confidence interval to indicate the accuracy of the regression analysis.

April - May 1996.

$$\Big[A\Big] = \begin{bmatrix} -0.146 \pm 0.066 & -2.08 \pm 2.808 \\ 0.004 \pm 0.002 & 0.020 \pm 0.090 \end{bmatrix} \left(d^{-1}\right) \tag{3.2}$$

$$\Big[B\Big] = \begin{bmatrix} 11.750 \pm 9.159 & 3.764 \pm 2.808 \\ -0.302 \pm 0.294 & -0.066 \pm 0.034 \end{bmatrix} \left(md^{-1}\right) \tag{3.3}$$

The positive value of A_{22}, suggests a positive feedback between a and $\dot{a}$. This seems

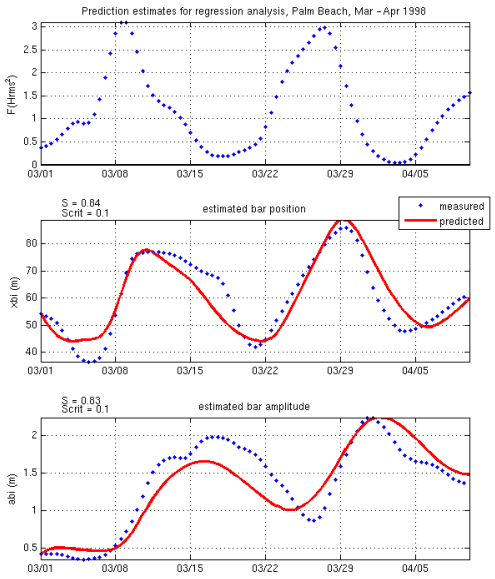

Fig. 3.5: Results for March - April 1998. Blue dots are measured data and red lines are predicted values based on forward prediction using regression results. (*top*) Wave forcing. (*middle*) Bar position. (*bottom*) Sinuosity.

sensible based on field observations of growing sinuosity under low wave conditions. However, the confidence intervals for the second column of A allow both these terms to change signs, therefore affecting the dynamical relationship and stability of the system. These terms suggest the influence of a on either x or itself may be weak, since both terms are not statistically different from zero. Little can be said about the off-diagonal terms, except that being non-zero indicates a dynamical relationship between x and a. The forcing matrix (B) is consistent with observations for increasing wave heights driving bars offshore and decreasing sinuosity (equation 3.3).

March - April, 1998.

$$\left[A\right] = \begin{bmatrix} -0.2968 \pm 0.082 & 2.950 \pm 2.004 \\ 0.009 \pm 0.003 & -0.131 \pm 0.063 \end{bmatrix} \left(d^{-1}\right) \tag{3.4}$$

$$\left[B\right] = \begin{bmatrix} 5.459 \pm 3.427 & 7.356 \pm 1.327 \\ -0.366 \pm 0.108 & -0.001 \pm 0.042 \end{bmatrix} \left(md^{-1}\right) \tag{3.5}$$

The results of this data set differ slightly from the previous in several ways. First, the diagonal terms of A (equation 3.4) are both negative, suggesting a stable system. The off-diagonal terms of A are not oppositely signed and therefore may also play a role in the overall stability of the system. The signs of all the terms in A do not change based on their confidence intervals, suggesting stronger links between individual parameters. In this instance, a actually encourages offshore bar migration (A_{12} is positive). This is an interesting result considering our hypothesis that the presence of sinuosity encourages onshore migration. This result may be more a mathematical fit to the system rather than highlighting the dynamics as the system starts out with a terrace (low sinuosity) and as the bar moves offshore, a is allowed to grow, and the system returns to a more terrace-like system again. As with the first data set, the terms in B indicate that increasing wave heights are accompanied by offshore sand bar migration and decreasing sinuosity (equation 3.5).

3.6.2 Equilibrium Values

Equilibrium values for each system are obtained by setting the left hand side of equation (3.1) equal to zero and rearranging:

$$\begin{bmatrix} x_o \\ a_o \end{bmatrix} = -[A]^{-1} B \begin{bmatrix} 1 \\ F \end{bmatrix} = B_o \begin{bmatrix} 1 \\ F \end{bmatrix}, \tag{3.6}$$

where x_o, a_o are the equilibrium values, and B_o describes the equilibrium coefficients in the presence of coupling, such that equilibrium values are a function of the external forcing (H^2).

April - May, 1996.

$$\begin{bmatrix} x_o \\ a_o \end{bmatrix} = \begin{bmatrix} 67.86 + 10.35F \\ 1.02 + 1.14F \end{bmatrix} \tag{3.7}$$

The equilibrium values are similar to those presented in *Plant et al.* (2006), indicating increasing (offshore) equilibrium bar position and sinuosity as a function of forcing. These results agree well with observations of bar position, but provide an inaccurate view of the system with respect to a. In nature, we observe a decreasing as the bar moves offshore with increasing H, usually during storms. Rarely do we observe the evolution of large a in the presence of large H and x, however this may be due to rarity in which constant wave forcing of this magnitude is also present.

March - April, 1998.

$$\begin{bmatrix} x_o \\ a_o \end{bmatrix} = \begin{bmatrix} -32.61 + 86.33F \\ -5.13 + 6.19F \end{bmatrix} \tag{3.8}$$

These equilibrium values are quite different, predicting negative values in the absence of forcing, but increasing x_o and a_o as forcing increases. It is hard to understand what this really means, but as we will discuss later, this particular data set sheds light on the strengths and weaknesses of the model chosen.

3.6.3 Stability Analysis

To further understand the dynamics of each system, we test the stability of each, and therefore its predictability. If a system is stable, then it is also predictable. Using eigenvalue analysis, we can determine the stability, response time, and the dynamic relationship between the different variables. A perturbation analysis is done assuming exponential growth with a timescale of λ:

$$\begin{bmatrix} x - x_o \\ a - a_o \end{bmatrix} = \begin{bmatrix} \xi \\ \alpha \end{bmatrix} e^{\lambda t}. \tag{3.9}$$

Expanding equation (3.1) about some equilibrium values, x_o, a_o,

$$\frac{d}{dt}\begin{bmatrix} x - x_o \\ a - a_o \end{bmatrix} = A \begin{bmatrix} x - x_o \\ a - a_o \end{bmatrix}, \tag{3.10}$$

and substituting equation (3.9) into equation (3.10),

$$\lambda e^{\lambda t}\begin{bmatrix} \xi \\ \alpha \end{bmatrix} = A \begin{bmatrix} \xi \\ \alpha \end{bmatrix} e^{\lambda t}, \tag{3.11}$$

leads to an eigenvalue problem:

$$\lambda \begin{bmatrix} \xi \\ \alpha \end{bmatrix} = A \begin{bmatrix} \xi \\ \alpha \end{bmatrix} \tag{3.12}$$

where λ are eigenvalues and ξ and α are eigenvectors of the system. The sign of the real part of λ indicates the stability of the system, where negative values indicate stability. The magnitude of this term is an indication of the response time. The decay timescale to return to equilibrium is given by $\Re(\lambda^{-1})$. The imaginary part of λ indicates an oscillation super-imposed on the decay timescale, where the period of oscillation is given by $T = (2\pi)\,\Im(\lambda^{-1})$. The complex phase shift, ϕ, indicates how a perturbation in one variable drives a response in the other. The complex phase shift is calculated as:

$$\phi = \tan^{-1}\left[\frac{\Im(\alpha/\xi)}{\Re(\alpha/\xi)}\right]. \tag{3.13}$$

A phase shift of zero indicates that the two variables are independent, while a 90° phase shift indicates that a perturbation in one (e.g. bar) causes a response in only the other variable (e.g. sinuosity). Partial quadrature indicates that the system is dynamically coupled.

April - May, 1996.

The two complex-valued eigenvalues are:

$$\lambda = -0.0616 \pm 0.0414i, \tag{3.14}$$

The real valued component is negative, indicating the system is stable, with a decay timescale of 16 days and a period of oscillation of 152 days. Since the decay timescale is much shorter than the period of oscillation, the system returns almost directly to its equilibrium value without oscillating around it. The resulting eigenvectors are:

$$\begin{bmatrix} \xi_1 & \xi_2 \\ \alpha_1 & \alpha_2 \end{bmatrix} = \begin{bmatrix} 1 & 1 \\ -0.0405 + 0.0206i & -0.0405 - 0.0206i \end{bmatrix}, \tag{3.15}$$

with

$$\phi = 153^\circ, \tag{3.16}$$

indicating the system is in partial quadrature and therefore, dynamically coupled.

March - April, 1998.

The two eigenvalues for this data are real-valued:

$$\lambda_1 = -0.0279 + 0i, \tag{3.17}$$

$$\lambda_2 = -0.400 + 0i. \tag{3.18}$$

The negative values indicate the system is stable, with decay timescales of 2.5 and 36 days. The lack of an imaginary component indicates there is no oscillation around the equilibrium and the system returns directly to its equilibrium value. This also produces two real-valued eigenvectors,

$$\begin{bmatrix} \xi_1 & \xi_2 \\ \alpha_1 & \alpha_2 \end{bmatrix} = \begin{bmatrix} 1 & -0.0912 \\ 1 & -0.035 \end{bmatrix}, \tag{3.19}$$

with a phase value of

$$\phi = 180^{\circ}, \tag{3.20}$$

indicating that an increase in one variable should cause a decrease in the other.

3.7 Discussion

A simple linear model relating bar position, sinuosity, and forcing was tested over a 4-year data set at Palm Beach, Australia. The model shows significant skill in predicting bar movement and changes in bar variability for all sample runs. The parameter estimates vary with changing data sets, but show that the system is stable and that the amount of cross-interaction is dependent on the system variables and forcing. The stability analysis was able to highlight some of the differences between the data sets. For example, the April - May 1996 data set showed a stable system, with decay times scales of the system much shorter than that from the oscillation and that there is significant cross-interaction between bar position and sinuosity. The March - April 1998 data set, however, was a stable system with two real-valued decay timescales and no oscillations. One of the decay timescales was much shorter in this case, indicating shorter response times and potentially a more forced system with respect to changing wave conditions. Looking at the coefficient matrices, we see that the self-interaction term for sinuosity is an order of magnitude greater in the second data set, but the forcing (matrix B) has an order of magnitude less of an influence on bar amplitude. This may be linked to the overall magnitude of forcing which is greater in the first case, with greater offshore bar movement. Alternatively, this may indicate that major storms cause the bar to become alongshore uniform, but a slight increase in forcing may move the bar offshore and increase the bar sinuosity/active surf zone width.

For the March - April 1998 data set, the three independent variables used in the regression (x, a, F) are all phase-lagged versions of each other (Fig. 3.5). This can cause interpretation problems in the linear regression analysis because variability can be assigned to a number of combinations to arrive at the same result. Particularly, this can

affect our interpretation on the interactions between x and a as depicted through our stability analysis of A. Although we can visually see the link between all three variables, the regression analysis weighted the B matrix much more heavily, suggesting a more 'forced system'. This also led to an eigenvalue analysis that suggested x and a were not in partial quadrature. This is not the case in the first data set where x and a varied on different timescales of wave forcing and the A matrix clearly defines the relationship between x and a.

3.8 Conclusions

The results indicate that inclusion of 2D circulation (modeled here by sinuosity) is important in producing correct on-shore bar migration rates for the data sets tested. The model had lower predictive skill for the Palm Beach data set compared to Duck data set taken during a hurricane event. However, the model was able to capture the fundamental dynamics during major storm resets (April - May 1996). Due to the nature of the bar evolution at Palm Beach, the linear model had limited ability to robustly separate bar evolution due to forcing and the effect of sinuosity in data sets where x, a, and F varied at similar time scales (March - April 1998). As well, the regression analysis was limited to short timescales (single storm events) due to the hysteresis of the natural system. Bar position and sinuosity are linked and therefore influenced each other at varying scales. Changes in one term drove changes in the other, however, unique values of x compared to a and H are not required. We conclude that such simple models can be useful at describing the nature of the dynamical feedback systems involved in bar evolution during major storm events on a storm by storm basis. However, for more forced systems, with variability in x and a directly linked to offshore wave conditions at short timescales, a more in-depth (physics-based) model with fewer free parameters may be required in order to examine the relationship between bar position and sinuosity.

4. A BEHAVIOR-ORIENTED DYNAMIC MODEL FOR SAND BAR MIGRATION AND 2DH EVOLUTION

4.1 Abstract

A new, nonlinear model is developed to study the influence of two-dimensional (horizontal, 2DH) circulation on alongshore-averaged cross-shore sand bar migration. The model uses an energetics-based formula to model sediment transport at the bar crest. The equations are reduced to a parametric form using the relationship between sand bar migration of a constant bed form and the underlying sediment transport pattern. Net sand bar migration is modeled based on an equilibrium approach in which temporal variations in the amount of wave breaking, and therefore the roller contribution to the undertow, is a significant contributor to sand bar migration. Due to the nonlinear form of the model, under non-breaking conditions sediment transport, and thus bar migration, is assumed to be negligible. The model includes the effects of 2DH currents on the alongshore-averaged sand bar migration rate through parameterizations based on the length scales of 2DH morphology and wave breaking. The model equations for cross-shore sand bar migration, $\dot{x}$, and changes in 2DH morphology, $\dot{a}$, are dynamically linked, such that changes in one term will drive changes in the other.

The model is tested on a subset of four years of data from Palm Beach, Australia. A total of 562 days surrounding eleven major storms and subsequent recovery are included. Model coefficients are subjectively chosen to best fit the spectral characteristics of the entire data set. The model is able to reproduce both onshore and offshore migration rates through multiple storm sequences with significant skill (95% level) for all data sets. Under less energetic wave conditions, the model predicts onshore migration, with rates influenced by the amount of 2DH variability present and the incident wave angle. The inclusion of 2DH terms are required to accurately reproduce the onshore migration rates

in the data. Offshore migration rates were also reproduced and attributed to dissipative wave conditions.

4.2 Introduction

Nearshore systems are highly dynamic in both space and time. While some beaches exhibit a monotonic cross-shore structure, most have offshore features, such as sand bars (e.g. *Keulegan* (1948); *Davis and Fox* (1972); *Plant et al.* (1999); *Ruessink et al.* (2003); *Alexander and Holman* (2004)). Observations show the morphology of these sand bars can rarely be considered alongshore uniform (e.g. *Zenkovich* (1967); *Sonu* (1973); *Wright and Short* (1984); *Lippmann and Holman* (1990); *Alexander and Holman* (2004); *van Enckevort et al.* (2004)). Thus a full description of the nearshore bathymetry, $h(x', y', t)$, requires specification of the cross-shore, x', alongshore,y', and temporal, t, dependencies. The prime is used to distinguish between spatial co-ordinates and measured bar crest position, x. For any particular survey, this might require bathymetry estimates at $O(10^4 - 10^6)$ locations, a daunting number of measurements to keep track of and model.

Several approaches have been used to reduce the dimensionality of the problem. It is often assumed that alongshore variability is negligible in the bathymetry and dynamics. Thus, models can be formulated that need only represent one horizontal dimension (1D), rather than both the alongshore and cross-shore (2DH) or all three, including the depth variation (3D). Alternately, bathymetry can be represented as either a continuous variable (although sampled at discrete survey locations) or as parametric functions that are assumed to adequately represent the bulk of the continuous profile variability with a few parameters such as the location, amplitude and width of Gaussian sand bar functions. Both approaches offer a compromise between simplicity and realism. On one hand, continuous models redistribute sand along the entire profile based on fluid-sediment interactions. This can lead to profile evolution that is unrealistic due to errors in the measured or modeled fluid forcing. Interpreting the skill of such models is also more subjective as they compare entire profiles versus a single parameter, such as bar crest

position. Alternatively, parametric models may be reduced to forms that mathematically represent the data, yet lack the necessary physical link between drivers of sediment transport and observations.

4.2.1 1DH Models

1DH bathymetric models assume that bathymetry can be represented as:

$$h(x',t) = \bar{h}(x') + \tilde{h}(x',t), \tag{4.1}$$

where $\bar{h}(x')$ represents the time-mean beach profile, and $\tilde{h}(x',t)$ the time variability about that mean. For sufficiently long data sets, $\bar{h}(x')$ is usually monotonic or planar, while $\tilde{h}(x',t)$ contains information on the cross-shore migration of sand bars (e.g. *Birkemeier* (1985); *Thornton et al.* (1996); *Gallagher et al.* (1998); *Plant et al.* (1999, 2001); *Ruessink et al.* (2003)), identified as the maxima in $\tilde{h}(x',t)$.

A number of process-based models of cross-shore transport have been proposed in the literature. Many are based on an energetics approach (e.g. *Bagnold* (1963); *Bowen* (1980); *Bailard* (1981)) and assume that cross-shore processes, such as undertow and velocity skewness, dominate the forcing terms (e.g. *Gallagher et al.* (1998)). An example of such a model is described in more detail in Section 4.3.1. Process-based models allow the user to examine the effects of individual components, such as the contribution of wave skewness to onshore migration or undertow to offshore migration.

Beach change in 1DH models is modeled as a continuous function of x', but results are often described in morphologic terms, for instance a judgment that a sand bar moved onshore or offshore, based on differences between two consecutive profiles. Offshore migrations (which occur under larger waves) are usually well predicted by energetics-based models (e.g. *Gallagher et al.* (1998)). However, models historically have failed to accurately predict the proper rates of onshore sand bar migration during more quiescent times. Recent work has examined the importance of previously unconsidered 1DH processes such as pressure gradients and the related wave acceleration skewness (e.g. *Drake*

and Calantoni (2001); *Hoefel and Elgar* (2003)), near-bed wave skewness (*Ruessink et al.*, 2007), and various boundary layer effects (*Henderson et al.*, 2004) in cross-shore sediment transport under wave driven environments. These models have shown improved skill under certain circumstances, but the problem is not considered solved despite the increasing complexity of the resolved processes.

Alternatively, parametric models assume that sand bars (or morphology) can be represented using a discrete set of parameters, such as bar position, whose variation with time can be modeled. Model equations are generally behavioral; distillations of known physics to a few essential elements that are assumed to dominate response. One well-known example is the breakpoint model (e.g. *King and Williams* (1949); *Greenwood and Davidson-Arnott* (1979); *Roelvink and Stive* (1989); *Marino-Tapia et al.* (2007)) that suggests sand bars exist at the location of initial wave breaking due to unspecified convergences in sediment transport. Since this model is based on an equilibrium response of the bar to a particular fluid forcing, it is strictly valid only when bar response is much more rapid than the rate of change of wave conditions. Under typical conditions, this is not true. Attempts to predict the time-varying location of bars under either instantaneous wave forcing or some time-average wave height have not usually been successful (*Sallenger and Howd*, 1989).

Plant et al. (1999) recognized the need to add a dynamic aspect to the breakpoint concept, modeling not the actual bar position but instead its rate of change. They proposed that the migration rate of the alongshore-averaged sand bar, $\dot{x}$, should depend on the disparity between its current position, $x(t)$, and a time-varying equilibrium location, $x_{eq}(t)$:

$$\dot{x} = -\alpha(t)\left[x(t) - x_{eq}(t)\right], \tag{4.2}$$

where $\dot{(\cdot)}$ represents the time derivative of the bracketed variable. x_{eq}, the time varying equilibrium sand bar position, is assumed to vary linearly with wave height, consistent with a breakpoint hypothesis:

$$x_{eq}(t) = a_2 H_o(t), \tag{4.3}$$

where $H_o(t)$ is the time varying offshore wave height and $\alpha^{-1}(t)$ is the response time, describing the rate at which bar location changes. Observations have shown response times due to changing wave conditions are dependent on wave height (e.g. *Wright and Short* (1984); *Plant et al.* (1999, 2001)), such that sand bars move offshore (during high waves) much faster than onshore (during milder wave conditions), and no migration occurs for $H = 0$. *Plant et al.* (1999) found a best-fit form for α to be dependent on the cube of the offshore wave height, H_o^3:

$$\alpha(t) = a_1 H_o^3(t), \tag{4.4}$$

Equations (4.2) - (4.4) represent a large improvement over the original breakpoint model. The dynamic nature of the equations acknowledge that bars are in continual pursuit of an equilibrium configuration but can only respond at a rate that depends on the cube of the wave height. Response to storms is found to be rapid while response to intervening quiet times is much slower. As a result, the mean bar position is weighted toward the large waves, offshore of the mean breakpoint. Using least squares fitting, values of parameters can be found such that model predictions reasonably match several long data sets.

Although simple in form and a useful representation of some aspects of bar behavior, the *Plant et al.* (1999) model has a number of acknowledged limitations. The model is not based on sediment transport principles but instead is a somewhat ad-hoc representation of reasonable behavior. For example, equation (4.2) requires a sand bar to move quickly when far away from its equilibrium and slow down as it approaches the location of wave breaking, similar in form to Hooke's Law ($F = -k\vec{x}$), where the restoring force, F, is related to the distance between current position and the equilibrium, $\vec{x}$, and a force constant, k. There is no obvious sediment transport basis for this assumption. Although

Plant et al. (1999) argued that sediment transport was related to H^p, by dimensional arguments, the units of a_1 must be $m^{-3}s^{-1}$, which is not an obvious result. Finally, this model assumes that alongshore variability is of no consequence and can be simply averaged out.

4.2.2 2DH Models

The assumption above of alongshore-uniformity is rarely valid. Observations show that 2DH morphology is quite common (e.g. *Wright and Short* (1984); *Lippmann and Holman* (1990); *Ranasinghe et al.* (2004)), especially during periods of onshore bar migration. For example, *Lippmann and Holman* (1990) found that sand bar morphology at Duck, North Carolina, was visibly alongshore-uniform for less than 7% of a two-year dataset of daily measurements. For periods of non-storm conditions (down-state transitions) changes in morphology were found to be more dependent on the prior state than on the wave forcing, suggesting a positive feedback system in which 2DH processes may influence the time-varying response of sand bars due to changing wave conditions.

Representation of a full 2DH bathymetry roughly squares the data requirements of modeling compared to the 1DH equivalent. 2DH or 3D models on general bathymetries have seen increasing research and often provide reasonable performance (e.g. *Reniers et al.* (2004); *Dronen and Deigaard* (2007)). The simulations are capable of reproducing the bulk characteristics of 2D systems (e.g. growing 2DH variability under low wave conditions), however, comparisons against measured bathymetric change (e.g. exact location and magnitude of developing 2D bathymetry) show limited skill. For this reason, and the lack of high resolution temporal and spatial bathymetry data, tests have been limited to a few field experiments. The logistics of fielding an operational capability at any field site would be severe.

Alternatively, a great deal of research has focused on the idea that alongshore variability is generally rhythmic and can be characterized by a single characteristic alongshore length scale of variability (e.g. *Bowen and Inman* (1971); *Guza and Inman* (1975); *Ko-*

mar (1983); *Wright and Short* (1984)). For example, *Bowen and Inman* (1971); *Guza and Inman* (1975); *Holman and Bowen* (1982) explained the generation of alongshore rhythmic features as a result of the dominant presence of edge waves of very particular frequencies. These models were subsequently shown to be inconsistent with extensive field observations (*Holland and Holman*, 1996, 1999).

An alternate explanation has been proposed by a number of authors (e.g. *Deigaard et al.* (1999); *Falques et al.* (1999); *Coco et al.* (2000); *Falques et al.* (2000); *Caballeria et al.* (2002); *Calvete et al.* (2005); *Garnier et al.* (2006)) based on instability analysis of various components of the nearshore system. For example, *Falques et al.* (1996) showed that longshore currents were unstable to bottom perturbations with length scales typical of oblique nearshore bars. Similarly, more complex two-dimensional (horizontal, 2DH) or quasi-3D models (e.g. *Reniers et al.* (2004); *Dronen and Deigaard* (2007)) have shown instabilities associated with pre-existing linear sand bars that had alongshore scales typical of rhythmic sand bars and rip channels. However, all of these models explain the initial generation of alongshore variability from an initially alongshore-uniform bathymetry. *Holman et al.* (2006) examined four years of nearshore morphology data from Australia to show that systems rarely return to an alongshore-uniform bar condition (i.e. system variability is rarely associated with the physics of initial generation) and that length scales of features were rarely rhythmic but instead occupied a spectral band of wavelengths.

Instead of treating alongshore variability in terms of a characteristic length scale, *Plant et al.* (2006) propose an alternate, parametric approach based on the bar sinuosity, a, the alongshore standard deviation of bar position for all alongshore length scales from 200 to 1000 m. While *Plant et al.* (1999) averaged out this variability on the assumption that it made no fundamental contribution to bar dynamics, *Plant et al.* (2006) explicitly explore their presence by modeling the dynamics of both x and a simultaneously as a function of wave forcing, represented by the offshore root mean square (rms) wave height squared, H_o^2. Their dynamic equations relating mean sand bar position and 2DH variability are:

$$\begin{bmatrix} \dot{x} \\ \dot{a} \end{bmatrix} = A \begin{bmatrix} x \\ a \end{bmatrix} + B \begin{bmatrix} 1 \\ F \end{bmatrix}. \tag{4.5}$$

The elements of the 2 x 2 matrix, A, represent the self and cross-interaction terms of x and a. For example, A_{12} represents the influence of a on the bar migration rate, $\dot{x}$. *Plant et al.* (2006) found this term to be significant suggesting that the presence of 2DH morphology is indeed required to predict correct onshore migration rates, i.e. $\dot{x} = f(a)$. The elements of B represent the influence of the forcing on the two sand bar variables.

The dynamic model proposed by *Plant et al.* (2006) provided the first simple parametric model to address the links between sand bar position and 2DH variability and allowed analysis of the stability of the system. However, it also had several weaknesses. The governing equations are again behavioral and lack a sediment transport basis, as with *Plant et al.* (1999). The linearized formulation allows bar movement even in the absence of wave forcing and lacks the clear response time characterization of *Plant et al.* (1999). The model is only valid for small perturbations about a mean, so can only be applied for short records (e.g. two months) and cannot be applied when the bar amplitude becomes limited by proximity to the shoreline. Finally, a unique least squares solution for the elements of A and B requires that the bar variables and the forcing vary on different time scales. Under forced conditions, when bar position and sinuosity vary on timescales of the wave forcing, the influence of sinuosity on bar migration may be masked due to the strong coupling with wave height.

We wish to build a hybrid model similar to *Plant et al.* (1999, 2006) to study the nonlinear feedbacks in 2DH sand bar migrations. We will develop a set of coupled equations that are dynamic (expressed in terms of time derivatives) and nonlinear, and are based on the principles of sediment transport. The model will not attempt to make predictions about the nature of 2DH morphology, such as rip channels, or the alongshore length scale of these features, but rather about the influence of 2DH morphology in general on net bar migration rates. Specifically, we test the hypothesis that alongshore

averaged sand bar migration rates, $\dot{x}$, and 2DH sand bar variability, a, are significantly coupled such that:

$$\dot{x} = f(a). \tag{4.6}$$

The paper is broken down as follows. In Section 4.3 we describe the proposed model. Section 4.4 describes the field site and data extraction from video time exposure images. In Section 4.5 we test the model and present results for several data sets. We conclude with a discussion of the model, limitations and relevant findings in sections 4.6 and 4.7.

4.3 Theory

Our goal is to develop a parametric model for bar variability that can be tested using commonly-available remote sensing data. These equations will be built from a sediment transport theory, the energetics-based equations of *Bagnold* (1963); *Bowen* (1980); *Bailard* (1981) (referred to as BBB herein). We first develop the equations in 1DH, looking at deviations about an equilibrium balance associated with changes in mean flows and the fraction of waves that are breaking. Extensions to 2DH will, of necessity, not be rigorous, but are based on observations and assumptions about the role of circulation cells and rip currents in net cross-shore transport. Highly developed 2DH systems are assumed to be partially self-stabilizing, so large wave heights are required to return the morphology to more 1DH conditions.

4.3.1 Alongshore-averaged Sand Bar Migration Rates ($\dot{x}$)

Parametric models provide a simplified representation of nearshore variability. However, prior to developing a parametric formulation, for example, for the cross-shore migration rate of a sand bar, we need to establish a link between bar migration and the sediment transport that caused that migration.

Connection Between Parametric and Transport-based Models

Bagnold (1941) showed that for a bedform undergoing strictly migration with no change in shape, the associated sediment transport pattern has the same shape as the bedform. In general, the bedform can be represented as

$$h(x',t) = h(x' + \delta x'(t)), \tag{4.7}$$

$$= h\left(x' + \int_0^t \dot{x}'(t)dt\right), \tag{4.8}$$

where x' is the domain of the bar shape function and $\delta x'(t)$ is a time varying offset of the basic bar form. Following *Bagnold* (1941), sediment transport is taken to have the same shape,

$$Q_x(x,t) = \frac{Q_{x_o}(t)}{\Delta} h(x',t), \tag{4.9}$$

where Q_{x_o} and Δ are the cross-shore transport at the bar crest and bar crest height, respectively. The two variables are linked by the conservation of mass equation,

$$\frac{\partial h}{\partial t} = \frac{1}{\mu}\frac{\partial Q_x}{\partial x}, \tag{4.10}$$

where μ is the sediment packing factor of settled sediment grains (set to 0.7 (*Thornton et al.*, 1996)). Substituting equation (4.7) and equation (4.9) into equation (4.10) we have

$$\frac{\partial h}{\partial t} = \frac{Q_{x_o}(t)}{\mu\Delta}\frac{\partial h}{\partial x}. \tag{4.11}$$

We see that mass is conserved if the migration rate, $\dot{x}$, is given by:

$$\dot{x} = \frac{1}{\mu}\frac{Q_{x_o}}{\Delta}, \tag{4.12}$$

where Q_{x_o} is the cross-shore sediment transport at the bar crest. This provides a convenient relationship between the bar migration rate, a parametric representation, and

the sediment transport at the bar crest, a geophysical variable, provided the sand bar migrates without change of shape.

Plant et al. (2001) carried out a similar analysis based on sixteen years of monthly beach profile data from Duck, North Carolina. Alongshore-averaged beach profiles were modeled as the superposition of a planar slope and a set of Gaussians, one for each sand bar. From the conservation of mass equation (4.10), changes in bathymetry between consecutive surveys could be inverted to find the associated sediment transport that caused the change. Because only Gaussian forms were allowed, these transport patterns could only look like Gaussians (bar movement) or bar growth and decay (Error functions). Even with these limited forms available, the vast majority of the variance was captured. *Plant et al.* (2001) then showed that the bulk of temporal changes of the profile between consecutive surveys were due to migration of constant form bars (transport had the same shape as the sand bar form). Thus, equation (4.12) should provide a good link between parametric bar migration rates and wave-driven sediment transport.

For the purposes of modeling bar evolution over extended periods of time, rather than collecting statistics from pairs of closely-spaced beach profiles as above, both the bar height and length scale vary as a function of cross-shore location (*Ruessink et al.*, 2003). Offshore bars with larger volumes should migrate more slowly than smaller onshore bars under the same magnitude of transport. The constant form transport equation (4.12) can be simply adapted to include a cross-shore dependency without altering the underlying assumption of constant form migration if the equation is rearranged as follows. As we are limited to the area of active wave-breaking, we assume that the bar height and length scale both vary linearly with cross-shore location, x':

$$\Delta(x') = \frac{\Delta_o}{x_o} x', \tag{4.13}$$

and

$$L_{bar}(x') = \frac{L_o}{x_o} x' \tag{4.14}$$

Δ_o and L_o are reference values of bar height and bar length, respectively, measured at some reference location, x_o. Since these values are measured at the bar crest location, $x' = x$. Rewriting equation (4.12) as

$$\dot{x} = \frac{1}{\mu} \frac{x_o^2}{\Delta_o L_o} \frac{Q_{x_o}}{x^2}, \tag{4.15}$$

we see that this is similar in form to equation (4.12) if we model the transport to include the normalization by x^2 and absorb x_0, Δ_0, and L_0 into empirical coefficients in the sediment transport relationships. In other words, the migration rates of bars with varying length scales can be equivalently modeled by normalizing the bar crest transport rate by that variation.

The ratio Δ_o/x_o is a site-specific parameter in the model. Based on an October 1999, survey of the field site, Palm Beach, Australia (*Brander*, 1999), the linear best-fit for the ratio Δ_o/x_o was 0.0076. Bar length, $L(x')$, was not determined from the single survey, such that the ratio L_o/x_o will be subsequently absorbed into a bulk empirical coefficient.

1DH Sediment Transport

The problem of predicting sand bar migration rates was shown above to depend only on predictions of cross-shore sediment transport rates at the bar crest, Q_{x_o}. In this section, we develop such a formulation based on the energetics models of BBB. If we assume that onshore and offshore transport terms balance under some wave conditions (equilibrium), then we can model the residual transport as deviations away from those conditions. Extending the ideas of *Plant et al.* (2001), we will represent deviations of wave forcing in terms of $\gamma_b = H_b/h_{bar}$, where H_b is the root mean square wave height at the breakpoint and h_{bar} is the depth at the bar crest.

We parameterize Q_{x_o} based on BBB-type equations, using the formulation similar to *Bowen* (1980), where

$$Q_x = \frac{K_b}{g}\left[\left\langle|u|^2U\right\rangle + \left\langle|u|^2u_w\right\rangle - \left\langle|u|^3\right\rangle\frac{\tan\beta}{\tan\phi}\right] + \frac{K_s}{gW}\left[\left\langle|u|^3U\right\rangle + \left\langle|u|^3u_w\right\rangle - \left\langle|u|^5\right\rangle\frac{\tan\beta}{W}\right], \tag{4.16}$$

and $\langle\cdot\rangle$ and $|\cdot|$ signify the time average and absolute value of a quantity. u, U, and u_w are the total velocity, depth-averaged cross-shore current, and wave orbital velocity, respectively. g is the acceleration due to gravity, W is the sediment fall velocity, $\tan\phi$ is the angle of repose for sediment, and $\tan\beta$ is the bed slope. K_b and K_s are the dimensionless bedload and suspended load transport coefficients:

$$K_b = \frac{\rho_w}{(\rho_s - \rho_w)}C_d\frac{\epsilon_b}{\tan\phi}, \tag{4.17}$$

$$K_s = \frac{\rho_w}{(\rho_s - \rho_w)}C_d\epsilon_s, \tag{4.18}$$

where ρ_w is the density of water, ρ_s is the density of the sediment, C_d is the drag coefficient, and ϵ_b and ϵ_s are the bedload and suspended load efficiency factors, respectively. *Bagnold* (1966) suggested $\epsilon_s = 0.01$ and $0.11 < \epsilon_b < 0.14$, values commonly used (e.g. *Bowen* (1980); *Bailard* (1981); *Gallagher et al.* (1998)). C_d is expected to have a range of $10^{-3} - 10^{-2}$. Based on *Church and Thornton* (1993) we set $C_d = 0.003$. W is set to 0.04 m/s based on a sediment grain size of 0.3 mm (*Dean and Dalrymple* (2002), p.32).

Several simplifications are made to equation (4.16) in order to isolate the main contributors to sand bar migration. We neglect the contribution due to bedload since its contribution is small in the surf zone (*Gallagher et al.*, 1998). We also neglect transport due to gravity ($\tan\beta$), since $\tan\beta$ is zero at the sand bar crest and the effect of this term is to change bar shape (spread the bedform out), and we have assumed the bedform shape to be unchanging, reducing equation (4.16) at the bar to

$$Q_{x_o} = \frac{K_s}{gW}\left[\left\langle |u|^3 U\right\rangle + \left\langle |u|^3 u_w\right\rangle\right]. \tag{4.19}$$

In the 1DH case, all the wave-driven shoreward mass transport must be returned by the undertow (U). In turn, this transport is composed of two contributions: the return flow due to Stokes drift (U_s) and that due to the wave roller (U_r) (*Svendsen*, 1984),

$$U = \left(c\left\langle\left(\frac{\eta}{h}\right)^2\right\rangle + bc\frac{\bar{e}}{h}\right)\cos\theta, \tag{4.20}$$

where c is the local wave celerity, $c = \sqrt{gh}$, η is the wave form, h is the local water depth, $\bar{e}$ is the roller area, $\bar{e} = 0.9H^2/L$, H is the local rms wave height, L is the local wavelength, and $\cos\theta$ is the wave angle with respect to shore normal. When only a fraction of the waves are breaking, we have modeled the contribution of the roller as being proportional to that fraction of breaking, b.

We assume that for some wave condition there is sufficient breaking that the terms in equation (4.19) balance and the system is in equilibrium ($Q_{x_o} = 0$):

$$Q_{x_o,eq} = \frac{K_s}{gW}\left[\left\langle |u|^3\left(U_s + 0.9b\frac{H_b}{T}\gamma_{eq}\right)\right\rangle + \left\langle |u|^3 u_w\right\rangle\right] = 0. \tag{4.21}$$

We have expressed this equilibrium condition in terms of an equilibrium value, γ_{eq}, of the non-dimensional breaker height, $\gamma_b = H_b/h_{bar}$.

Deviations away from this equilibrium condition will determine the net transport. A full representation of the dependencies of each term in equation (4.21) with varying conditions will be complex. Instead, we will assume that changes in the Stokes drift and skewness contributions stay roughly in balance leaving a residual that is related to variations in the roller term. Thus, we will model the primary variation of transport away from equilibrium as depending on $b\,(\gamma_b - \gamma_{eq})$. This term has sensible behavior over a range of conditions.

During storms, wave breaking is saturated over the bar and much of the surf zone. To balance the saturated roller transport, the undertow is large and predominantly 1DH,

such that net transport is in the offshore direction (positive values). Under calm conditions, no waves will be breaking. Skewness-based transport will likely dominate (e.g. *Guza and Thornton* (1985); *Doering and Bowen* (1987); *Thornton et al.* (1996); *Plant et al.* (2001); *Ruessink et al.* (2007)), but is assumed negligible compared to breaker-driven processes. Inclusion of the fraction of breaking in our formulation will force transport to go to zero. Under intermediate conditions, partial breaking over the bar can drive sediment transport in either the onshore or offshore direction depending on the wave height. Our final model for net 1DH cross-shore transport is

$$Q_{x_o} = 0.9 K_s \left\langle |u|^3 \right\rangle g^{-1} b \Omega \left(\gamma_b - \gamma_{eq}\right). \tag{4.22}$$

where $\Omega = H_b/TW$ is the dimensionless fall velocity term, a parameter that has been associated with beach response by a number of authors (e.g. *Shepard* (1950); *Bascom* (1954); *Dean* (1973); *Wright and Short* (1984)). Equation (4.22) can be separated into a magnitude ($\hat{Q}_{x_o}$) and a direction component:

$$Q_{x_o} = \hat{Q}_{x_o}(\gamma_b - \gamma_{eq}), \tag{4.23}$$

where

$$\hat{Q}_{x_o} = \frac{9}{80} K_s b \gamma_{bar}^3 h_{bar} \sqrt{g h_{bar}} \Omega, \tag{4.24}$$

and we have replaced the local orbital velocity at the bar crest by its phase-averaged shallow water form $\left(\left\langle |u|^3 \right\rangle = \gamma_{bar}^3/8 g h_{bar} \sqrt{g h_{bar}}\right)$.

Inclusion of 2DH Terms

When morphology becomes alongshore variable, the requirement to balance wave mass transport through undertow at each cross-shore transect is removed. Instead, horizontal circulation may occur, with onshore-directed flow over the typically broad shoals and offshore-directed flows concentrated in narrow rip channels (e.g. *Haller et al.* (2002);

Reniers et al. (2004); *Aagaard et al.* (2006); *Garnier et al.* (2006); *Falques et al.* (2008); *Garnier et al.* (2008)). Water mass is still balanced in the alongshore average, but not locally.

Most sand bar models assume that the alongshore-average migration rate of bars is unaffected by the presence of alongshore variability, or, in parametric variables, $\dot{x} \neq f(a)$. This assumption is the sediment transport analog to the requirement that fluid mass must be balanced in the alongshore-average, independent of whether circulation is present or not. However, sediment transport is a nonlinear function of velocity. It is quite plausible that onshore transport over the broad shoals could dominate over the offshore transport associated with rip channels (or visa versa, although this seems contrary to observation).

We hypothesize that the presence of alongshore variability has two consequences on the alongshore-averaged bar migration rate. First, we suggest that the presence of horizontal circulation due to alongshore bathymetric variability facilitates net onshore sediment transport, hence the rate of onshore sand bar movement (i.e. $\hat{Q}_{o_x,2D} = f(a)\hat{Q}_{x_o}$). Second, since fluid mass transport need not be balanced at each cross-shore transect for an alongshore-variable system, we suggest that γ_{eq} will also be a function of a (i.e. $\gamma_{eq,2D} = f(a)\gamma_{eq}$), with much larger waves sustainable over a 2DH sand bar morphology than over an alongshore-uniform equivalent system. These functionalities are implemented using a modified equation for the alongshore-averaged cross-shore sediment transport for 2DH conditions:

$$Q_{o_x,2D} = \alpha_1 \hat{Q}_{x_o} \left(\gamma_b - \kappa_a \gamma_{eq}\right) \kappa_a, \tag{4.25}$$

where κ_a represents the influence of 2DH processes on the alongshore-averaged cross-shore bar migration,

$$\kappa_a = 1 + \alpha_2 \frac{a}{x} \frac{b\zeta}{(\beta - \Delta_o/x_o)\gamma_b^2}, \tag{4.26}$$

where b is the fraction of breaking at the bar crest position, ζ describes the effect of

oblique waves on 2DH circulation, a is the 2DH variability in the morphology, x is the alongshore-averaged bar position, β is the beach slope, Δ_o/x_o is the ratio of the bar crest height to current position, γ_b is the non-dimensional relative breaking wave height.

The main objective of κ_a is to capture the effect of 2DH circulation and the relative influences of existing morphology versus the incident fluid forcing. Deviations of κ_a from unity represent the influence of a on cross-shore migration rates. The details of this fluid-sediment system are complex, but three phenomena should be represented. First, the effect of a is assumed to scale with a/x (i.e. the impact of alongshore variability scales with its size, expressed as a fraction of offshore bar distance) and only has an impact if waves are breaking over the morphology ($b \neq 0$) driving 2D currents. Second, under storm conditions, when wave breaking begins well beyond the sand bar location (large relative wave height, γ_b), the effect of alongshore bar variability will be severely reduced due to the presence of more alongshore uniform breaking and the resulting 1DH currents. Based on empirical tests of wave conditions associated with changes from 2DH to 1DH morphology, *Holman et al.* (2006) suggested that the influence of wave height on reducing alongshore bar variability should scale as wave height squared. We represent this in equation (4.26) by dividing the a dependence by γ_b^2, (i.e. using wave height squared, but normalized by bar crest depth). Finally, the above processes occur for near shore-normal wave incidence ($\zeta \sim 1$). However, as the wave angles become oblique and drive a mean alongshore current, v_0, it has been commonly observed that the effect of alongshore-variable forcing or morphology becomes muted (e.g. *Yu and Slinn* (2003)), so the dependence on a should be reduced.

Wilson et al. (in review) discuss this problem in detail. They partition the wave forcing into alongshore-uniform and alongshore-variable components, F_0 and F_1 respectively, and the forced longshore current into corresponding steady and variable components, v_0 and v_1. For the example case of a sinusoidally-varying forcing with wavenumber, k_y, they show that v_1 is both reduced and alongshore-shifted by the presence of v_0 as:

$$v_1 = \zeta \frac{F_1}{\rho_w C_f u_o} \sin\left[k_y y - sin^{-1}(\zeta)\right], \tag{4.27}$$

where C_f is the wave friction factor, taken to be 0.01. Both the attenuation and phase shift of v_1 depend only on the non-dimensional parameter, ζ, which in turn, depends only on the shallow water Reynolds number:

$$\zeta = \frac{1}{\sqrt{1 + Re_s^2}}, \tag{4.28}$$

where,

$$Re_s = \frac{k_y h_{bar} v_o}{C_f u_o}, \tag{4.29}$$

where $k_y = 2\pi/L_y$ is the representative length scale of alongshore variability of the bar, h_{bar} is the local water depth (taken at the bar crest), u_o is the maximum horizontal velocity of the waves evaluated at the breaker location, and v_o is the alongshore current, measured at mid-surf zone. Using the approximation $v_o = 2.7 u_o \sin\theta \cos\theta$ (*Komar and Inman*, 1970), Re_s can be simplified to:

$$Re_s = \frac{2.7}{C_f} k_y h \sin\theta \cos\theta. \tag{4.30}$$

As the wave angle increases, the effect of alongshore bathymetric variability is damped out, reducing v_1 and by continuity, u_1, the alongshore-variable component of the cross-shore current. For a typical longshore length scale of $L = 150$ m for Palm Beach, this formulation suggests wave angles greater than roughly 5 degrees at the breakpoint reduce the effects of 2DH variability by 50%.

Finally, equation (4.15) can be written as

$$\dot{x} = \alpha_1 M \left(\gamma_b - \kappa_a \gamma_{eq}\right) \kappa_a, \tag{4.31}$$

where

$$M = \frac{1}{\mu}\frac{x_o^2}{\Delta_o L_o}\frac{\hat{Q}_{x_o}}{x^2}, \tag{4.32}$$

and κ_a represents the influence of 2DH variability on the alongshore-averaged bar migration rate. α_1 and α_2 are free parameters in the model, solved for based on a best-fit analysis of the data.

4.3.2 Temporal Changes of 2DH Surf zone Variability ($\dot{a}$)

Using the above equations, forward prediction of bar position, given variability and forcing can be obtained. We can examine the influence of 2DH morphology on onshore transport rates, but in order to study the dynamic relationship between alongshore-averaged bar position and 2DH variability of the bar, equations describing the changes in 2DH variability, $\dot{a}$, are required. Similar to the development of $\dot{x}$, the magnitude of $\dot{a}$ is related to the magnitude of sediment transport, $\hat{Q}_{x_o}$, as well as the bar volume and the sediment packing factor, μ, such that large sand bars develop 2DH variability slower than small sand bars. Using this formulation (e.g. equation (4.32) also drives sediment transport, and thus $\dot{a}$, to zero in the absence of breaking. Although many mechanisms have been postulated as to why sand bars develop 2DH variability (see *Coco and Murray* (2007) and references therein for a complete discussion), equations detailing the time-evolution of variability, $\dot{a}$, are not generally available. We develop a behavior-oriented set of equations based on sediment transport and the assumption that 2DH variability is due to self-organization processes associated with 2DH currents (e.g. *Reniers et al.* (2004); *Dronen and Deigaard* (2007); *Garnier et al.* (2008)) and can be modeled as an instability such that

$$\dot{a} = \Lambda a. \tag{4.33}$$

Equation (4.33) represents exponential growth or decay of the alongshore variability, a, depending on the sign of Λ. The rate is expressed in terms of an e-folding time, given

by Λ^{-1}. The magnitude of Λ is related to the magnitude of sediment transport, $\hat{Q}_{x_o}$, through equation (4.32), such that $\Lambda = \alpha_3 MG$. α_3 is an empirical coefficient and G is the unknown parameter representing the different physical processes that affect the growth and decay of 2DH morphology of sand bars under varying wave conditions. Although there is no simple formulation for G, we choose one based on sensible behavior, based on several observations such as:

- The growth of 2DH variability is associated with intermediate forcing conditions ($2 < \Omega = H/TW < 5$) (e.g. *Wright and Short* (1984); *Lippmann and Holman* (1990)).
- The magnitude of 2DH bar variability (a) cannot exceed the surf zone width (x), such that when a bar has run into shore, the growth of 2DH variability tends to subside, suggesting an upper bound to a.
- Under low wave conditions (low Ω), rip channels can be filled in with sediment (at a rate that depends on M) and form low-tide terraces (*Wright and Short*, 1984), thus decreasing the system 2DH variability under extreme low waves.
- The timescales of growth are influenced by tidal range, Δ_{tide} (*Wright et al.* (1987); *Castelle* (2004)), mean wave period, T (*van Enckevort et al.*, 2004), and wave angle, θ (*Garnier et al.*, 2008).
- Both large waves (large γ_b) and oblique waves (small ζ) will cause a reduction in the variability toward a linear bar configuration.

We combine these concepts into a single equation for G, balancing potential growth and decay terms:

$$G = \frac{T}{T_o}\left(1 - \frac{3a}{x}\right) - \alpha_4 \frac{\Omega \gamma_b}{\zeta}, \tag{4.34}$$

where a reference value of T_o is included such that α_3 and α_4 are non-dimensional. For simplicity, we set T_o to the approximate mean value of the data used ($T_o = 10$ s). The

influence of tidal range has been included in the breaking parameterization, b, which affects the total magnitude of sediment transport. The term $(1 - 3a/x)$ represents a reduction (and potentially reversal) of growth as the landward portions of the variable bar become limited by the shoreline. 2D systems generally revert to linear bars when $H^2/\cos\theta > 2.2$ (*Holman et al.*, 2006). We use this observation as a basis for the 2DH decay term. We choose a non-dimensional form that includes the effect of relative wave height, γ_b, and non-dimensional fall velocity, Ω. As in the formulation of $\dot{x}$, we assume that the reduction of alongshore variability due to strong longshore currents can be represented in terms of ζ. Large wave angles (small ζ), as well as large waves (large Ω) breaking seaward of the bar (large γ_b) tend to return the bar back to a 1DH configuration. The final form of equation (4.33) is therefore

$$\dot{a} = \alpha_3 M \left(\frac{T}{T_o} \left(1 - \frac{3a}{x} \right) - \alpha_4 \frac{\Omega \gamma_b}{\zeta} \right) a. \tag{4.35}$$

Similar to equation (4.31), α_3 and α_4 are free parameters solved for by best-fit methods. The rate of $\dot{a}$ is determined by the magnitude of sediment transport, M, and 2DH morphology$a$. Finally, the predicted time evolution of the alongshore-averaged sand bar, $\hat{x}$, and 2DH variability, $\hat{a}$, are solved for using simple forward integration:

$$\hat{x}(t+1) = \hat{x}(t) + \dot{x}(t)dt, \tag{4.36}$$

$$\hat{a}(t+1) = \hat{a}(t) + \dot{a}(t)dt. \tag{4.37}$$

Selection of a time step in the model that is excessively large can lead to overshooting of both parameters. To prevent either $\hat{x}$ and $\hat{a}$ becoming negative due to discretization, limits for both $\dot{x}$ and $\dot{a}$ are set such that $|\dot{x}| < 0.9x$ and $|\dot{a}| < 0.9a$ when $\dot{x}$ or $\dot{a}$ are negative. As well, $\hat{x}$ and $\hat{a}$ are constrained to be greater than 1. Alternatively, higher order finite-difference methods can be implemented to avoid such issues.

4.4 Data

4.4.1 Field Site Description

The study site to test our hypotheses was Palm Beach, a 2 km-long, east facing, open ocean embayment, located approximately 30 km north of Sydney, Australia (Fig. 4.1). The beach extents are defined by the Barrenjoey headland to the north and the Little Head headland to the south. The location is micro-tidal and swell-dominated, with no significant seasonal variability in the wave conditions (*Short and Trenaman*, 1992). The dominant wave direction is from the SSE with the occasional E and NE swell and wave heights averaging 1.5 m but can reach 3-6 m during storm conditions (*Short and Trenaman*, 1992). The nearshore beach slope is 0.03 (*Wright et al.*, 1980) and the median grain size is 0.30 mm (*Wright et al.*, 1980).

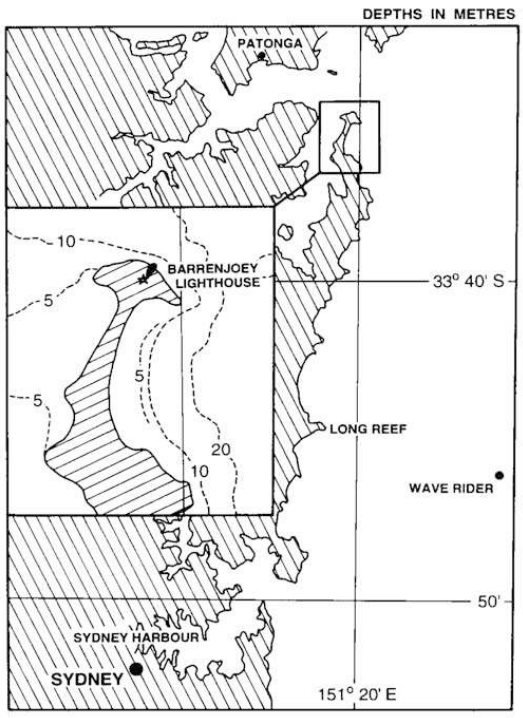

Fig. 4.1: Map of Palm Beach, Australia.

Under the *Wright and Short* (1984) classification scheme, Palm Beach is considered an intermediate beach. However, the beach morphology at Palm Beach is very dynamic,

ranging from dissipative, with a longshore uniform sand bar during major storms, through all four intermediate beach states described by *Wright and Short* (1984) during milder wave conditions. The most observed state is the transverse sand bar rip occurring about 55% of the time (*Ranasinghe et al.*, 2004). State changes occur quite rapidly, with rhythmic sand bars and rip channels developing usually within a week of a major storm. Although no preferential rip locations were found in a study by *Holman et al.* (2006), *Alexander and Holman* (2004) found a significant correlation at Palm Beach between offshore significant wave height and inverse rip spacing at short lags ($\sim$ day) indicating that morphology responds very rapidly to changing wave conditions.

4.4.2 Wave and Tide Characterization

Tide data was acquired from a tide gauge at Patonga, slightly NW of Palm Beach (Fig. 4.1). The offshore wave characteristics (significant wave height, H_s, wave angle, θ, and significant wave period, T_s) were obtained from a directional wave rider buoy located at Long Reef, 20 km south of Palm Beach, in a depth of 80 m (Fig. 4.1). Waves recorded at this buoy can undergo considerable refraction to reach the roughly east-facing beach. Hourly wave height, period, and direction were input into the 2D HISWA wave refraction model (*Holthuijsen et al.*, 1989) and propagated to the 10 m contour. Root mean square wave heights, H_{10}, were smoothed using a 25-point running mean and then decimated at daily intervals. Breaking wave heights, H_b, were defined following *Komar* (1974), setting the breaking parameter, γ, to 0.42 (*Thornton and Guza*, 1982):

$$H_b = \left(\frac{\gamma}{g}\right)^{1/5} \left[H_{10}^2 c_{g,10} cos\theta_{10}\right]^{2/5}. \tag{4.38}$$

Similarly, local wave heights at the bar location were calculated using linear wave theory and conservation of energy flux (e.g. *Dean and Dalrymple* (1991)):

$$H_{bar} = H_{10}\sqrt{\frac{c_{g,10}}{c_{g,bar}}}\sqrt{\frac{\cos\theta_{10}}{\cos\theta_{bar}}} \tag{4.39}$$

where H_{10} (H_{bar}), $c_{g,10}$ ($c_{g,bar}$), θ_{10} (θ_{bar}) are the wave height, wave group velocity and angle of incidence calculated at 10 m water depth (bar), respectively. Wave heights defined at the location of the bar in the model were set to the minimum of the local wave height (H_{bar}), the breaking wave height (H_b) or $0.5h$.

4.4.3 Fraction of Breaking (b)

The fraction of wave breaking (utilized in the roller contribution) depends on the non-dimensional wave height, $\gamma = H/h$, in a way that was parameterized using a sigmoid curve:

$$b = \frac{1}{1 + e^{\frac{-(\gamma_b - \gamma_o)}{\Gamma}}}, \tag{4.40}$$

$\gamma_b = H_b/h_{bar}$ is a mixed variable, comparing the wave height at one location, the break point, to the depth at another location, the bar crest. The values of $\gamma_o = 0.39$, $\Gamma = 0.055$ were chosen to best fit wave breaking data from Duck94 (hourly statistics for October 11-12) and NSTS (November 1978) (Fig. 4.2).

Tidal variation affects the percent of breaking, for example allowing some breaking at low tide even if no breaking would be predicted at mean tide. Since the subsequent analysis will be based on daily or semi-daily estimates of wave forcing, these variations must be parameterized. Using equation (4.40), hourly curves of breaking fraction were computed for a wave height and tide range (Δ_{tide}) values, then integrated to yield tidally-adjusted curves (e.g. Figure 4.3). Equation 4.40 was adjusted for tidal effect by defining a new Γ_t:

$$\Gamma_t = \Gamma \left[1 + \gamma_b \frac{\Delta_{tide}}{h} \right]. \tag{4.41}$$

At Palm Beach, the tide range is 1 m, and therefore not expected to significantly affect the spread of Γ (Fig. 4.3).

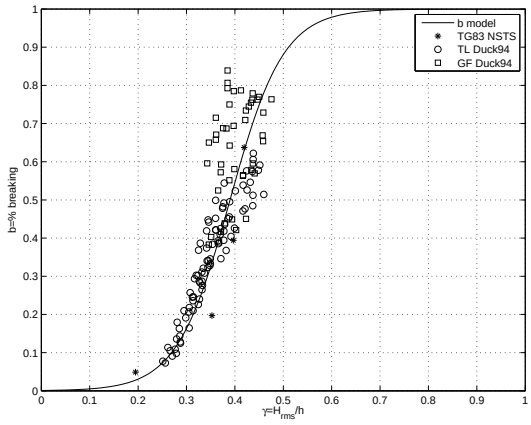

Fig. 4.2: Breaking curve b fit to 3 field data sets. NSTS data digitized from *Thornton and Guza* (1983), Fig. 11. Duck94 data provided by T. Lippmann for Oct. 11-12.

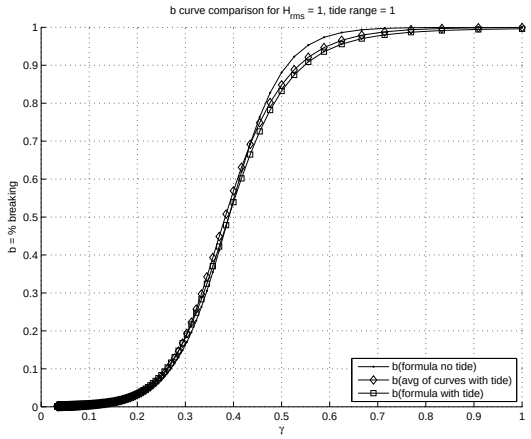

Fig. 4.3: Variation of breaking curve b for a tidal range of 1 m and varying wave heights.

4.4.4 Beach Characterization

Video Data

A two-camera Argus video-imaging station (*Holman and Sallenger*, 1993; *Aarninkhof and Holman*, 1999; *Holman et al.*, 2003) was installed in the Barranjoey lighthouse in January, 1996 (Fig. 4.1). The cameras are located 115 m above mean sea level and face south towards Palm Beach. Only the wide-angle lens camera, C1, was used as it provides a view of 90% of the study area. During camera installation, the location of the camera and several visible ground control points (GCPs) were surveyed relative to a

known benchmark. Calibration of the camera pointing parameters was computed based on the image locations of these GCPs (*Holland et al.*, 1997).

To extract sand bar locations, images were first rectified to an overhead (plan) view using standard photogrammetric transformations. The shoreline at Palm Beach is curved (Fig. 4.4b), therefore images were transformed to a straightened co-ordinate system following the method and using the values of *Alexander and Holman* (2004).

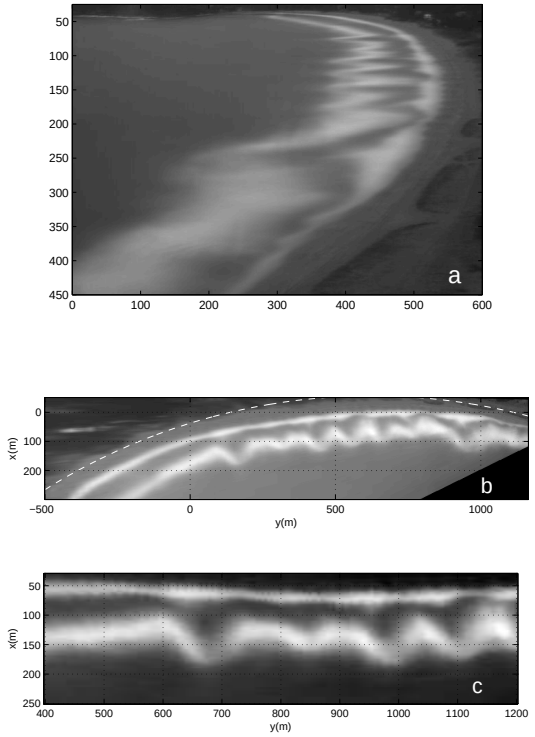

Fig. 4.4: Example rectification and straightening of images for Palm Beach.(a) Oblique time exposure image for May 18, 1996. (b) Rectified time exposure image showing the curve fit (dashed line) used to straighten out the beach. (c) Time exposure image remapped onto straightened beach coordinates.

Shoreline Position

The intertidal zone (the part of the beach that is submerged only part of the time) has the largest range of intensity in the images between high and low tide and can be easily identified due to wave breaking near the shoreline at high tide (a bright intensity

signal) and wetted sand at low tide (a darker intensity signal). The shoreline, $x_s(y)$, was determined as the shoreward most point of the intensity difference ($I_{high} - I_{low}$) peak above an empirically defined threshold (*Alexander and Holman*, 2004). Shoreline estimates were then filtered using a 25-pt Hanning window to remove any short scale features or anomalous data. The estimated shoreline for May 18, 1996 is shown in Fig. 4.5 and agrees well with the imaged shoreline, depicted as the shoreward edge of the shoreline breaker.

Sand bar Position

Daily sand bar positions, $x_b(y)$, were obtained optically from daytimex images (images showing the average of all ten-minute time-exposure images from any particular day) based on preferred wave breaking patterns that correspond to topographical highs, such as sand bars (*Lippmann and Holman*, 1989; *van Enckevort and Ruessink*, 2001; *Alexander and Holman*, 2004). Bar positions were estimated at 5 m intervals in the alongshore direction using a Bar Line Intensity Maximum (BLIM) tool that searches for the local intensity maximum in a cross-shore intensity profile within a user defined region of interest. Mean sand bar position, x, was defined as the alongshore-averaged distance between the measured sand bar position, $x_b(y)$, and the shoreline, $x_s(y)$:

$$x = \frac{1}{N_y} \sum_{y_i=1}^{N_y} (x_b(y_i) - x_s(y_i)). \tag{4.42}$$

Surf zone Variability

Daytimex images are used to identify intensity patterns associated with breaking over the sand bar. However, the contrast between breaking and non-breaking waves varies as a function of distance away from the camera due to variations in grazing angle and ambient light. To account for these lighting artifacts in the image and to enhance the contrast between breaking and non-breaking, each daytimex image was adjusted as follows. The intensity trend due to grazing angle was obtained by taking the intensity values at the

most offshore location of the image ($I_{trend}(y)$), where no breaking was assumed to be occurring.

The intensity image was remapped based on the variation in the image between the offshore trend and the maximum intensity possible ($I = 1$):

$$I_{new}(x, y) = \frac{I(x, y) - I_{trend}(y)}{1 - I_{trend}(y)}. \tag{4.43}$$

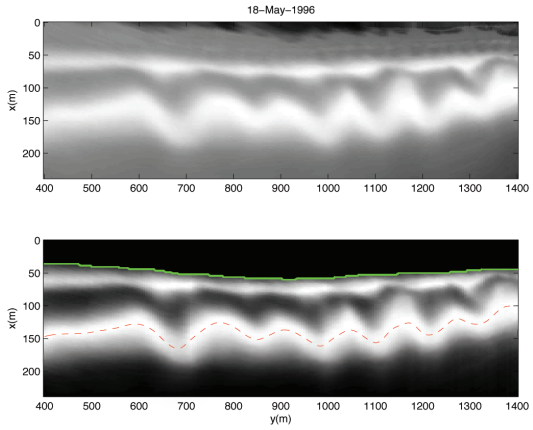

Fig. 4.5: Example of de-trending image to highlight bar position.(*top*) Day time exposure image for May 18, 1996. (*bottom*) De-trended intensity image, May 18, 1996 with shoreline (solid) and sand bar (dash).

The surf zone variability index, a, is a proxy for 2DH currents, which in turn are a function of the bathymetry and the incoming wave field. *Plant et al.* (2006) proposed a method to estimate a based on the band-passed root mean variance of the alongshore bar position. The method works well when sand bars are offshore and not overly 2DH, such that the identified cross-shore location of the sand bar, $x_b(y)$, also represents the center of breaking. As the sand bar becomes more 2DH, the cross-shore extent of breaking can also vary in a way that bears on expected 2DH circulation but may not be represented by a.

Ranasinghe et al. (2004) uses the Variance of the band-pass Filtered Longshore cross-shore integrated Intensity Profile ($V - FLIP$) as a proxy for alongshore variable breaking patterns and morphology. $V - FLIP$ measurements have slightly linear increases in

magnitude as sand bars move onshore and then decrease again under low-tide terrace regimes. Having both end member states (low-tide terraces and longshore-bar-trough) with similar variance values leads to a non-unique description of the beach state. This method also assumes that cross-shore integrated intensities will vary in the alongshore for 2DH sand bars, which is not the case for alongshore uniform width of breaking over a slightly 2DH sand bar. Thus, a hybrid approach of the two methods is used.

Bar positions ($x_b(y)$) were identified as described in section 4.4.4 (Fig. 4.5, 4.6). Landward ($b_m(y)$) and seaward ($b_p(y)$) limits to the region of active breaking were defined by first exceedances of intensity above a threshold of 0.8 times the maximum intensity at $x_b(y)$, subsequently smoothed with a 50 m Hanning filter to remove small-scale variations (Fig. 4.6 top). Similar to *Ranasinghe et al.* (2004), Longshore Intensity Profile ($LIP(y)$, Fig. 4.6 bottom) was found by cross-shore integration of intensities between these limits:

$$LIP(y) = \sum_{b_m(y)}^{b_p(y)} I_{break}(x,y)\partial x. \tag{4.44}$$

Finally, a composite Longshore Bar Breaking Profile ($LBBP$, Fig. 4.6 bottom) combining bar crest position and width of breaking information was then defined as:

$$LBBP(y) = x - x_b(y) + LIP(y). \tag{4.45}$$

The surf zone variability index (a) was calculated once per day using the spectral method described in *Plant et al.* (2006). The input signal ($LBBP$) was first de-meaned and de-trended and Fourier transformed. a was defined as the root mean variance in the band 30 m $< L <$400 m.

4.5 Results

A subset of the four years of data presented in *Alexander and Holman* (2004) and *Holman et al.* (2006) was used to test the model. Seven data sets were chosen based on reset events described in *Holman et al.* (2006) and varied in length from 1 - 6 months, totaling

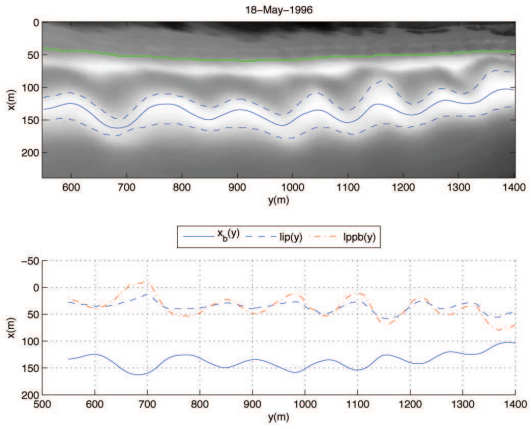

Fig. 4.6: Example of isolating bar position and active breaking.(*top*) Daytimex image for May 18, 1996, with sand bar position ($x_b(y)$) (solid) and $I_{break}(y)$ bounds ($b_m(y)$,$b_p(y)$) (dash) (*bottom*) Bar position ($x_b(y)$)(solid), Longshore Intensity Profile (LIP)(dash), and Longshore sand Bar Breaking Profile ($LBBP$) (dash-dot).

562 days. All data sets included at least 1 major storm and in most cases, also contained several minor storms in which full resets did not occur. General statistics are summarized in Table 4.1.

Table 4.1: Data set statistics used in analysis, including major storm resets as defined by *Holman et al.* (2006).

Date	days	resets	$\overline{H}(\sigma_H)$	$\overline{T}(\sigma_T)$	$\overline{\cos\theta}(\sigma_{\cos\theta})$
April 1996	20	1	1.13 (0.61)	9.67 (1.31)	0.94 (0.04)
July 1996	162	4	0.84 (0.46)	8.72 (1.38)	0.94 (0.06)
May 1997	72	1	1.18 (0.65)	9.66 (1.34)	0.96 (0.05)
October 1997	83	1	0.77 (0.40)	8.40 (1.44)	0.93 (0.07)
March 1998	38	1	0.96 (0.52)	9.88 (1.64)	0.94 (0.05)
May 1998	95	2	0.98 (0.63)	9.74 (1.36)	0.94 (0.08)
April 1999	89	1	1.27 (0.59)	10.34 (1.60)	0.96 (0.05)

4.5.1 Initial Testing

Prior to coupling equation (4.31) and equation (4.33) to form the dynamic model, each equation was individually tested in forward prediction mode. There are 5 free parameters (α_1-α_4 and γ_{eq}) for which appropriate values must be chosen. The criteria for selecting γ_{eq}

was based on matching overall rates and magnitudes of offshore migration when $\kappa_a = 1$, such that only 1DH processes were considered. Values greater than ~ 0.42 indicate waves breaking offshore of the bar. A value of 0.65 corresponds to $\sim 100\%$ breaking according to Fig. 4.2, or that for offshore bar migration to occur, all waves must be breaking seaward of the current bar location.

α_1 and α_3 represent overall magnitude terms, while α_2 indicates the influence of a on $\dot{x}$, and α_4 balances relative growth and decay of a. In selecting α_1 and α_2 we used equation (4.31) with measured a, H, T, and θ and for α_3 and α_4, we used equation (4.33) with measured x, H, T, and θ. A least-squares solution using the entire data set to solve for the α coefficients was initially attempted. Values estimated by the least-squares method did not represent the observed magnitude of short-scale variability when tested on individual data sets. The α coefficients ($[\alpha_1\ \alpha_2\ \alpha_3\ \alpha_4] = [352\ 0.0165\ 50\ 0.035]$) damped out all the higher frequency variability, but were able to capture the low-frequency trends. This is easily seen by comparing the frequency cross-spectra of the observed values of mean bar position versus that modeled using the least-squares solution. Comparing data sets this way allows us to objectively identify model skill over a wide range of frequencies. Figure 4.7 shows the least-squares solution captured the low-frequency energy of the system but under-estimated the energy in the higher frequency range for x (Fig. 4.7). Predicted and measured values of x were also coherent for signals longer than roughly 15 days. Comparisons of a and predicted a showed that the energy in the low-frequency band was again being captured by the least-squares fit. High frequency data was not well modeled using these coefficients. As well, coherence between the two data sets dropped off quickly (Fig. 4.8), suggesting a is not well modeled using these coefficients.

Alternatively, α coefficients were subjectively determined from a visual best-fit to data ($[\alpha_1\ \alpha_2\ \alpha_3\ \alpha_4] = [1100\ 0.017\ 85\ 0.035]$). Comparing the spectra of the true values of mean bar position versus that modeled using the subjectively-defined values showed that these matched both the low and higher-frequency components of x (Fig. 4.9) and a (Fig. 4.10). The coherence shows good agreement for signals longer than roughly 6 days

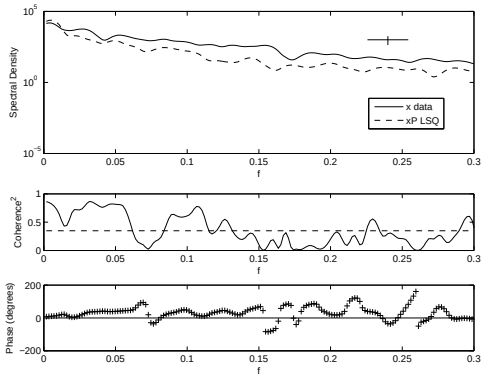

Fig. 4.7: Comparison of spectra between measured x values and predictions based on least-squared fit for α values. $[\alpha_1\ \alpha_2] = [352\ 0.0165]$. Frequency units are cycles/day.

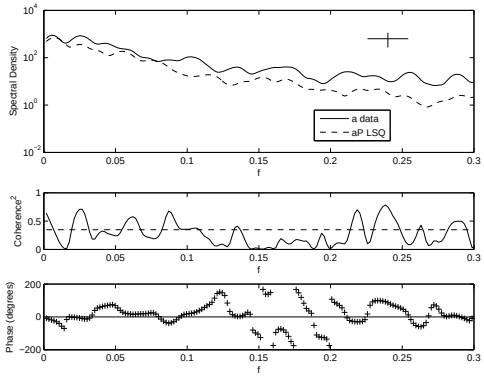

Fig. 4.8: Comparison of spectra between measured a values and predictions based on least-squared fit for α values. $[\alpha_3\ \alpha_4] = [50\ 0.035]$.

in x. Comparisons of a were again less telling with coherence similar to the least-squares solution, again suggesting a may not be well-modeled using these coefficients. We use the subjectively-defined coefficients in testing individual data sets because they provide a better representation of the data variability at all scales.

Model skill, $S = R^2$, based on the correlations between measured (e.g. x) and predicted (e.g. $\hat{x}$) values for each run were compared against a critical skill, S_{crit}, at the 95% level (Table 4.2). S_{crit} was determined from the average value based on long-lag correlations and the pdf method. For $\dot{x}$ (4.31), all data sets showed significant skill in predicting the time evolution of $\hat{x}$ (e.g. Figs. 4.11, 4.13). Results for $\dot{a}$ (4.33) were similar, but with only 3 of the 7 data sets showing significant skill at predicting $\hat{a}$ (e.g.

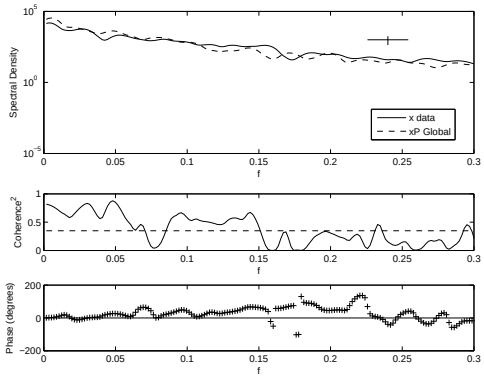

Fig. 4.9: Comparison of spectra between measured x values and predictions based on subjectively-determined α values. $[\alpha_1\ \alpha_2] = [1100\ 0.017]$.

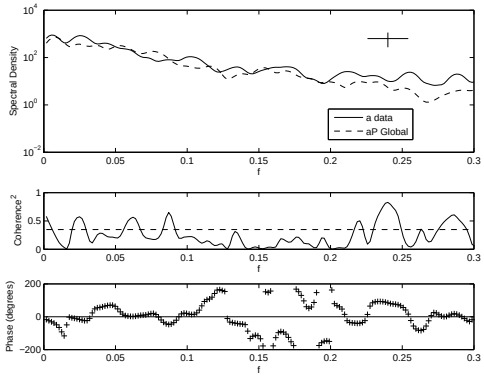

Fig. 4.10: Comparison of spectra between measured a values and predictions based on subjectively-determined α values. $[\alpha_3\ \alpha_4] = [85\ 0.035]$.

Fig. 4.12).

Table 4.2: Data set skill values for individual equations using subjectively-determined α values.

Date	$R^2_{x\hat{x}}$	S_{crit}	$R^2_{a\hat{a}}$
April 1996	0.92	0.41	0.66
July 1996	0.42	0.07	0.02
May 1997	0.31	0.14	0.11
October 1997	0.28	0.12	0.33
March 1998	0.61	0.24	0.65
May 1998	0.41	0.11	0.04
April 1999	0.27	0.11	0.03

The July - December 1996 data set was the longest run tested. The model did

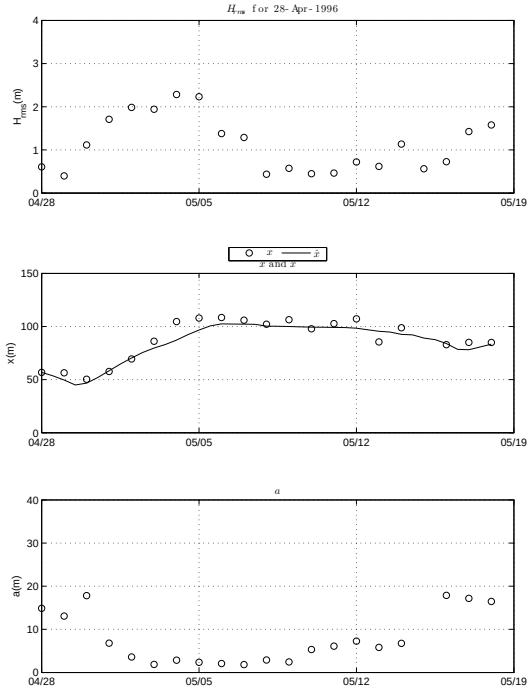

Fig. 4.11: Results for forward testing of $\dot{x}$ for April - May 1996 storm. The model skill was significant at the 95% level with $R^2 = 0.92$. Raw data (circle) and predicted values (line).

surprisingly well (Fig. 4.13), capturing short term variability as well as the longer term trends in bar position given correct input data of wave conditions and 2DH variability. To our knowledge, this is the longest continuous modeling of cross-shore bar migration to include short-term variability from multiple storm-sequences and subsequent recovery. The predicted evolution of a was less accurate (Fig. 4.14).

Table 4.3: Data set skill values for dynamically coupled model using subjectively-determined α values.

Date	$R^2_{x\hat{x}}$	S_{crit}	$R^2_{a\hat{a}}$
April 1996	0.90	0.41	0.76
July 1996	0.18	0.07	0.05
May 1997	0.61	0.14	0.05
October 1997	0.35	0.12	0.14
March 1998	0.59	0.24	0.52
May 1998	0.40	0.11	0.04
April 1999	0.22	0.11	0.03

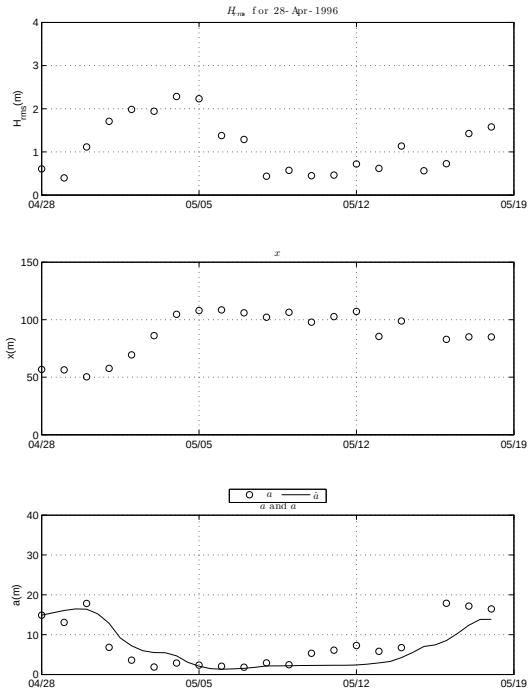

Fig. 4.12: Results for forward testing of $\dot{a}$ for April - May 1996 storm. The model skill was significant at the 95% level with $R^2 = 0.66$.

Based on the results for the individual equations, the model equations were coupled and dynamic forward predictions ($\hat{x}$, $\hat{a}$) were computed. $\hat{x}$ was predicted with significant (95% level) (e.g. Fig. 4.15) in all cases, while $\hat{a}$ was significant for 3 of the 7 cases (Table 4.3). The subjectively-determined parameters did surprisingly well on the more complex data sets (those spanning multiple minor storms and in some cases, multiple major storms), suggesting that a single set of parameters can be used to model complex systems. For example, the March 1998 data set (Fig. 4.16), had $R^2_{x\hat{x}} = 0.59$ and $R^2_{a\hat{a}} = 0.52$. In this data set, the morphology started out as a terrace system, became linear as the bar moved offshore, and then rapidly grew 2DH features and moved back onshore, reforming terraces.

4.5.2 Regression Analysis on Individual Data Sets

Although the subjectively-determined α coefficients chosen in the initial testing provided reasonable results, we would like to know if predictions could be improved by using a

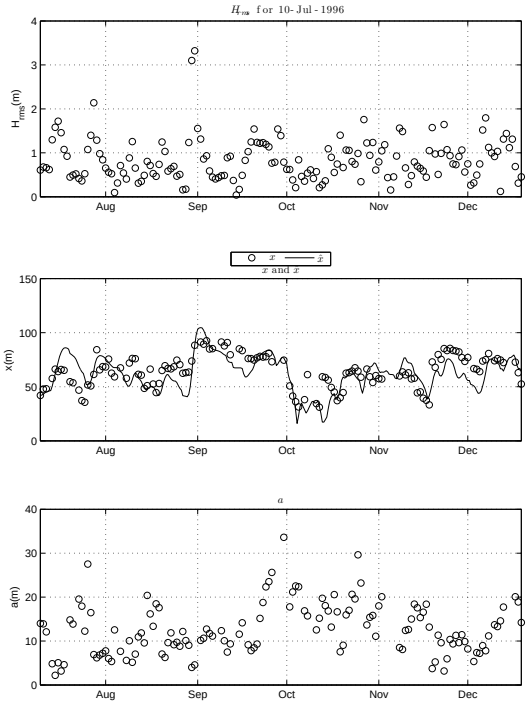

Fig. 4.13: Results for forward testing of $\dot{x}$ for July - December 1996 data set. The model skill was significant at the 95% level with $R^2 = 0.42$. Raw data (circle) and predicted values (line).

nonlinear least-squares fit to the data to solve for the unknown coefficients for each data set. In this way, we may also gain insight into the variability and importance of these terms under different scenarios. Initial guesses for the α coefficients were set to the subjectively-determined values mentioned above. Upper and lower bounds were also set, constraining the solution to within a reasonable range of physically accepted values (for instance, $\alpha > 0$). The nonlinear least-squares fit was based on comparisons of values (e.g. x versus $\hat{x}$) rather than gradients (e.g. $\dot{x}$ versus $\hat{\dot{x}}$). This method was preferred since gradients can be very noisy, while the overall temporal evolution may be much smoother. Table 4.4 summarizes the regression results.

Using the nonlinear least-squares fit α values, 5 out of the 7 predictions had a better combined mean ($(S_x+S_a)/2$) skill. In some instances, this increase in skill was substantial (e.g. Fig. 4.17 versus Fig. 4.18), however, a number of the estimated α coefficients, namely α_1 and α_3 were equal to the lower or upper bound values, suggesting the solution

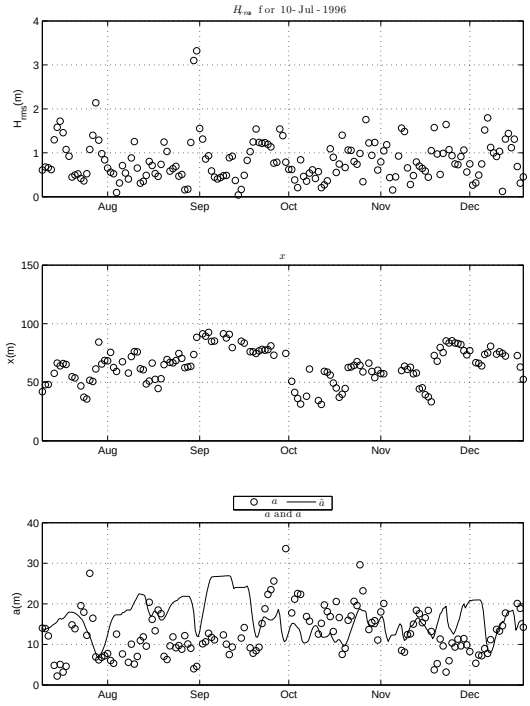

Fig. 4.14: Results for forward testing of $\dot{a}$ for July - December 1996 data set. The model skill was not significant at the 95% level with $R^2 = 0.02$. Raw data (circle) and predicted values (line).

Table 4.4: Regression coefficients based on nonlinear least squares regression fit to full data set. 95% confidence intervals are also given. For the mean values ($\pm$ 2σ). Initial estimates = $[\alpha_1\ \alpha_2\ \alpha_3\ \alpha_4]$ = [1100 0.017 85 0.035]. Lower bounds = [800 0 50 0]. Upper bounds = [2000 1 150 1].

Date	α_1	α_2	α_3	α_4
April 1996	1050 $\pm$ 116	0.03 $\pm$ 0.003	98 $\pm$ 86	0.04 $\pm$ 0.008
July 1996	800 $\pm$ 118	0.02 $\pm$ 0.007	50 $\pm$ 87	0.05 $\pm$ 0.013
May 1997	800 $\pm$ 66	0.02 $\pm$ 0.002	77 $\pm$ 25	0.04 $\pm$ 0.006
October 1997	800 $\pm$ 114	0.03 $\pm$ 0.001	150 $\pm$ 71	0.04 $\pm$ 0.007
March 1998	800 $\pm$ 76	0.05 $\pm$ 0.002	150 $\pm$ 25	0.04 $\pm$ 0.007
May 1998	800 $\pm$ 83	0.02 $\pm$ 0.007	50 $\pm$ 36	0.04 $\pm$ 0.002
April 1999	800 $\pm$ 83	0.01 $\pm$ 0.001	150 $\pm$ 29	0.06 $\pm$ 0.008
Mean	835 $\pm$ 188	0.03 $\pm$ 0.02	104 $\pm$ 92	0.04 $\pm$ 0.02

may have been artificially constrained. Using unbounded solutions produced lower skill values as the nonlinear regression technique tended to emphasize the low-frequency trends and not capture the high-frequency variability.

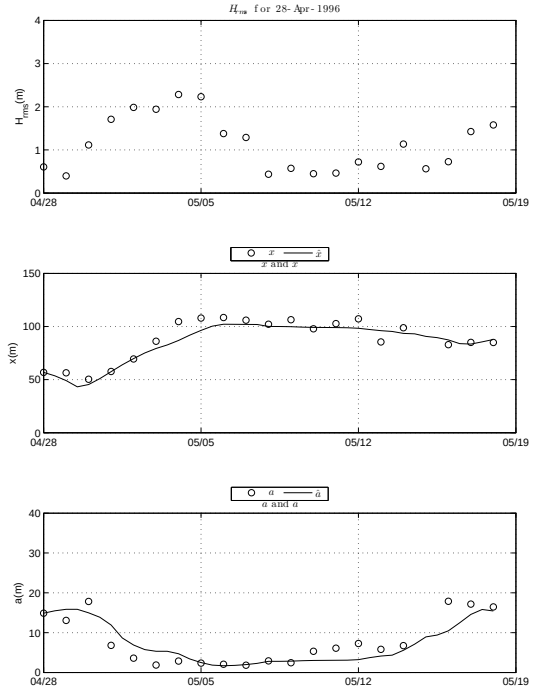

Fig. 4.15: Results for forward testing of the coupled dynamic model for April - May 1996 storm. The model skill was significant at the 95% level with $R^2_{x\hat{x}} = 0.90$ and $R^2_{a\hat{a}} = 0.76$.

Table 4.5: Data set skill values using nonlinear least-squares α values for each data set.

Date	$R^2_{x\hat{x}}$	S_{crit}	$R^2_{a\hat{a}}$
April 1996	0.91	0.41	0.86
July 1996	0.23	0.07	0.06
May 1997	0.79	0.14	0.36
October 1997	0.31	0.12	0.09
March 1998	0.53	0.24	0.52
May 1998	0.47	0.11	0.23
April 1999	0.33	0.11	0.09

4.5.3 Model Stability

Although the model was formulated based on an equilibrium approach to sand bar migration and 2DH morphology, it is convenient to know if the model coefficients are indeed stable. To test this, the model was run in prediction mode with each set of the regression coefficients using constant wave forcing conditions and starting at the initial (t=1) values

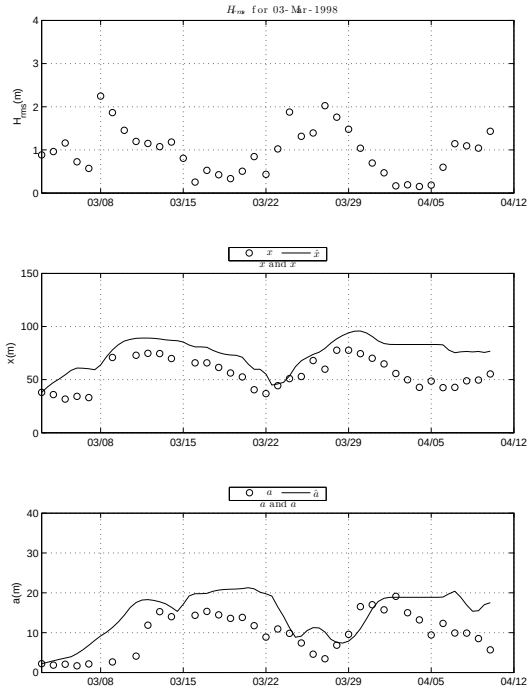

Fig. 4.16: Results for forward testing of the coupled dynamic model for March - April 1998 data set. The model skill was significant at the 95% level with $R^2_{x\hat{x}} = 0.59$ and $R^2_{a\hat{a}} = 0.52$.

for x and a. In all cases, the model converged on a solution pair (x_o and a_o), unique to the set of α coefficients. This analysis was repeated using the subjectively-determined α values to determine if initial positions influenced the final equilibrium position. All data sets converged on the same equilibrium solution, indicating that initial position had no influence on the dynamic equilibrium and the systems were indeed predictable.

4.6 Discussion

Ideally we would like to be able to model the nearshore system using fully 3D models that are capable of capturing all the necessary physics for driving nearshore flows and sediment transport. However, our understanding of the physics that govern sediment transport is still lacking, as many models are unable to predict accurate rates of onshore and offshore sediment transport. These more complex models are also sensitive to initial and boundary conditions, requiring accurate knowledge of bathymetry and waves in

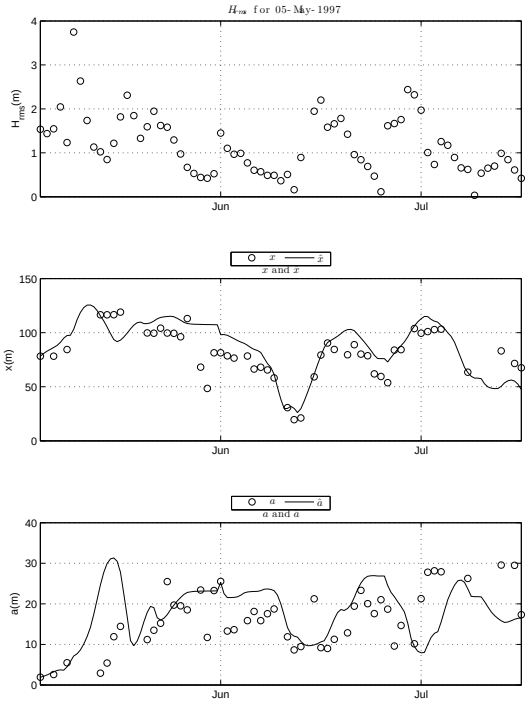

Fig. 4.17: Results for forward testing of the coupled dynamic model for May - July 1997 data set using subjectively-determined alpha coefficients. The model skill was significant at the 95% level with $R^2_{x\hat{x}} = 0.61$ and $R^2_{a\hat{a}} = 0.05$.

order to accurately predict morphology change. Small errors in either input can cause solutions to diverge from the true solution. The use of fully 3D models is also computationally expensive, although becoming more feasible as computer power becomes more readily available. Alternatively, parametric models can be designed in such a way to gain understanding of certain relationships between forcing and sediment transport. These models are simple and efficient, requiring knowledge of bulk terms, such as bar position or offshore wave height, rather than bathymetry and wave height variation over the domain. These models also trade the more complex physics-based equations for more observation-based parameterizations. Here we attempt to merge parametric and physics-based approaches. Sediment transport is modeled using energetics-based equations (BBB-type). Equations are then transformed to a parametric form based on the relationship between bar migration of a constant form and the resulting sediment transport pattern. The model is then extended to include the effects of 2DH currents on

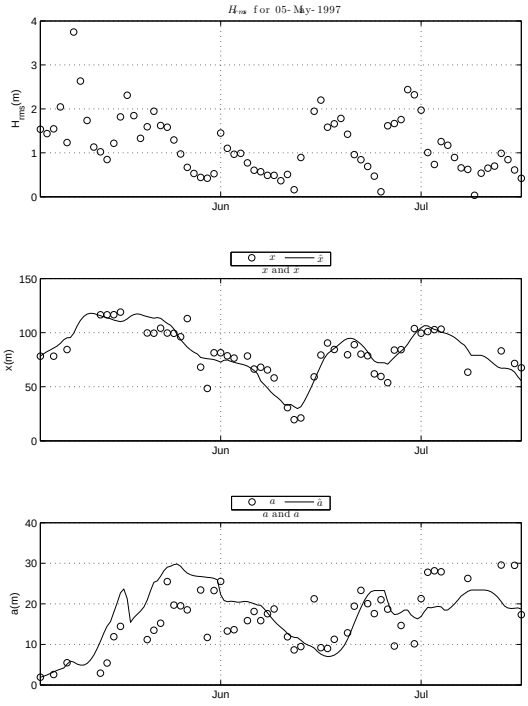

Fig. 4.18: Results for forward testing of the coupled dynamic model for May - July 1997 data set with α coefficients solved for using nonlinear least squares fit to the data. The model skill was significant at the 95% level with $R^2_{x\hat{x}} = 0.79$ and $R^2_{a\hat{a}} = 0.36$.

alongshore-averaged sand bar migration.

4.6.1 The Effect of 2DH Variability on $\dot{x}$

One of the driving forces behind this research was the common assumption that 2DH processes have a negligible influence on cross-shore sand bar migration rates. *Plant et al.* (2006) first questioned this assumption, introducing a parametric model dynamically linking the alongshore-averaged sand bar position and 2DH variability (sinuosity). The modeled parameters (bar position and sinuosity) were shown to be dynamically coupled and that the sinuosity term had a positive influence on onshore migration rates. Using this formulation, they were able to accurately predict onshore and offshore sand bar migration over a two month period at Duck, North Carolina.

The model presented here is an extension of this theory. Using a non-linear model,

we test whether cross-shore sand bar migration rates are influenced by 2DH currents through a proxy modeled as the presence of 2DH sand bar variability. We find that both onshore migration rates increase under 2DH conditions with respect to a 1DH version of the model and that 2DH systems can sustain higher wave conditions without resetting due to the fact that return flow does not need to return as undertow, but rather as 2DH currents. By including a proxy for 2DH currents through the 2DH variability influence factor, κ_a, we isolated the importance of including such a term in future models.

Values of κ_a ranged from 1(at full breaking) to 2.5 (Fig. 4.19). Plotting κ_a against γ_b shows the maximum influence of κ_a exists under mid-range γ_b ($0.4 < \gamma_b < 0.75$) with negligible influence at low and high values of γ_b (i.e. $\kappa_a = 1$). Similar relationships are seen for κ_a versus Ω. As γ_b approaches 0, bar migration/sediment transport ceases. As γ_b increases, the magnitude of onshore transport also increases, up to a maximum around $\gamma_b \approx 0.6$. There is a sharp decline in onshore migration with a reversal in direction and increasing magnitude of offshore migration as γ_b exceeds roughly 0.8.

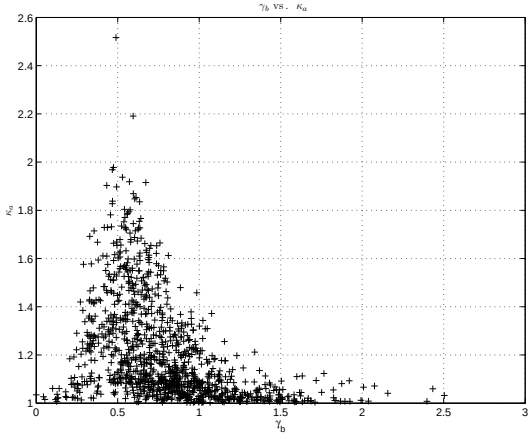

Fig. 4.19: Comparison of κ_a versus γ_b.

The influence of κ_a not only provides the increased rates of onshore transport, but also a shift in the effective γ_{eq} for onshore/offshore transport. This is easily seen comparing the sign of $\dot{x}$ versus γ_b values. There is a distinct shift between onshore and offshore migrations around $\gamma_b \approx 0.75$ (Fig. 4.20). Recalling that $\gamma_{eq} = 0.65$, onshore migrations are occurring up to values of $\gamma_b \approx 1$, suggesting a strong influence of 2DH variability in

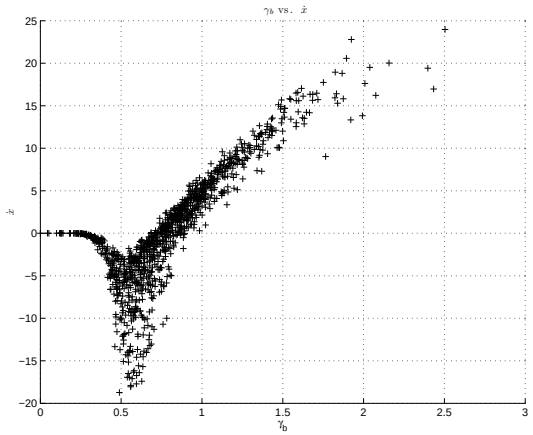

Fig. 4.20: Comparison of modeled $\dot{x}$ versus γ_b.

maintaining onshore migrations during higher wave conditions that could not be predicted using a simple 1DH approach. The result is hysteresis in the bar system response to varying wave forcing.

4.6.2 Relation to Ω

The influence of κ_a is most dominant at low-medium energy conditions ($1 < \Omega < 3$) (Fig. 4.21). There are distinct changes between onshore and offshore migrations as a function of Ω. Transitions between onshore and offshore migrations, however, happen at lower values of Ω than expected. Onshore migrations can be linked to lower energy conditions ($\Omega < 6$) and therefore longer response times, while offshore migrations occur during both intermediate ($2 < \Omega < 6$) and dissipative conditions ($\Omega > 6$), linked to much shorter response times.

4.6.3 1DH Model Comparison

The model was run in 1DH mode (setting $a = 0$, thus $\kappa_a = 1$) using the same coefficient values for $\alpha_1 - \alpha_4$ and γ_{eq}. The results were compared against the results of the 2DH model. The model skill for the 1D model was significantly lower for most data sets. When compared against incident wave angle, the largest decreases in skill coincided with low wave angles ($|\theta| < 20$), when 2DH currents are expected to influence onshore migration

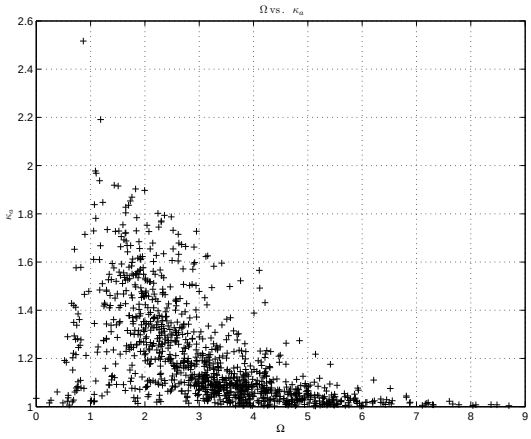

Fig. 4.21: Comparison of κ_a versus Ω.

rates (Fig. 4.22). According to *Wilson et al.* (in review), wave angles greater than 20° are equivalent to roughly a 75% decrease ($\zeta = 0.25$) in 2DH currents, such that 1DH dynamics dominate and we expect similar skill from both 1DH and 2DH models.

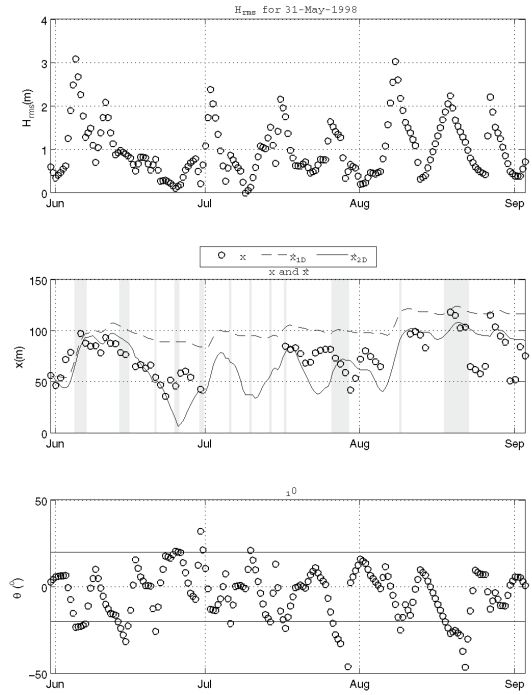

Fig. 4.22: Comparison of 1D model (dash) and 2D model (solid) for predominantly low wave angle case. Shaded areas represent times when offshore wave angles were greater than 20 degrees and 1DH processes should dominate.

4.6.4 Range of α Coefficients

One of the issues with using a nonlinear least squares regression approach is that there are multiple local minimum solutions. Also, due to the dynamic nature of the model, we simultaneously solve for a best fit to both equation (4.36) and equation (4.37), therefore a better fit in one data set may yield a worse fit for the other. As well, using the least-squares fit to solve for α coefficients is sensitive to local errors in $\dot{x}$ and $\dot{a}$, such that in some instances, the model might have predicted a larger offshore migration than measured but then mapped the rest of the variability well (appearing as an offset between modeled and measured x) (e.g. Fig. 4.16). In these instances, the least-squares solution chose smaller α_1 and α_3 values and subsequently damped out the short scale variability. Sensible initial estimates and bounds were chosen to converge on meaningful solutions. An alternative method for determining α coefficients may provide increased model skill, however, the subjectively-determined values chosen seem to model a wide variety of conditions successfully such that we are satisfied with the choices.

4.6.5 Bathymetry Representation

The full problem describing sediment transport in the nearshore region requires knowledge of $h(x', y', t)$, i.e. depth and its evolution everywhere. Our analysis includes a number of assumptions and potential sources of error including the reduction of bathymetry data to two variables, x and a, and the estimation of those variables from images. Without extensive surveys of the beach, which is prohibitive for large areas over long timescales, proxies for the beach morphology are required. The use of Argus video data is critical to this problem as it allows us to map out large spatial and temporal extents of the morphology that could not be attained in any other reasonable way.

The estimation of alongshore-averaged bar position from Argus images is based on the link between the peak in breaker intensity in an image and the sand bar location (e.g. *Lippmann and Holman* (1989); *Aarninkhof* (1996); *Aarninkhof and Holman* (1999); *van Enckevort and Ruessink* (2001, 2003a,b)). This method works best under typical non-

storm wave conditions, where waves are expected to break over the sand bar. Under storm conditions the entire surf zone is often saturated, making bar identification challenging. Likewise, under extreme calms, when no waves are breaking, bars cannot be located. Fortunately, bar movement is minimal in calm periods, so bar position can be interpolated from previous and subsequent days. In several instances, errors could be attributed to only partial exposure of a complex or double bar system due to limited wave breaking (e.g. the 3 day period in mid June 1997 (see Fig. 4.17). The sharp onshore migration at low wave heights is due to limited breaking over the bar. As wave heights increase slightly, the breaking over the bar is observed to move back offshore.). A subsequent increase in wave height could reveal the full offshore extent of the bar, thus could appear to cause an artificial offshore migration.

The proxy for 2DH currents, measured through a, may be more difficult to capture as the relationship between breaking patterns and the induced 2DH circulation is not well understood. For this reason, the parametric constraints on modeling a are also less rigorous. For instance, terrace morphologies, often incised with rip channels, were difficult to represent. Narrow channels in an otherwise alongshore uniform system could have small values of a, but not necessarily negligible 2DH circulation (which is what a is attempting to represent). Under some 2DH conditions, the breaking pattern had longshore gaps that were spatially interpolated over to provide an estimate of $x_b(y)$. Because wave height and breaking patterns can induce a fair amount of noise into the measurement of x and a, modeling the time evolution of x and a rather than $\dot{x}$ and $\dot{a}$ provides a more stable solution.

4.6.6 Wave Data

The closest available wave data was 20 km away in 80 m depth. Due to the orientation of the beach with respect to the dominant wave direction and the location of the beach in relation to the wave buoy, we required a model to transform to local conditions. The HISWA model was used to transform wave heights to the 10 m contour. The parameters

used to shoal and refract the waves were tuned to best-fit inshore measured root mean square wave height during RDEX, October 1999 (see *Reniers et al.* (2001) for data comparisons). However, on several occasions there were obvious discrepancies between the amount of breaking in images and that expected for the model wave heights (e.g. Fig. 4.23). Buoy wave data were represented by only three parameters, H_s, a representation of the total variance, T_p, and $\cos\theta_p$, the period and direction of the highest spectral peak. If wave energy is instead directionally spread (for example in a bimodal spectrum) a large portion of the expected energy may never reach the beach, so forcing will be in error.

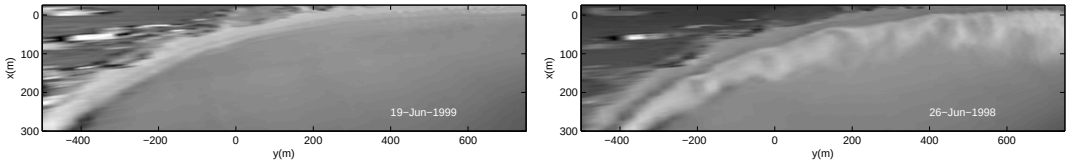

Fig. 4.23: Example images of mismatch between measured and observed wave heights. June 19, 1999: Measured wave heights were ≈ 0.55 m, while no breaking appears in the image, suggesting much smaller wave heights were present. June 26, 1998: Measured wave heights were ≈ 0.25 m, while lots of breaking existed in the image.

4.6.7 Model Limitations

Introduction of a physics-based link between parametric bar behavior (bar migration rate) and the sediment transport that caused migration is an important part of this model. The link is based on the assumption that the bar shape has a quasi-constant form. This is a good parameterization for offshore features, but is violated in highly 2DH systems, where large terraces or shoals close to shore adjacent to cuts (rips channels) dominate the morphology. We assume that this will induce detail errors, but not seriously affect the bulk physical processes being modeled.

Including a cross-shore dependency on the height and width of the bar agrees well with observations at this location. Under the cross-shore extents that we examine in the present model it is observed that as bars migrate offshore, they gain volume and

therefore have reduced migration rates. Similarly, as they approach the shoreline, they continue to reduce in size, increasing their migration rates (for a constant wave height) but only up to a certain point. However, as bars run into the shoreline, they maintain a significant volume (in the form of shoals) that will require significant transport to move. Thus, under terrace conditions, the model over-predicts onshore migration rates (e.g. mid-November 1997, Fig. 4.24).

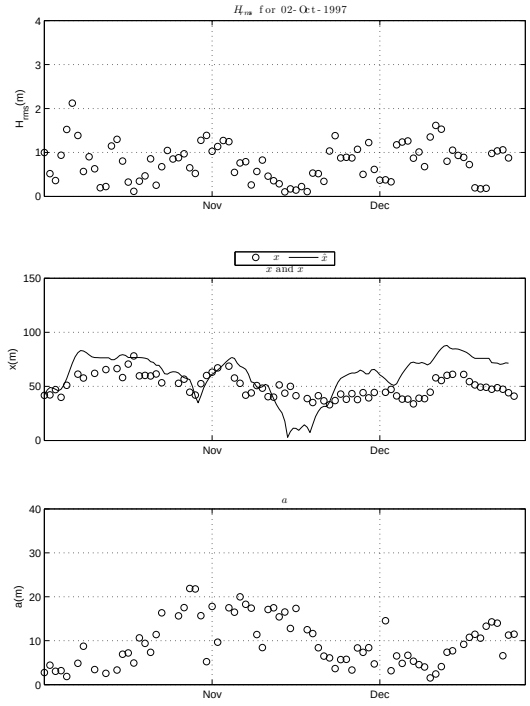

Fig. 4.24: Results for forward testing of the$\hat{x}$ model for October 1997 data set, highlighting over-prediction of onshore migration for terrace systems. Notice in mid-November through mid-December bar position remains fairly static (terrace system), while the model predictions show a continued onshore migration and then recovery.

Cross-shore sediment transport, Q_x, was formulated using energetics-type equations (BBB), simplified to focus on contributions due to the roller term, neglecting bedload, return flow due to Stokes drift, downslope, and skewness terms on the assumption that their net effect is insignificant compared to breaker driven processes. The original formulation looked at changes around this defined equilibrium in terms of variations in the

fraction of breaking (b). However, for most conditions values of b at the bar crests were close to 1.0, so that b had a very limited dynamic range. For example, large storms were indistinguishable from average wave conditions. Alternatively, γ_b had a much larger dynamic range and is a better representation of changing wave heights and storms influence on the direction and rate of cross-shore transport.

The extension of the BBB-based 1D sediment transport equation to 2D cannot be similarly derived from simple heuristic arguments. Instead, assumptions of the form of a as well as its influence on cross-shore transport processes were required. The parameterizations used in the model are sensible extensions, based on observations of onshore bar migration under 2DH morphology. However, there is no direct proof that the equations presented here offer a unique solution to the problem. Despite these simplifications, the equations showed strong skill at modeling a wide variety of conditions and allow us to focus our thinking on the influence of 2DH morphology on cross-shore sand bar migration.

4.7 Conclusions

A new, nonlinear behavioral model has been developed to study sand bar response to changing wave forcing. The bar system is represented by two parameters: the alongshore mean bar position (x) and 2DH bar variability about that mean (a). Cross-shore bar migration is driven by a physics-based sediment transport formulation (BBB) under the assumption of constant bar form, modified to allow increasing bar volume with offshore distance. The presence of alongshore variability, a, is assumed to cause horizontal circulation with potentially important consequences to bar variability, represented by empirical terms. The final form of the model has two coupled equations describing the time evolution of x and a.

The model was tested using video images from Palm Beach, Australia. Seven data sets, totaling 562 days and 11 major storms over a four-year period were used. Measurements of x and a were extracted from wave breaking patterns in daily-averaged time exposure images. Using subjectively-determined values for the model coefficients, model

skill was significant at the 95% level for all data sets in predicting x. Spectra were well reproduced and coherent with the data for most frequencies less than 1 in 6 days. The model was less successful at predicting a. Model skill was improved using least-squares solutions for the α coefficients for individual data sets although coherence of x predictions was reduced at higher frequencies. To our knowledge, this is the first model to reasonably predict bar response for multi-storm time scales.

The model was capable of reproducing onshore migration and growth of 2DH variability under mild wave conditions as well as offshore migration and straightening during storms. The influence of a, modeled here as κ_a, was found to increase onshore migration rates during moderate wave conditions, a role that has usually been assumed negligible. In addition, alongshore variability appears to stabilize 2DH systems against larger waves by reducing undertow in favor of circulation. This effect introduces hysteresis into the system. When waves were highly oblique ($> 20°$), these 2DH effects are highly reduced due to the parameterized role of longshore advective terms. Migration rates were also dependent on the amount of wave breaking, becoming insignificant during non-breaking conditions.

5. ESTIMATION OF NET SEDIMENT TRANSPORT FROM 2D CHANGES IN BATHYMETRY

5.1 Abstract

In this chapter we explore the possibility of obtaining unique 2D sediment transport patterns from changes in bathymetry through the 2D conservation of mass equation. The problem is under-determined, having two unknowns and one known variable. Measurements of changes in depth, $\Delta h/\Delta t$ can be obtained through classical survey methods. However, the contributions of the alongshore component of sediment transport, Q_y, and the cross-shore component of sediment transport, Q_x are unknown. Therefore, additional constraints are required in order to invert transport from changes in bathymetry. We assume that that the cross-shore integral of Q_x is closed, such that no sand enters or exists the system in this direction. By conservation of mass, this requires changes in volume of the cross-shore transect to be due to gradients in Q_y. Here we test six rules for distributing Q_y: three constraints describing one component of alongshore transport, Q_y^r, and three describing the cross-shore distribution of the excess volume component, Q_y^e. Initial results suggest that requiring sediment to travel down slope ($Q_y^r = f(\beta_y)$) is a possible parameterization for describing transport of distinct perturbations. Alternatively, basing the relationship of Q_x^r and Q_y^r on spatial lag correlations of the bar form between two surveys showed good results for identifying transport associated with alongshore migrating features. This method, however, did not do well under strictly onshore migration of 2D features, where alongshore transport was not predicted. A hybrid approach, using both the down-slope constraint and spatial correlation lags may provide more robust predictions on sediment transport patterns in complex environments. Due to the lack of closed boundaries in the alongshore, knowledge of $Q_y(x, y_0)$ is required to obtain net sediment transport patterns. Alternatively, spatial patterns of the transport

gradients provide useful insight into the system behavior without requiring $Q_y(x, y_0)$.

5.2 Introduction

Sand bars are one of the most prominent features of nearshore morphology. Bars act as natural buffers to the beach against storm wave action, dissipating wave energy offshore and away from the valued beach and dune system and human activity. They are also extremely variable, moving onshore and offshore in response to changing wave conditions and changing among a suite of shapes and morphologies. The transport processes associated with sand bar generation and migration are not well understood, making it a challenge for scientists and planners to accurately predict the natural cycles of the nearshore region. It is certainly true that bars develop where sediment transport patterns converge. Thus, early models assumed an initial featureless profile on which sand bars were generated by sediment transport convergence caused by any of a variety of mechanisms (e.g. *Bowen and Inman* (1971); *Holman and Bowen* (1982)).

Another well-known example is the breakpoint model (e.g. *King and Williams* (1949); *Greenwood and Davidson-Arnott* (1979); *Roelvink and Stive* (1989); *Marino-Tapia et al.* (2007)) that suggests that sand bars are generated at the location of initial wave breaking due to unspecified convergences in sediment transport. For depth limited breaking, this location is determined by the saturation condition for breaking, $\gamma = H_{rms}/h < 0.42$, where H_{rms} is the local root mean square (rms) wave height and h is the local water depth (*Thornton and Guza*, 1982, 1983). Taken literally this model predicts that as wave heights change, the sand bar will instantaneously move to the location along a smooth background bathymetry profile where this condition is true.

There are two flaws in this concept. First, because sediment transport rates are finite, bar response cannot be instantaneous and must continually lag behind the forcing. Thus, several recent papers have attempted to model this pursuit of equilibrium in terms of simplified dynamical equations (e.g. *Plant et al.* (1999, 2006); *Splinter et al.* (submitted)). Second, once sand bar response to forcing becomes significant (depth at the bar changes

appreciably), the location of initial wave breaking will also change, rendering the earlier prediction invalid. This feedback between the transport patterns forced by waves and the effect of the resulting bathymetry changes on those forcing patterns is fundamental to understanding changing sand bar morphologies.

Nearshore profile (1DH) and area (2DH) models that include sediment transport modules and allow bathymetry to respond appreciably will naturally include these feedbacks between an existing bar and the fluid forcing. For example, *Gallagher et al.* (1998) observed and described the feedbacks between undertow and the existing morphology. Specifically, under large waves, the maximum in undertow is located over the bar crest, causing offshore directed sediment transport and convergences on the seaward face of the bar. This shifts the bar and therefore the breakpoint and the maximum in the undertow seaward, reinforcing offshore migration until waves are no longer able to break over the bar. Similarly, *Ruessink et al.* (2007) showed that feedbacks between near-bed wave skewness, bedload transport, and the bar morphology are significant in describing onshore migration. These models utilize a variety of sediment transport formulations, based on wave and flow characteristics. Yet most, if not all models lack the proper physics to model both onshore and offshore bar migrations and the associated changes in 2DH variability of the bar form.

Parametric models, wherein the sand bar morphology is represented by a few variables, such as the bar crest position, have also been used to study the feedbacks between existing morphology and sediment transport. For example, *Plant et al.* (2001) (hereafter PFH01) provided a framework for analyzing the 1DH behavior of a natural sand bar system that we will try to extend to 2DH in this paper. The goal of PFH01 was to understand the relationship between any sand bar and the sediment transport induced by the bar under varying wave forcing. This required both accurate measurements of bathymetry and sediment transport.

Continuous cross-shore profiles of accurate sediment transport data are not generally available. However, one of the contributions of PFH01 was their use of an accurate

method to invert data on bathymetry change to yield transport. In general, bathymetry changes are related to sediment transport by the equation for the conservation of mass:

$$\mu\frac{\partial}{\partial t}h(x,y,t) = \frac{\partial}{\partial x}Q_x(x,y,t) + \frac{\partial}{\partial y}Q_y(x,y,t), \tag{5.1}$$

where μ is the sediment packing factor, $h(x,y,t)$ is the depth field, a function of cross-shore location x measured positive from the shoreline, y the alongshore location and t, time, and Q_x and Q_y are the depth integrated net cross-shore and alongshore sediment transport, respectively. PFH01 analyzed alongshore-mean bathymetry profiles so that the second term of equation (5.1) was identically zero and the equation reduced to:

$$\mu\frac{\partial h(x,t)}{\partial t} = \frac{\partial Q_x(x,t)}{\partial x}. \tag{5.2}$$

For two profile surveys, separated in time by Δt, the left hand side can be approximated by the finite difference form, $\Delta h/\Delta t$. Equation (5.2) can then be integrated in x starting at some point landward of any profile change to yield the profile of cross-shore transport that was needed to explain the observed profile change:

$$Q_x(x) = \int_0^x \mu\frac{\Delta h}{\Delta t} \tag{5.3}$$

Equation (5.3) is a powerful tool in this analysis, providing accurate estimates of cross-shore sediment transport everywhere without the need for any in-situ measurements or temporal averaging. The results are, by definition, the correct transport profiles to explain the observed profile changes. Given good data on both the evolving profile and the accurate net sediment transport between surveys, PFH01 were then able to study the feedbacks in the system, that is the relationship between sand bars and the sediment transport they cause, as a function of wave conditions.

To proceed, PFH01 modeled each beach profile in terms of a set of Gaussians superimposed on a background planar slope. Sediment transport profiles were then fit using corresponding Gaussians and error functions (the orthogonal function to a Gaus-

sian) such as any signal can be decomposed into sines and cosines by Fourier transform. Fits were usually excellent, with R^2 usually greater then 0.8. Continuing the analogy to Fourier analysis, the relationship between the two signals could then be expressed in terms of a magnitude and a relative phase, computed from the relative contributions of the error function and Gaussian. A relative phase of 0 (transport looks like the Gaussian bar) will lead to simple offshore bar movement, much like ocean waves wherein orbital velocity and wave form are in phase. A phase of π corresponds to onshore progression with no change in form. Phases of $\pm\pi/2$ represent bar growth/decay, respectively.

Through this analysis PFH01 showed that the majority of temporal changes of the profile were due to migration of a constant bar form (phase equal to 0 or π almost exclusively). They then further related the observed phase to the non-dimensional breaking parameter, $\gamma_{bar} = H_{bar}/h_{bar}$, and found distinct jumps between onshore and offshore transport at $\gamma_{bar} \approx 0.3$, or the onset of wave breaking. This value is slightly lower than the one suggested by *Thornton and Guza* (1982, 1983). Since experiments were performed under different field conditions (PFH01 on a barred beach at Duck, North Carolina and *Thornton and Guza* (1982, 1983) on an planar beach at Torrey Pines, CA), it is difficult to quantify differences.

Using a simple approach that was based solely on alongshore-average bathymetry data, PFH01 were able to demonstrate the presence and nature of the fluid-forced sediment transport over a nearshore sand bar. They showed that the induced sediment transport was coherent with the bar form (explaining most of the variance) and that variability was mainly due to progressive motions alternating between on and offshore, depending on the presence of wave breaking.

Observations show that sand bar morphologies are usually highly two-dimensional (horizontal, 2DH) (e.g. *Zenkovich* (1967); *Sonu* (1973); *Wright and Short* (1984); *Lippmann and Holman* (1990); *Alexander and Holman* (2004); *van Enckevort et al.* (2004)). Analogous to the 1DH results of PFH01, we expect that strong feedbacks between the bar profile and induced sediment transport patterns likely exist under typical 2DH condi-

tions as well. Both *Lippmann and Holman* (1990) and *Ranasinghe et al.* (2004) examined long records of daily morphological beach states (*Wright and Short*, 1984) and found that under accretional conditions, "down-state' transitions were more dependent on the previous morphological state than on the current wave forcing, suggesting a positive feedback system where 2DH processes influence the time-varying response of sand bars to changing wave conditions. Recent work by *Plant et al.* (2006) and *Splinter et al.* (submitted) have studied the dynamical link between onshore bar migration and 2DH variability, further supporting the importance of feedbacks between 2DH morphology and sediment transport patterns.

We hypothesize that strong feedbacks exist between existing morphology and the resulting sediment transport patterns that determine the evolution of the system. In order to understand these systems, we require accurate knowledge of directional sediment transport under varying wave conditions. Such data are not currently available. Extending the work of PFH01, it is the objective of this research to develop methods for inverting 2D bathymetry change data to obtain unique solutions of 2D sediment transport associated with onshore bar migration. As part of this work, we examine the consequences of different assumed constraints used to close the problem and the resulting net sediment transport patterns. Initial testing is done on synthetic beaches and later tested on bathymetry collected during the SandyDuck field experiment.

5.3 Approach

The fundamental equation for this work is the 2D equation for the conservation of mass (equation 5.1) that relates the directional components of sediment transport (Q_x, Q_y) to bathymetric change. Unlike the 1DH case, the 2D equation has two unknowns, Q_x and Q_y, and only one known, $\Delta h/\Delta t$, so is under-determined. Therefore, it is necessary to make further assumptions in order to get a unique solution for net sediment transport. Here we discuss several options, using information available from bathymetry surveys. For simplicity, all terms will be considered a function of (x, y), unless otherwise stated.

For illustration, Fig. 5.1 shows several examples of synthetic beach changes for which associated sediment transport pathways can be imagined. The differences between two profiles ($\Delta h/\Delta t$) have unique patterns based on the morphological change. For instance, onshore migration of a linear bar appears as Fig. 5.1a. A slightly more complex pattern exists for a linear bar that becomes 2DH variable (Fig. 5.1b). A bar that continues to grow in 2DH variability, while moving onshore has a $\Delta h/\Delta t$ that looks like Fig. 5.1c. A 2DH alongshore variable bar that is both growing and migrating alongshore has a $\Delta h/\Delta t$ pattern that looks like Fig. 5.1d. Understanding the relationship between patterns of 2D bathymetry change data and the associated sediment transport will help us understand the dynamics of coastal change.

For a closed, idealized system, the change in volume ($\Delta V/\Delta t$) for a given time is zero, such that mass is conserved. In real world examples, $\Delta V/\Delta t = 0$ is not required. If our cross-shore domain is large enough, we can constrain the solution such that no sediment enters ($Q_x(0) = 0$) or exits ($Q_x(\infty) = 0$) at the boundaries. Therefore, any changes in volume are due to converges or divergences in the alongshore transport (Q_y). Excess volume for a given cross-shore transect ($\Delta V(y)/\Delta t$) is determined by

$$\frac{\Delta V(y)}{\Delta t} = \int_{x=o}^{\infty} \frac{\Delta h(x)}{\Delta t} dx, \tag{5.4}$$

$$= \int_{x=0}^{\infty} \frac{\partial Q_y(x)}{\partial y} \frac{1}{\mu} dx, \tag{5.5}$$

where $\Delta h/\Delta t = (h_f - h_i)/\Delta t$, where subscripts f, and i indicate final and initial conditions and $\Delta h/\Delta t > 0$ indicates erosion. μ is the sediment packing factor (set to 0.65).

Rules can be defined for Q_x, Q_y, or both. We begin by placing constraints on Q_y, which we will denote by Q_y^r and Q_y^e. Knowing that volume must be conserved, we define the total alongshore transport to be

$$Q_y = Q_y^r + Q_y^e + Q_y(0), \tag{5.6}$$

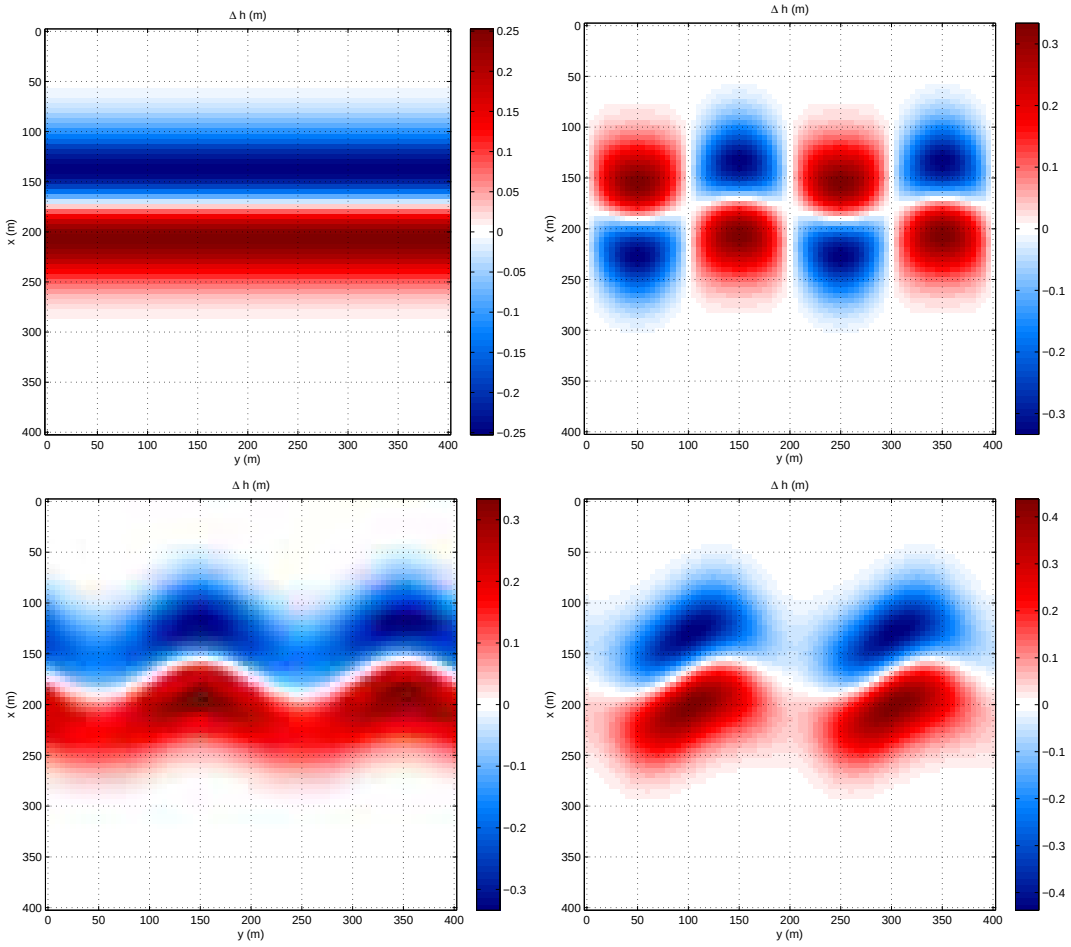

Fig. 5.1: $\Delta h/\Delta t$ patterns for various morphological changes. $\Delta h/\Delta t < 0$ indicates accretion. (a) Purely onshore migration of a linear bar. (b) Linear bar that transforms into a 2DH bar, with sinusoidal lengthscales $20\sin(2\pi y/L_y)$. (c) 2DH bar that both moves onshore and gains 2DH variability. Original bar crest location $x_{b1} = 180 + 15\sin(2\pi y/Ly)$. Final bar crest location $x_{b2} = 165 + 20\sin(2\pi y/L_y)$. (d) 2DH bar growth plus an alongshore shift. Same form as (c) but $x_{b2} = 165 + 20\sin(2\pi(y + 20)/L_y)$.

where Q_y^e is the excess Q_y required to conserve mass for a given cross-shore transect and $Q_y(0)$ is a constant of integration required to account for net alongshore transport. The cross-shore distribution of Q_y^e is unknown, but must be reasonable. For example, it is unlikely for this term to be significant seaward of the limit of measurable profile change. We will assume the excess is distributed according to some function F that we will specify later. Thus,

$$\frac{\partial Q_y^e}{\partial y} = \frac{\Delta V'(y)}{\int_{i=1}^{\infty} F(i)dx} F, \tag{5.7}$$

where

$$\Delta V'(y) = \Delta V(y) - \int_{i=1}^{\infty} \frac{\partial Q_y^r(i)}{\partial y} dx. \tag{5.8}$$

For any rule, r, and function, F, $\partial Q_y/\partial y$ is specified, such that the remaining bathymetry change not already specified is related to cross-shore gradients in Q_x:

$$\frac{\partial Q_x}{\partial x} = \frac{\Delta h'}{\Delta t}, \tag{5.9}$$

$$= \mu \frac{\Delta h}{\Delta t} - \frac{\partial Q_y^r}{\partial y} - \frac{\partial Q_y^e}{\partial y}. \tag{5.10}$$

Since we've specified no cross-shore transport enters from the shore boundary ($Q_x(0) = 0$), equation (5.9) can be directly integrated to determine Q_x. No similar constraint exists for $Q_y(x, y_0)$ that could serve as a constant of integration in y. Under special circumstances (i.e. at a jetty where $Q_y(x, y_0) = 0$ or identically rhythmic bathymetry where $Q_y(x, y_0) = Q_y(x, y_2)$), net transport can be uniquely determined in 2D. In more general cases, gradients in Q_y may be the only available solution as determining $Q_y(x, y_0)$ requires extensive knowledge of the 2D flow and sediment transport along the boundary.

We examine several options for constraints, r and F. We allow r to be:

- $Q_y^r = K$, where K is some constant form,
- $Q_y^r = K(\beta_y)$, where β_y is the alongshore slope, thus requiring Q_y to go down slope, and
- $Q_y^r = f(\tan^{-1}(\Delta y/\Delta x))$, where Δy, Δx are alongshore and cross-shore distances based on best-fit spatial lag correlations between the sand bar position in two adjacent surveys.

We allow F to be:

- $F_1 = \sigma_y(\Delta h/\Delta t)$, the alongshore standard deviation of the bathymetry change,
- $F_2 = \sigma_y(\overline{h})$, the alongshore standard deviation of the time mean profile, and
- $F_3 = h_o - \overline{h}$, where h_o is the long term equilibrium profile (planar beach) and $\overline{h}$ is the time mean profile.

The spatial distribution of F_1 and F_2 are similar for the synthetic examples. The cross-shore distribution resembles a double hump. F_3 has both a longshore and a cross-shore dependence. The cross-shore distribution is a single, Gaussian shaped hump.

We consider these rules under three different scenarios. Bathymetry, $h(x, y, t)$, is modeled using the formulation provided in *Plant et al.* (2001), based on an approximate fit to Duck, North Carolina, assuming a single alongshore sand bar. In all instances, the initial bar has the following form:

$$x_{b_i}(y) = x_{b_o} + A_b \sin\left(\frac{2\pi y}{L_y}\right), \tag{5.11}$$

where x_{b_i} defines the bar crest location with respect to the shoreline, x_{b_o} is the alongshore-averaged bar position, set to 180 m, A_b is the cross-shore amplitude of the bar position, set to 15 m. L_y is the length of the domain. Bar width, L_b, is set to 50 m and bar height, h_b, to 1 m. The first case is for an onshore migrating bar that grows in 2D variability, whose bar width and bar height are unchanging. The final bar crest position is

$$x_{b_f}(y) = 165 + 20 \sin\left(\frac{2\pi y}{L_y}\right). \tag{5.12}$$

The second case has the same onshore migration and increase in variability but also allows for a change in bar shape, such that

$$L_{b_f}(y) = 50 - 10 \sin\left(\frac{2\pi y}{L_y}\right), \tag{5.13}$$

such that bars closer to shore are larger, attempting to mimic shoals. The third case has the same onshore migration and increase in variability but also includes an alongshore

shift (Δy) in the bar position,

$$x_{b_f} = 165 + 20\sin\left(\frac{2\pi(y+\Delta y)}{L_y}\right). \tag{5.14}$$

5.3.1 Constant Q_y

The simplest form is to constrain $Q_y^r = K$, where K is a constant, thus reverting to the 1DH continuity equation if $\Delta V(y)/\Delta t = 0$. For linear bar migration, this provides sensible sediment transport patterns. However, if we consider an alongshore variable bar, constant in shape, the resulting sediment transport patterns do not match the assumed hydrodynamic patterns based on existing bathymetry (Fig. 5.2). In this scenario, we would assume alongshore variable wave breaking would induce 2DH circulation and that 2DH currents would transport sand that was mobilized by the waves, causing rotational sediment transport (shorewards over the shoreward maxima of the 2D bar and offshore directed at the seaward maxima of the 2D bar). Likewise, if we allow volume to change, we would assume similar sediment transport patterns, with enhanced transport over the growing regions. The modeled result is onshore directed transport everywhere with sediment converging at the shoreward maxima of the 2D bar.

5.3.2 Q_y is a function of the bathymetric alongshore slope (β_y)

A second option is to require $Q_y^r = f(\partial\overline{h}/\partial y)$, such that sediment travels down slope under gravitational effects as proposed by *Bagnold* (1963). Here we set Q_y^r to

$$Q_y^r = K\frac{\partial\overline{h}}{\partial y}, \tag{5.15}$$

where $K = 600$, is a scaling factor and $\overline{h}$ is the mean profile ($(h_f + h_i)/2$). We solve for Q_x using equation (5.9).

For an alongshore uniform bar on a planar beach, this reverts to the 1D model. For a 2DH bar, the resulting sediment transport pattern for growing 2DH variability and onshore migration resembles possible 2DH current patterns (Fig. 5.3) in contrast to the

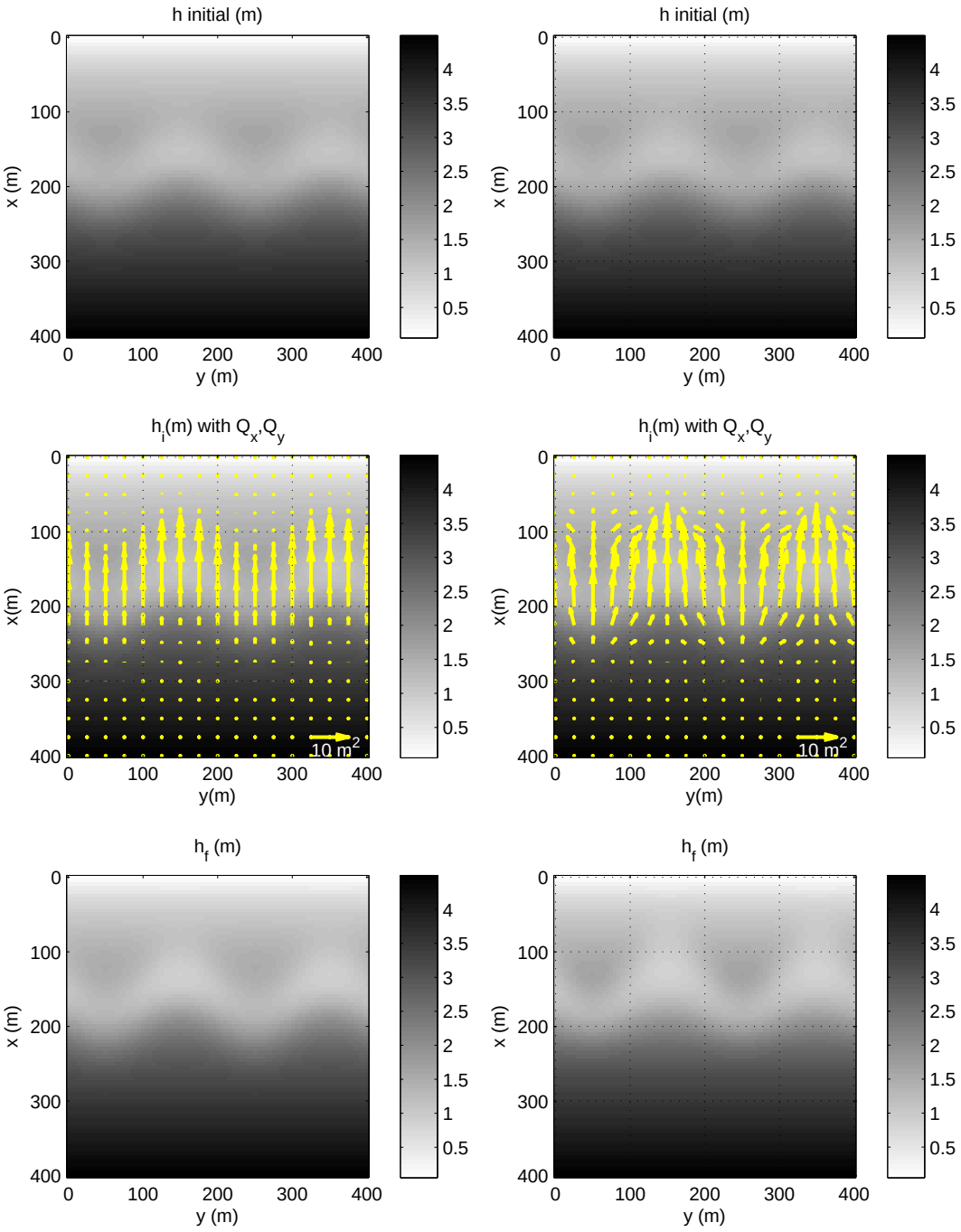

Fig. 5.2: Sediment transport patterns with the assumption of $Q_y = K$. (*left*) $\Delta V/\Delta t = 0$. (*right*) $\Delta V/\Delta t \neq 0$ with F_1 used to distribute excess volume.

previous assumption of $Q_y^r = K$. However, the downslope term is a destructive contributor (this term causes the bar to flatten out), requiring Q_x to compensate. The resulting

sediment transport pattern has strong onshore directed transport over the shoreward maxima of the 2D bar and offshore transport over the seaward maxima of the 2D bar (Fig. 5.3). There are regions where the vector transport is required to travel along slope, despite the assumption that alongshore transport should be down-slope directed. These areas are near the rotation axes as the bar moves onshore and grows in cross-shore amplitude.

This works reasonably well for growing 2DH bars. If we allow changes in volume to occur, the distribution of Q_y^e becomes more critical. Using F_1 or F_2, the resulting transport no longer resembles 2DH circulation patterns (Fig. 5.4(left)). However, the use of F_3 to distribute excess volume still maintains a similar circulation pattern (Fig. 5.4(right)), suggesting an alongshore variable distribution of Q_y^e may be more realistic.

For an alongshore migrating bar that is also increasing in 2DH variability, the resulting net sediment transport patterns still resemble 2DH circulation patterns. In these instances, we might assume oblique waves approaching the beach, driving an alongshore variable current over the bar. The current will potentially undulate along the variable bathymetry. However, the predicted sediment transport still resembles more 2DH circulation, albeit slightly skewed down stream (Fig. 5.5).

If a constant of integration is known, such that a (potentially) cross-shore variable alongshore transport can be superimposed onto the net sediment transport, the result may resemble the hydrodynamics. For this reason, it may be a more sensible option to examine the patterns of $\partial Q_y/\partial y$ and $\partial Q_x/\partial x$ rather than Q_y and Q_x in 2D. The resulting gradients resemble an alongshore shifting bar (alongshore skewed pattern) and slight onshore shifting (Fig. 5.6)). The results of the gradient transport seem sensible for the cases examined. Of the three choices for distributing the excess volume, F_3 appeared to be slightly better than F_1 or F_2 when comparing net sediment transport patterns for these cases.

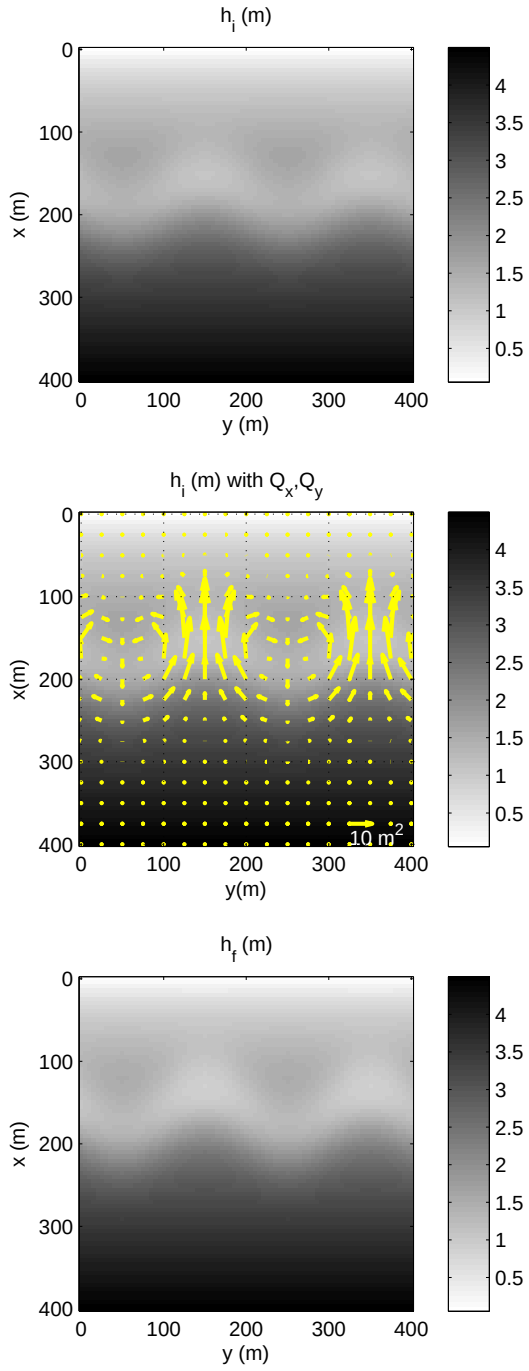

Fig. 5.3: Sediment transport patterns with the assumption of $Q_y = K\partial h/\partial y$.

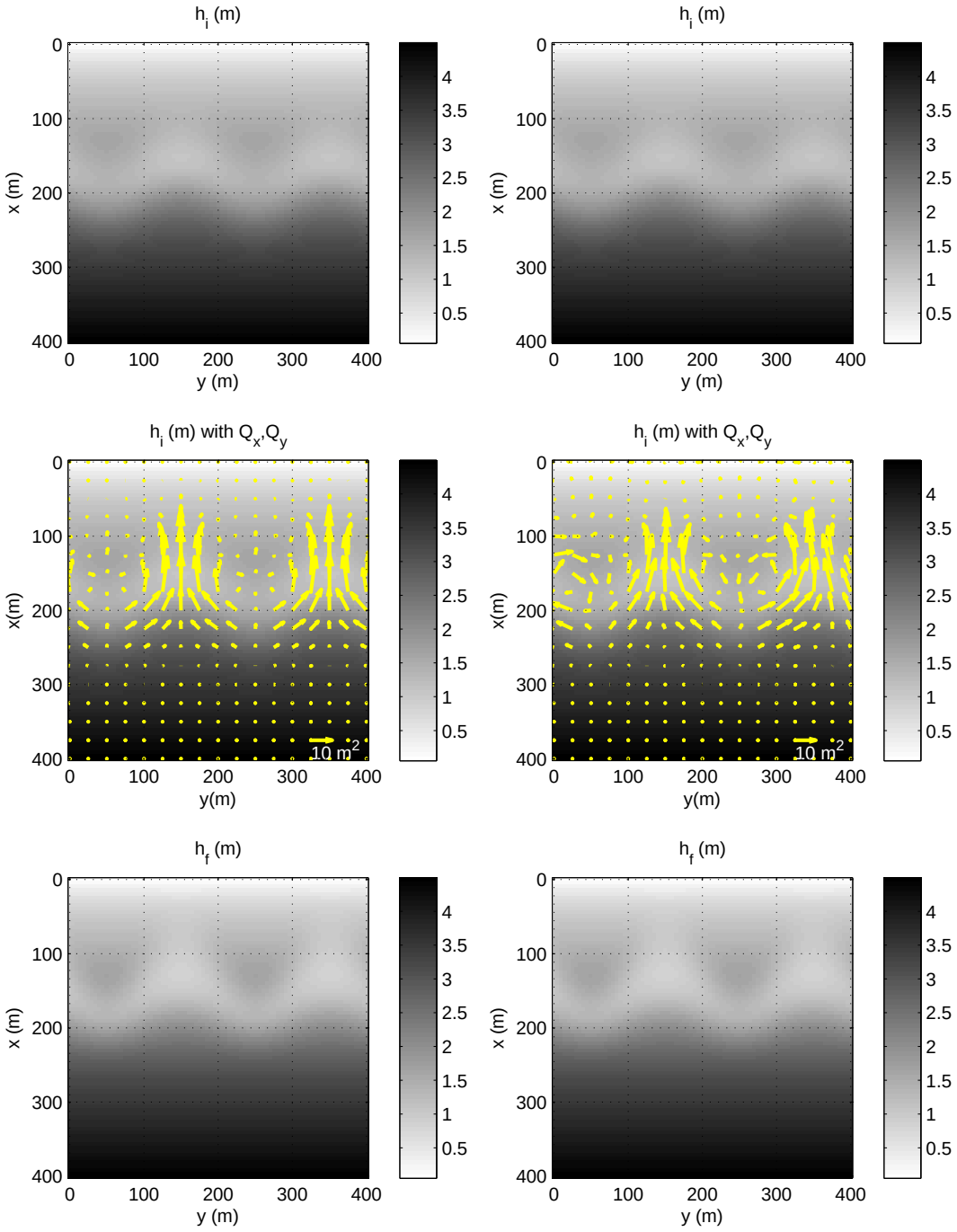

Fig. 5.4: Sediment transport patterns with the assumption of $Q_y = K\partial h/\partial y$ with a change in volume. (*left*) Using F_2 to distribute excess sand. (*right*) Using F_3.

5.3.3 Isolating Alongshore Variability in $\Delta h/\Delta t$

Alternatively, we can examine the alongshore variation of $\Delta h/\Delta t$ (or $\overline{h}$) to potentially gain information about 2DH sediment transport patterns. For alongshore uniform sand

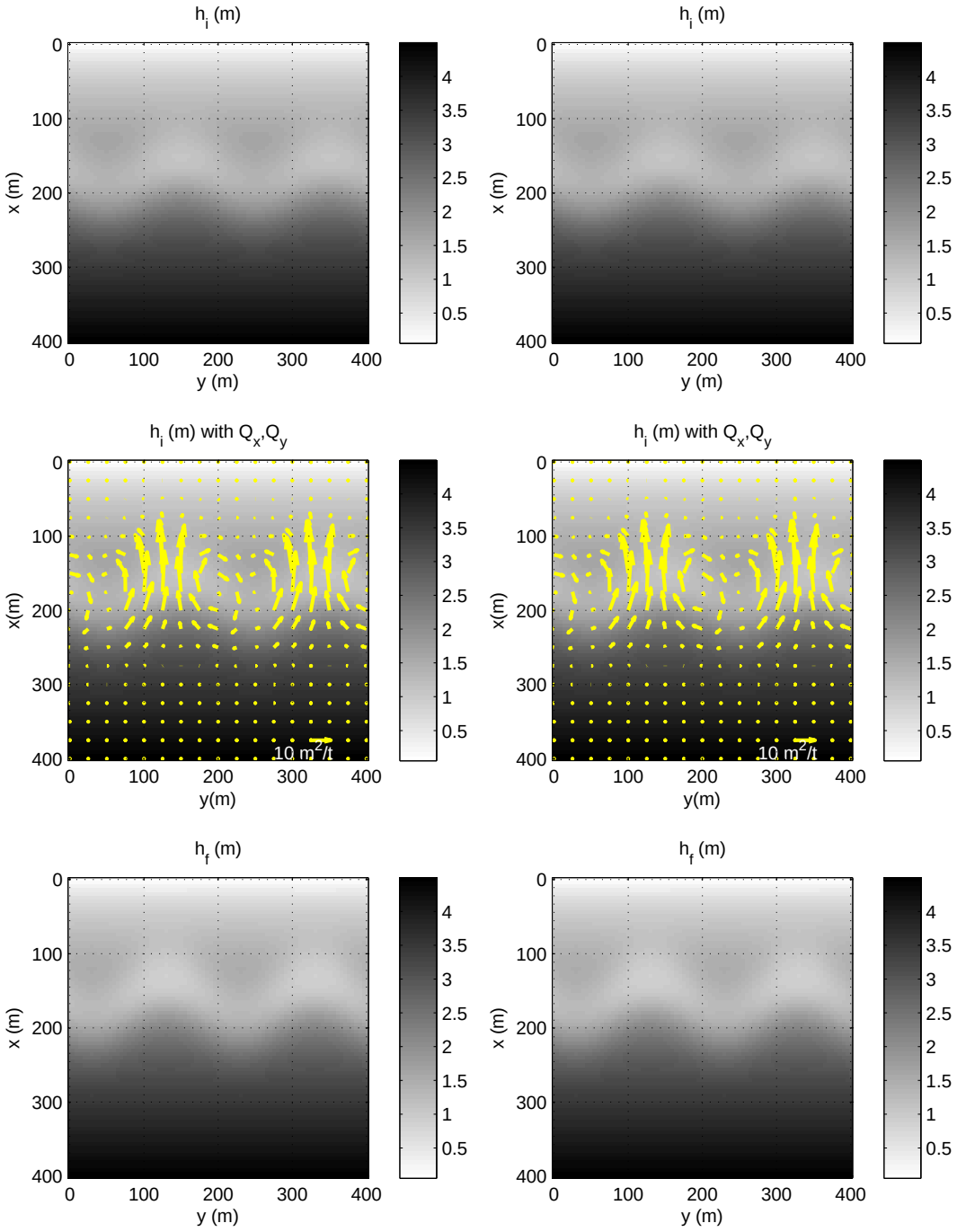

Fig. 5.5: Sediment transport patterns with the assumption of $Q_y = K\partial h/\partial y$ with an alongshore shift. (*left*) Using F_2 to distribute excess sand. (*right*) Using F_3.

bars, a cross-shore transect of the profile is equal to the alongshore mean bar ($< h >_y (x)$) profile and we assume gradients in Q_y to be negligible. Variations about the alongshore

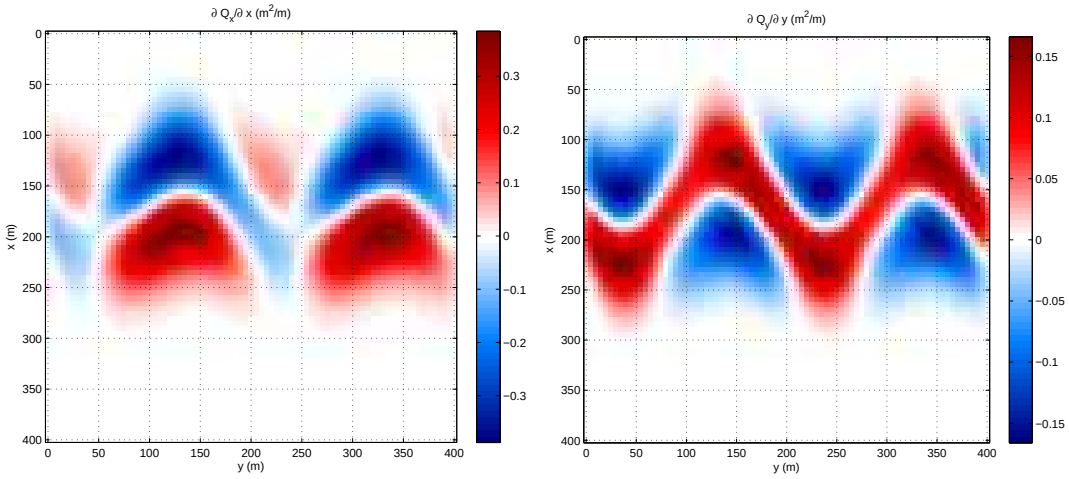

Fig. 5.6: Gradients in sediment transport patterns with the assumption of $Q_y = K\partial h/\partial y$ with a shifting bar. (*left*) $\partial Q_x/\partial x$. (*right*) $\partial Q_y/\partial y$ with F_2 to distribute excess sand.

mean can indicate 2DH sediment transport. We begin by determining the alongshore variable component of $\Delta h/\Delta t$:

$$\frac{\Delta h'}{\Delta t}(x,y) = \frac{\Delta h}{\Delta t}(x,y) - \langle \frac{\Delta h}{\Delta t} \rangle_y(x). \tag{5.16}$$

In most instances, the perturbations in the long term mean profile (i.e. the sand bars) are the most visible indication of sediment transport gradients. If sand bars can be identified such that the use of spatial lag correlations between adjacent surveys can provide a proxy for directional transport, the solution can be further constrained. Comparing bar crest position, $x_b(y)$, between two adjacent surveys, correlations are found at distinct spatial lags in both the alongshore and cross-shore directions. For the alongshore direction, the maximum correlation between two surveys is used to identify the alongshore spatial lag, or shift, Δy. In the cross-shore, there are two options: to calculate a cross-shore shift, Δx, based on the spatial lag correlations between alongshore mean bar positions ($< h >_y (x)$), or to calculate the shifts at each alongshore location and then find a mean value. We opted for the second approach, such that the shift is defined as the mean difference in the cross-shore bar peak ($x_{bf}(y) - x_{bi}(y)$) between the two profiles.

The initial profile is first shifted, based on the alongshore lag (Δy) prior to finding the cross-shore shift. Assuming that the relation between Δy and Δx is an indication of the relative magnitudes of sediment transport in the alongshore and cross-shore direction, a relative angle, defining the relation between the magnitudes of the alongshore and cross-shore shifts is defined as

$$\theta(y) = \tan^{-1} \frac{|\Delta x|}{|\Delta y|}. \tag{5.17}$$

Contributions of $\partial Q_x^r/\partial x$ and $\partial Q_y^r(x,y)/\partial y$ are

$$\frac{\partial Q_x'}{\partial x} = \sin\theta \mu \Delta h', \tag{5.18}$$

$$\frac{\partial Q_y'}{\partial y} = \cos\theta \mu \Delta h'. \tag{5.19}$$

We define the distribution of excess volume, $\partial Q_y^e/\partial y$ by equation (5.7). The remaining bathymetry change (equal to the alongshore-average bar change, $\mu < \Delta h/\Delta t >_y (x)$) is attributed to gradients in cross-shore transport,

$$\begin{aligned} \frac{\partial Q_{x_m}}{\partial x} =& \mu \frac{\Delta h}{\Delta t} - \frac{\partial Q_y^r}{\partial y} - \frac{\partial Q_x^r}{\partial x} - \frac{\partial Q_y^e}{\partial y}, \\ =& \mu \langle \Delta h \rangle_y (x). \end{aligned} \tag{5.20}$$

The final solutions for Q_x and Q_y are

$$Q_x = Q_x^r + Q_{x_m}, \tag{5.21}$$

$$Q_y = Q_y^r + Q_y^e. \tag{5.22}$$

For a purely onshore migrating bar this method has the same solution as $Q_y^r = K$,

suggesting that including the slope dependent term is also necessary in these instances to estimate net sediment transport patterns. For the case of the alongshore propagating bar, a much different pattern of sediment transport gradients compared to $Q_y^r = \beta_y$ exists (Fig. 5.5 versus Fig. 5.7).

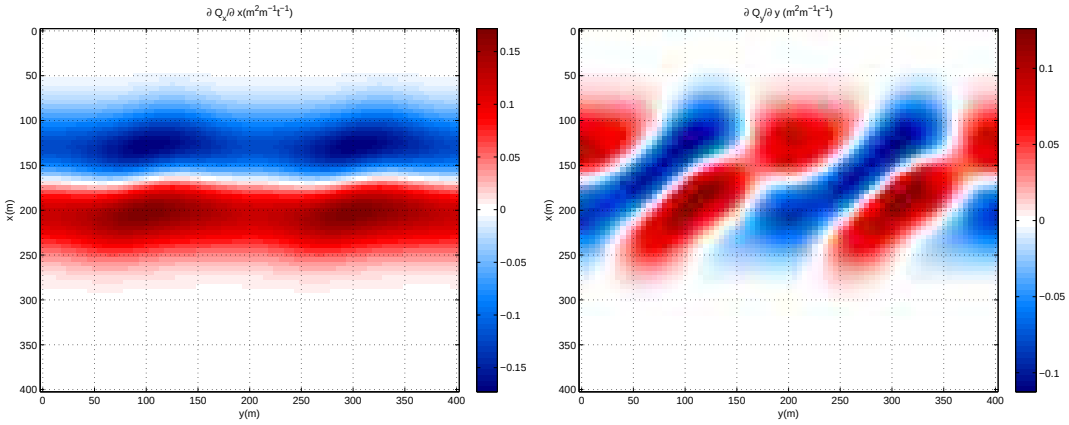

Fig. 5.7: Gradients in sediment transport patterns with the assumption of $Q_y = f(\Delta x/\Delta y)$ for an alongshore migrating bar. F_3 is used to distribute excess sand. (*left*) Cross-shore sediment transport gradients, $\partial Q_x/\partial x$. (*right*) Alongshore sediment transport gradients, $\partial Q_y/\partial y$

The convergence pattern for $\partial Q_y/\partial y$ indicates an alongshore migrating feature. The convergence patterns for $\partial Q_x/\partial x$ indicate a predominantly onshore migrating bar. Alongshore variability in both terms represent the growth of the feature. Integrating $\partial Q_x/\partial x$ in x gives Q_x. Since the cross-shore is a closed integration ($Q_x(0) = 0$, $Q_x(\infty) = 0$), the solution is unique. Integrating $\partial Q_y/\partial y$ in y however, does not lead to a unique solution since there is no requirement for $Q_y = 0$ at either of the alongshore boundaries.

5.4 Evaluation of Constraints on Field Data

Bathymetric surveys from SandyDuck are used to test the above theories. SandyDuck was a multi-institutional experiment undertaken at the US Army Corps Field Research Facility (FRF), Duck, North Carolina during September - November 1997. The main goal of the experiment was to gain a greater understanding of the processes that cause beaches to change. Daily profile lines were sampled using the CRAB at 18 alongshore

locations, spaced 25 m apart within the instrument area and 50 m apart everywhere else. All lines began at the base of the dune system and extended to approximately 550 m offshore (roughly 6 m depth). At the seaward boundary $\Delta h/\Delta t$ was negligible that we can consider the domain to extend out past the point of active transport, such that $Q_x(\infty) = 0$. Measured bathymetry was interpolated onto a 2 m x 2 m grid using a linear Loess interpolation scheme. Initial testing for the survey dates October 15-16, 1997 are discussed here. These dates are chosen because of the clear $\Delta h/\Delta t$ pattern that could allow for simple analysis of the techniques so far discussed (Fig. 5.8).

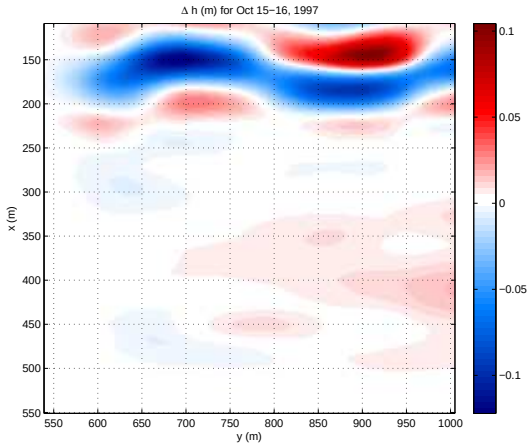

Fig. 5.8: $\Delta h/\Delta t(m)$ for Oct. 15-16, 1997 at Duck, North Carolina.

We first test $Q_y^r = f(\beta_y)$. The alongshore migrating feature does not have a significant slope, such that this term is quite small throughout most of the domain. No significant transport is associated with the feature (Fig. 5.9). The left side of the domain does have some feature that has a much larger slope resulting in large localized gradients in both cross-shore and alongshore transport. The resulting gradients in sediment transport are shown in figures (5.9) and (5.10). The spatial patterns predicted by this approach do not seem reasonable for the given change in bathymetry. The large amount of transport predicted at $y = 600$ is obviously erroneous and is a result of an over-prediction of alongshore transport gradients and the requirement to conserve mass. $\partial Q_y/\partial y$ does not resemble any particular pattern seen in $\Delta h/\Delta t$. Particularly, the 2D feature appears to be migrating alongshore, yet this method does not predict coherent alongshore transport.

Alternatively, we can test the third method, seeing if we can find spatial lags in the data in order to constrain the solution.

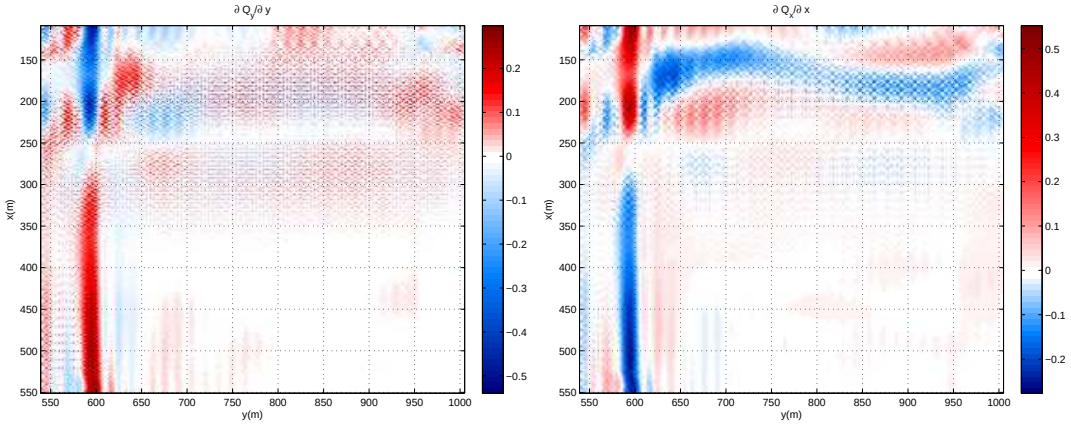

Fig. 5.9: Predicted sediment transport gradients using slope constraint and distribution of excess volume according to F_2. (*left*) $\partial Q_y/\partial y$. (*right*) $\partial Q_x/\partial x$.

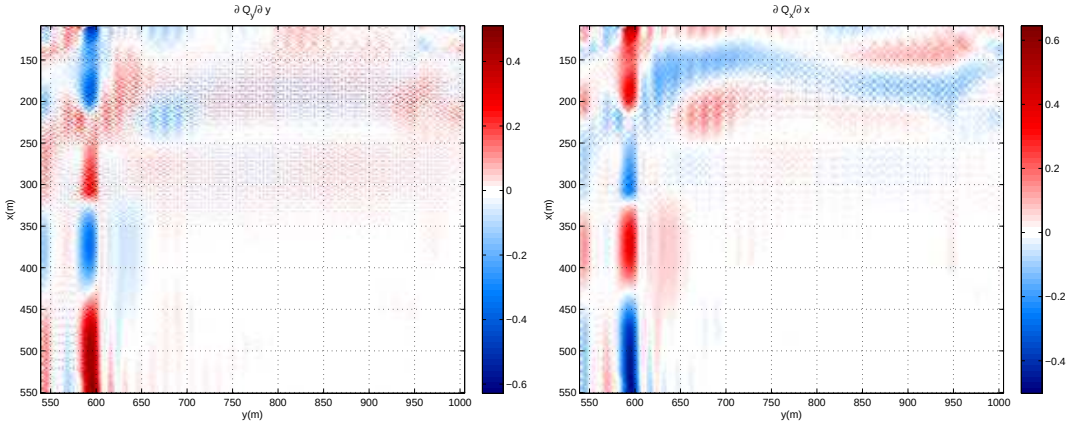

Fig. 5.10: Predicted sediment transport gradients using slope constraint and distribution of excess volume according to F_3. (*left*) $\partial Q_y/\partial y$. (*right*) $\partial Q_x/\partial x$.

Within the SandyDuck data set, multiple positive perturbations (bars) existed, not always continuous in the alongshore, which forced us to refine our spatial lag correlation scheme. In order to calculate the spatial lag correlation between the adjacent surveys, several methods are tested. We find that regions of active transport are not necessarily limited to the location of the largest sand bar, such that determining spatial lags of this feature did not provide information about the direction of transport. 2D correlations

between the two bathymetries are also not useful at identifying the direction of sediment transport because only a small region actually exhibited noticeable $\Delta h/\Delta t$. We chose to isolate the analysis to the region of active sediment transport, defined by the cross-shore extents where $|\Delta h/\Delta t| > 0.05$ m. Sand bars, or positive perturbations were identified based on the maximum in the perturbation profile within the region of interest (Fig. 5.11).

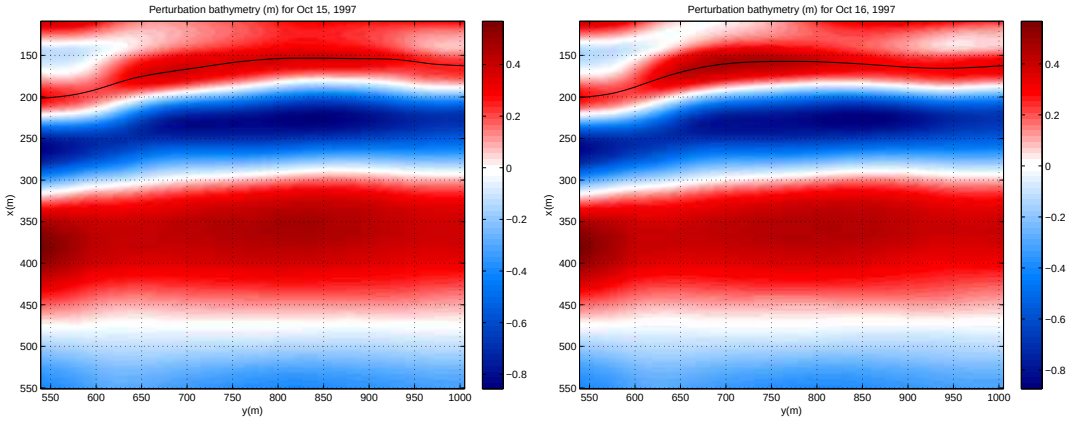

Fig. 5.11: Perturbation profiles with identified bar positions (solid black line) for Oct. 15 - 16, 1997 at Duck, North Carolina. Region of interest for determining bar features was defined as 126 m$< x <$ 200 m.

2D spatial lag correlations of the identified bar positions determined a best-fit with a cross-shore shift of 4 m (offshore) and an alongshore shift of -66 m. The resulting sediment transport convergence/divergence patterns (Fig. 5.12) based on equations (5.7), (5.18), (5.20), and (5.21) describe a predominantly alongshore migrating 2D bar (checker pattern of $\partial Q_y/\partial y$) with a slight offshore shift (alongshore uniform pattern of $\partial Q_x/\partial x$). Integrated sediment transport requires knowledge of mean alongshore transport to give sensible results as discussed above.

5.5 Discussion

The extension of *Plant et al.* (2001) to include the alongshore component of sediment transport is complicated by the fact that the equation is under-constrained, with two unknown parameters: the alongshore and cross-shore components of sediment transport

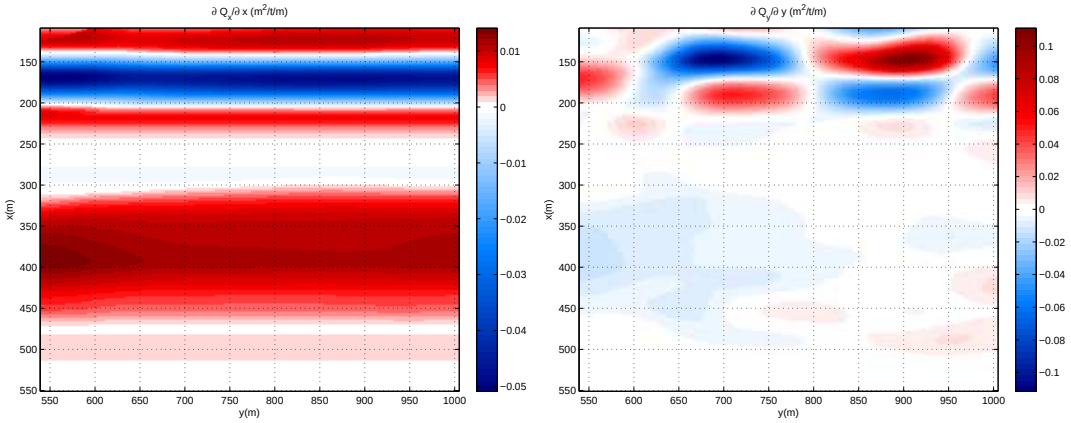

Fig. 5.12: Estimated convergence/divergence patterns of sediment transport for bathymetric change between Oct. 15-16, 1997 at Duck, North Carolina. Positive values indicate areas of erosion.

and only one known parameter: changes in bathymetry. Although we can often consider the cross-shore system to be closed, such that no sediment enters or exits at the cross-shore boundaries, the same cannot be said for the alongshore direction. Several constraints are needed to obtain a unique solution. Since the original 2D equation for conservation of mass is under-constrained, we require some knowledge of either Q_y or Q_x. We can assume a closed system in the cross-shore, such that Q_x can be directly integrated if all other terms are known. However, the alongshore component has no such constraint unless a feature, such as a jetty, exists at one end of the domain so $Q_y(x, y_0)$ can be determined. Thirdly, if we assume $Q_x(0) = Q_x(\infty)$, such that the cross-shore integral is 0, we require all excess volume to be a function of $\partial Q_y/\partial y$. The cross-shore distribution of this term is another unknown in the problem.

Initial testing of several theories for the distribution of $\partial Q_y/\partial y$ provided plausible extensions, but also highlighted limitations. We examined three methods for distributing the component of Q_y due to some rule (Q_y^r) and three methods for describing the distribution of excess volume (Q_y^e). The major contributor to the final spatial patterns of Q_y was Q_y^r. The resulting net sediment transport differences based on the distribution of Q_y^e were not significant in most cases.

Any change in volume was attributed to convergences/divergences in Q_y due to our

constraint on $Q_x = 0$ at the cross-shore boundaries. Although the total amount of sand required to account for the volume change could be calculated, its cross-shore distribution was unknown. Three options were tested. Two methods had an alongshore uniform distribution (F_1 and F_2), while method three (F_3) varied in both the alongshore and the cross-shore. Under growing features, the cross-shore distribution of the excess volume played a significant role in the final solution when Q_y^r was a function of β_y. Under field conditions, F_3 may contain more than just the perturbation features if a strong fit to the background profile is not found. For this reason, methods F_1 or F_2 might be more sensible. However, an alongshore uniform distribution seems unjustified for highly 2D bathymetry. Determining the best method to distribute this volume is still unknown as none of the methods tested seemed robust to a variety of conditions.

Requiring $Q_y^r = K$, where K is a constant, resulted in sediment transport patterns that seemed reasonable for 1DH systems. However, for 2DH systems, this constraint did not predict sediment transport patterns that matched expected hydrodynamics. Constraining Q_y^r to go down slope was an improvement. In some instances, this constraint required net transport to follow contours, despite the down slope term. The resulting sediment transport pattern for growing 2DH bar systems resembled the expected hydrodynamics. However, this method produced net sediment transport patterns that were inconsistent with the alongshore transport of features. Under these circumstances, we would assume that maximum Q_y should exist over the mean bar position (or perturbation), similar to the 1DH model. Gradients in sediment transport resembled the underlying bathymetry with a slightly skewed pattern in the direction of alongshore transport. The inclusion of a constant of integration in solving for Q_y may provide a more reasonable net sediment transport result in these cases.

The third method tested required knowledge of correlation lags between the perturbation features in adjacent surveys. Determining how much transport was due to 1D versus 2D dynamics required some sort of separation of the 2D profile from the alongshore uniform component. Our initial choice was to remove the alongshore mean profile.

If the profile was an alongshore uniform bar, then no 2D transport was expected. The remaining 2D perturbation profile was used to determine 2D transport based on lag correlations, while the remaining alongshore mean profile was used solely to determine the remaining portion of Q_x. This method could not reproduce Q_y transport for onshore migrating features since there was no alongshore lag. In these instances, this method was the same as $Q_y^r = K$. Under alongshore migrating features, this method produced a very different pattern for sediment transport gradients compared to $Q_y^r = f(\beta_y)$. In this case, the alongshore transport gradients did not resemble the existing bar form, but more an alongshore migrating feature of roughly constant form.

The slope dependent and correlation lag methods were tested on a field example. Due to the lack of significant longshore slope in the data in the area of active sediment transport, the slope dependent method did not produce reasonable results. The slope constraint was unable to identify the feature in the field data and reproduce sensible sediment transport patterns associated with its migration. As well, a large amount of sediment transport was required to compensate for the slope dependent term on the left hand side of the survey. The correlation method provided a slightly better solution due to the fact that it could be constrained to the area of noticeable $\Delta h/\Delta t$. The resulting sediment transport gradients for this method showed an alongshore propagating feature that moved slightly offshore, consistent with data.

The field data was far less idealized than the synthetic data which was composed of a monotonically increasing depth with a super-imposed Gaussian bar. Sand bars are far less apparent in the field data, such that isolating sand bars on the basis of positive perturbations requires accurate removal of the background trends. Linear regression of the bathymetry from the approximate shoreline to the offshore boundary removed the planar slope dependency and any offset in the data, leaving both positive (bar) and negative (trough) perturbations. Bar positions, or features, are much more prominent in the alongshore averaged profile, which facilitates the identification and mapping of bars required to do correlation lags. Applying the methods to field data highlighted some

of these limitations. The identification of features to both determine spatial lags and cross-shore distribution of $\partial Q_y^e/\partial y$ are areas of future research. *Plant et al.* (2001) were able to parametrically model the alongshore average profile, thus isolating bar forms and enabling them to relate sediment transport patterns to the mean bar profile. Utilizing such an approach in 2D may improve the above analysis techniques.

Identification of the dominant direction of transport seems key to determining unique solutions. This initial work focused on using lag correlations to determine the potential contributions of Q_x and Q_y. This required the correct identification of features (in our case, the bar) that were actively changing height or shape. This may not be feasible over a wide range of conditions, such as broken or shore-parallel bars. Alternative methods for determining direction, potentially from $\Delta h/\Delta t$ patterns, is another future topic of research.

Mapping sediment transport of 2D bathymetry is far more complex than of the alongshore-averaged profile. Small scale bumps and variability can be smoothed out through alongshore averaging, removing a large component of complexity. For example, the alongshore average profiles for October 15 and 16, 1997 (Fig. 5.13) clearly shows a small perturbation feature around $x = 175$ m and $x = 325$ m. As well, there is very little change between the two alongshore averaged profiles, suggesting minimal sediment transport occurred between the two days. This however, is contradicted when we look at the 2DH pattern of $\Delta h/\Delta t$ (Fig. 5.8) that indicates considerable transport.

This also raises the question on the validity of the assumption that if the cross-shore mean change ($(\Delta h)_{net}$) between two consecutive surveys is significantly less than the root mean square changes ($(\Delta h)_{rms}$), transport is predominately in the cross-shore direction. Both *Gallagher et al.* (1998) and *Ruessink et al.* (2007) use this comparison to justify the use of a 1DH sediment transport model. If we apply such a test to the October 15 - 16, 1997 surveys, the result is that cross-shore transport dominates the change in morphology. This conclusion does not match the observed changes in morphology. If we consider a 2DH bar, constant in volume and shape, yet migrating in the alongshore direction, the above

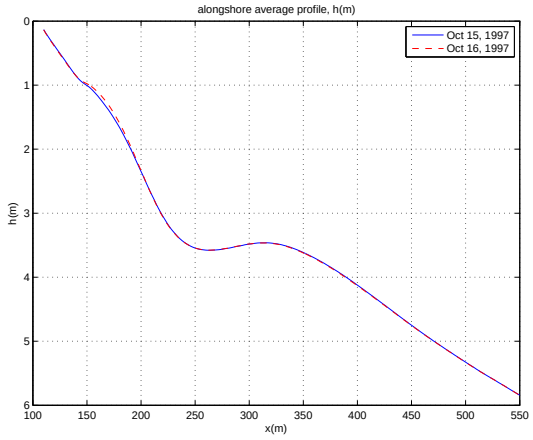

Fig. 5.13: Alongshore-averaged profiles for Oct. 15-16, 1997 at Duck, North Carolina.

analysis would indicate cross-shore transport dominated, yet none actually occurred. In the case of October 15 - 16, 1997, a 2DH bar is migrating predominately in the alongshore, such that changes in morphology could be attributed (falsely) to cross-shore transport. In this manner, this simple test seems valid only when the morphology is predominately alongshore uniform and we assume gradients in cross-shore transport to dominate the $\Delta h/\Delta t$ signal.

5.6 Conclusions

Complex bathymetry patterns cannot be explained by simple 1D sediment transport equations. The use of a 2D sediment transport inversion technique from changes in bathymetry requires knowledge of the relationship between Q_x, Q_y, and the observed bathymetry change. Initial tests produced non-intuitive results and sparked further analysis on the constraints chosen. Constraining Q_y to be a function of the beach slope resulted in sediment transport patterns that were physically plausible during shore-normal waves. For alongshore propagating features, the knowledge of a boundary condition to constrain $Q_y(x, y_0)$ is necessary to obtain sensible net sediment transport patterns. Alternatively, spatial patterns of the gradients of transport are much more easily obtained and may provide information about the relationship between Q_x, Q_y and bathymetry change in 2D environments.

The use of spatial 2D correlations between perturbation (bar) features showed promising results in identifying the main direction of sediment transport and further constraining the solution. A combined method, including slope dependent terms and correlation-lags may provide the necessary constraints to obtain unique solutions for gradients in transport over a wide variety of conditions. $\Delta h/\Delta t$ patterns are very complex in 2D such that unique solutions of net 2D sediment transport may be beyond the scope of the methodology presented here without further constraints, specifically retrieving the constant of integration for Q_y. Alternatively, unique spatial gradients in Q_x and Q_y, which ultimately define bar migration seem attainable with further research.

6. CONCLUSIONS

Within this dissertation we examined the interactions and feedbacks between bathymetry, waves, currents, and sediment transport. The first two projects focused on the use of remote sensing techniques to expand our knowledge of the nearshore. Utilizing remotely sensed wave refraction patterns of nearshore waves, we were able to estimate bathymetry gradients in the nearshore through the 2D irrotationality of wave number equation. Remotely sensed images of wave breaking over complex bathymetry were used to study the nonlinear feedbacks between 2DH morphology and cross-shore migration rates of the alongshore averaged bar. The last project, while preliminary, utilized bathymetry measurements to gain further understanding of 2D sediment transport.

The goal of the bathymetry estimation from refraction patterns of surface waves was to provide an alternative method for providing bathymetry when time-series data was unavailable. Due to the plethora of snap-shot data that is available from satellites and made available through such programs as Google Earth, having a method that can determine bathymetry from spatial wave patterns would be highly valuable. An algorithm was developed to estimate nearshore bathymetry based on the changing direction of refracting waves. The model used an augmented form of the refraction equation that relates gradients in bathymetry to gradients in wavenumber and wave angle through the chain rule. The equations are cast in a form that is independent of wave period, so can be solved using wavenumber and direction data from a single snapshot rather than the normally-required time series of images.

Three methods for extracting wave number, k, and wave angle, θ, from images were tested. Under monochromatic conditions, all methods performed well. However, for cases with high-frequency noise or a non-ideal wave field, the two gradient methods for determining k, θ were found to be unusable. The tomographic approach of the nonlinear

PHH08 method was robust to these complications and had the added advantage of providing skill estimates that allowed objective identification of unacceptable results. For some cases, waves are simply too broad-banded for representation by a single direction and wavelength. These can be identified objectively by low skill values and disregarded. Synthetic testing of the model using monochromatic waves on three bathymetries of increasing complexity, showed that the model accurately estimated 2D bathymetry gradients, hence bathymetry, with a mean bias of 0.01 m and mean root mean square error over the three beaches of 0.17 m. While the model is not useful for cases of complex seas or small refraction signals, the simplified data requirement of only a single snapshot is attractive. The model is perhaps best suited for shorter period swell conditions, for example from a semi-enclosed sea, where strong refraction patterns are visible and k, θ easily extracted from a single frame image.

Future work should be focused on image processing and data extraction techniques, such that robust measurements can be obtained from a single image. Alternatively, time series data may be required in order to provide robust estimates of complex environments. The largest limitation of this work is the requirement for smooth wavenumber and wave angle measurements from images. For the synthetic cases, this was achieved using the PHH08 method. However, for field data, even this method had limited success in extracting information from raw images. This is mainly due to the high noise to signal ratios within the data. As well, the waves in an image appear as spikes/dips, rather than sinusoidal forms.

The goal of the second project was to determine if 2DH currents (indicated by the presence of 2DH bathymetry) had a noticeable influence on cross-shore migration of the alongshore-averaged sand bar. We began by testing a linear model on a four year data set at Palm Beach, Australia. Although the linear model suggested that 2DH bathymetry was indeed linked to cross-shore bar migration rates, the results also highlighted several short comings of the linear model. The primary limitation was that variations in bar position and variability had to be temporally uncorrelated with forcing in order to achieve

meaningful results. For large storms, this is indeed the case. However, many smaller storms seen at Palm Beach, showed that changes in bar position and variability were correlated with forcing. This led to the development of a physics based, nonlinear model.

The nonlinear model had several advantages over the linear model. First, it included the physics of sediment transport in the equations that the linear model did not. Initial equations were formulated from commonly accepted sediment transport theory using energetics-type equations. Equations were then parameterized based on the relationship between sediment transport and bar migration of a constant form. Cross-shore transport was based on the deviations around an equilibrium amount of breaking and the resulting contribution due to the roller effect. The nonlinearity of the model forced sediment transport to zero in the absence of wave breaking. The extension to 2DH was based on parameterizations of bar variability and the associated 2DH circulation. The presence of 2DH morphology had two effects: both increasing onshore transport rates and stabilizing the system against larger waves. The model was able to span multiple storms, accurately predicting bar migration for both onshore and offshore events. The longest individual data set tested was approximately 6 months. Using subjectively determined values for the coefficients, $\hat{x}$ was predicted with an $R^2 = 0.42$ over this time period. Discrepancies between model and measured data could usually be attributed to errors in measured inputs (wave height, bar position, and amplitude). During onshore events, the inclusion of 2DH variability enhanced the predicted migration rates to match the data. A 1DH version of the model was also tested to compare against 2DH results. The 1DH model showed limited skill at predicting onshore migration rates, suggesting again that the inclusion of 2DH terms is key. Under highly oblique waves the 2DH model reduced to the 1DH form, predicting much slower onshore migration rates, in accordance with measured values. The majority of work for the project was on model development and showing the links between 2DH variability and onshore bar migration. Further work can include more in-depth study of the key terms in the equations and under what circumstances does 2DH variability play a key role in onshore migration.

In the fourth paper we explore the possibility of obtaining unique 2D sediment transport patterns from changes in bathymetry through the 2D conservation of mass equation. The problem is under-determined, having two unknowns (Q_y) and (Q_x) and only one known ($\Delta h/\Delta t$) such that a series of rules must be applied in order to invert transport. We assume that that the cross-shore integral of Q_x is closed, such that no sand enters or exists the system in this direction. By conservation of mass, this requires changes in volume of the cross-shore transect to be due to gradients in Q_y. We explored six constraints for distributing Q_y: three rules describing the initial longshore transport (Q_y^r) and three describing the cross-shore distribution of the excess volume component (Q_y^e). Initial results suggest that requiring sediment to travel down slope ($Q_y^r = f(\beta_y)$) is a reasonable choice for describing transport of distinct perturbations. Under field tests, this method did not perform well for the given example, however, further work refining the problem may provide improved solutions. Alternatively, basing the relationship of Q_x^r and Q_y^r as a function of spatial correlation lags between two surveys showed good results for identifying transport associated with alongshore migrating features. This method, however, did not do well under strictly onshore migration of 2D features, where alongshore transport was not predicted. A hybrid approach, using both the down-slope constraint and spatial correlation lags may provide more robust predictions on sediment transport patterns in complex environments. Due to the lack of closed boundaries in the alongshore, knowledge of $Q_y(x, y_0)$ is required to obtain sensible net sediment transport patterns. Alternatively, spatial patterns of the transport gradients provide useful insight into the system behavior without requiring $Q_y(x, y_0)$.

BIBLIOGRAPHY

Aagaard, T., M. Hughes, R. Møller-Sørensen, and S. Andersen (2006), Hydrodynamics and sediment fluxes across an onshore migrating intertidal bar, *Journal of Coastal Research*, *22*, 247–259, doi:doi:10.2112/04-0214.1.

Aarninkhof, S. (1996), Quantification of bar bathymetry from video observations, Msc thesis, Delft University, Delft, The Netherlands.

Aarninkhof, S., and R. Holman (1999), Monitoring the nearshore with video, *Backscatter*, *10*(2), 8–11.

Aarninkhof, S., and B. Ruessink (2004), Video observations and model predictions of depth-induced wave dissipation, *IEEE Transactions on Geoscience and Remote Sensing*, *42*(11), 2612–2622, doi:10.1109/TGRS.2004.835349.

Adler-Golden, S. M., P. K. Acharya, A. Berk, M. W. Matthew, and D. Gorodetzky (2005), Remote bathymetry of the littoral zone from aviris, lash, and quickbird imagery, *IEEE Transactions on Geoscience and Remote Sensing*, *43*(2), 337–347.

Alexander, P. S., and R. A. Holman (2004), Quantitative analysis of nearshore morphological variability based on video imaging, *Marine Geology*, *208*(1), 101–111.

Bagnold, R. (1941), *The Physics of Blown Sand and Desert Dunes*, Methuen, New York.

Bagnold, R. (1963), Mechanics of marine sedimentation, in *The Sea*, vol. 3, edited by M. Hill, pp. 507–528, Wiley-Interscience, New York.

Bagnold, R. (1966), An approach to the sediment transport problem from general physics, *Professional Paper 422-I*, U.S. Geological Survey.

Bailard, J. (1981), An energetics total load sediment transport model for a plane sloping beach, *Journal of Geophysical Research*, *86*(C11), 10,938–10,954.

Bascom, W. (1954), *Waves and beaches*, Anchor Books, Garden City, N.Y.

Bell, P. S. (1999), Shallow water bathymetry derived from an analysis of X-band marine radar images., *Coastal Engineering*, *37*, 513–527.

Bendat, J. S., and A. G. Piersol (1986), *Random Data: Analysis and Measurement Techniques*, 2nd ed., Wiley-Interscience, New York.

Birkemeier, W. A. (1985), Time scales of nearshore profile change, in *19th International Conference on Coastal Engineering*, pp. 1507–1521, ASCE, New York.

Birkemeier, W. A., and C. Mason (1984), The CRAB: A unique nearshore surveying vehicle, *Journal of Survey Engineering*, *110*, 1–7.

Bowen, A. J. (1980), Simple models of nearshore sedimentation; beach profiles and longshore bars, in *The Coastline of Canada*, vol. Paper 80-10, edited by S. McCann, pp. 1–11, Geological Survey of Canada.

Bowen, A. J., and D. L. Inman (1971), Edge waves and crescentic bars, *Journal of Geophysical Research*, *76*(36), 8662–8671.

Brander, R. (1999), Field observations on the morphodynamic evolution of a low-energy rip current system, *Marine Geology*, *157*, 199–217.

Caballeria, M., G. Coco, A. Falques, and D. Huntley (2002), Self-organizatino mechanisms for the formation of nearshore crescentic and transverse sand bars, *Journal of Fluid Mechanics*, *465*, 379–410.

Calvete, D., N. Dodd, A. Falques, and S. van Leeuwen (2005), Morphological development of rip channel systems: Normal and near normal wave incidence, *Journal of Geophysical Research*, *110*(C10006), doi:doi:10.1029/2004JC002803.

Castelle, B. (2004), Modélisation de l'hydrodynamique sédimentaire au-dessus des barres sableuses soumises á l'action de la houle: application á la côte aquitaine, Ph.D. thesis, Université Bordeaux I, France.

Church, J., and E. Thornton (1993), Effects of breaking wave induced turbulence within a longshore current model, *Coastal Engineering*, *20*, 1–28.

Coco, G., and A. Murray (2007), Patterns in the sand: From forcing templates to self-organization, *Geomorphology*, *91*, 271–290.

Coco, G., D. Huntley, and T. O'Hare (2000), Investigation of a self-organization model for beach cusp formation and development, *Journal of Geophysical Research*, *105*(C9), 21,991–22,002.

Davis, R. A., and W. T. Fox (1972), Coastal processes and nearshore sand bars, *Journal of Sedimentary Petrology*, *42*, 401–412.

Dean, R. G. (1973), Heuristic models of sand transport in the surf zone, in *Conference on Engineering Dynamics in the Surf Zone*, p. 7, Sydney, N.S.W.

Dean, R. G., and R. A. Dalrymple (1991), *Water Wave Mechanics For Engineers and Scientists*, vol. 2, World Scientific Publishing Co.

Dean, R. G., and R. A. Dalrymple (2002), *Coastal Processes with Engineering Applications*, Cambridge University Press.

Deigaard, R., N. Dronen, J. Fredsoe, J. Jensen, and M. Jorgensen (1999), Morphological stability analysis for a long straight barred coast, *Coastal Engineering*, *36*, 171–195.

Doering, J., and A. Bowen (1987), Skewness in the nearshore zone: A comparison of estimates from marsh mcbirney current meters and collocated pressure sensors, *Journal of Geophysical Research*, *92*, 13,173–13,183.

Drake, T. G., and J. Calantoni (2001), Discrete particle model for sheet flow sediment transport in the nearshore, *Journal of Geophysical Research*, *106*(C9), 19,859–19,868.

Dronen, N., and R. Deigaard (2007), Quasi-3-d modelling of the morphology of longshore bars, *Coastal Engineering*, *54*, 197–215.

Dugan, J. P., C. Piotrowski, and J. Z. Williams (2001), Water depth and surface current retrievals from airborne optical measurements of surface gravity wave dispersion, *Journal of Geophysical Research*, *106*(C8), 16,903–16,915.

Falques, A., A. Montoto, and V. Iranzo (1996), Bed-flow instability of the longshore current, *Continental Shelf Research*, *16*(15), 1927–1964, doi:doi:10.1016/0278-4343(96)00031-3.

Falques, A., A. Montoto, and D. Vila (1999), A note on hydrodynamic instabilities and horizontal circulation in the surf zone, *Journal of Geophysical Research*, *104*(C9), 20,605 – 20,615.

Falques, A., G. Coco, and D. Huntley (2000), A mechanism for the generation of wave-driven rythmic patterns in the surf zone, *Journal of Geophysical Research*, *105*(C10), 24,017 – 24,087.

Falques, A., N. Dodd, R. Garnier, F. Ribas, L. MacHardy, R. Larroudé, D. Calvete, and F. Sancho (2008), Rhythmic surf zone bars and morphodynamic self-organization, *Coastal Engineering*, *55*, 622–641.

Feddersen, F. (2007), Breaking wave induced cross-shore tracer dispersion in the surf zone: Model results and scalings, *Journal of Geophysical Research*, *112*(C09012), doi:doi:10.1029/2006JC004006.

Flampouris, S., F. Ziemer, and J. Seemann (2008), Accuracy of bathymetric assessment by locally analyzing radar ocean wave imagery (February 2008), *IEEE Transactions on Geoscience and Remote Sensing*, *46*(10), 2906–2913.

Gallagher, E., R. Guza, and S. Elgar (1998), Observations of sand bar evolution on a natural beach, *Journal of Geophysical Research*, *103*(C2), 3203–3215.

Garnier, R., D. Calvete, A. Falques, and M. Caballeria (2006), Generation and nonlinear evolution of shore-oblique/transverse sand bars, *Journal of Fluid Mechanics*, *567*, 327–360.

Garnier, R., D. Calvete, A. Falques, and N. Dodd (2008), Modelling the formation and the long-term behavior of rip channel systems from the deformation of a longshore bar, *Journal of Geophysical Research*, *113*(C07053), doi:doi:10.1029/2007JC004632.

Greenwood, B., and R. G. D. Davidson-Arnott (1979), Sedimentation and equilibrium in wave-formed bars: a review and case studies, *Canadian Journal of Earth Sciences*, *16*, 312–332.

Guenther, G. C. (1985), Airborne laser hydrography: System design and performance factors, *Professional paper series*, NOAA, Rockville, MD: NOS, NOAA.

Guza, R., and E. Thornton (1985), Velocity moments in nearshore, *Journal of Waterway, Port, Coastal, and Ocean Engineering*, *111*, 235–256.

Guza, R. T., and D. L. Inman (1975), Edge waves and beach cusps, *Journal of Geophysical Research*, *80*(21), 2997–3012.

Haller, M., R. A. Dalrymple, and I. A. Svendsen (2002), Experimental study of nearshore dynamics on a barred beach with rip channels, *Journal of Geophysical Research*, *107*(C6), doi:10.1029/2001JC000955.

Havlicek, J. P., D. S. Hardin, and A. C. Bovik (1996), The multi-component AM-FM image representation, *IEEE Transactions on Image Processing*, *5*(6), 1094–1100.

Havlicek, J. P., J. W. Havlicek, and A. C. Bovik (1997), The analytic image, in *IEEE International Conferene on Image Processing*, pp. 446–448, IEEE, Santa Barbara, CA.

Havlicek, J. P., J. W. Havlicek, N. D. Mamuya, and A. C. Bovik (1998), Skewed 2d hilbert transforms and computed am-fm models, in *IEEE International Conference on Image Processing*, pp. 602–606, IEEE, Chicago, IL, USA.

Henderson, S., J. Allen, and P. Newberger (2004), Nearshore sandbar migration predicted by an eddy-diffusive boundary layer model, *Journal of Geophysical Research*, *109*, C06,024, doi:10.1029/2003JC002137.

Hickman, G. D., and J. E. Hogg (1969), Application of an airborne pulsed laser for near-shore bathymetric measurements, *Remote Sensing of Environment*, *1*(1), 47–58.

Hoefel, F., and S. Elgar (2003), Wave-induced sediment transport and sandbar migration, *Science*, *299*(5614), 1885–1887.

Holland, K., and R. Holman (1996), Field observations of beach cusps and swash motions, *Marine Geology*, *134*, 77–93.

Holland, K., and R. Holman (1999), Wavenumber-frequency structure of infragravity swash motions, *J. Geophys. Res.*, *104*(C6), 13,479–13,488.

Holland, K., R. Holman, T. Lippmann, J. Stanley, and N. Plant (1997), Practical use of video imagery in nearshore oceanographic field studies, *IEEE Journal of Ocean Engineering*, *22*(1).

Holland, T. K. (2001), Application of the linear dispersion relation with respect to depth inversion and remotely sensed imagery, *IEEE Transactions on Geoscience and Remote Sensing*, *39*(9), 2060–2072.

Holman, R., A. J. Sallenger., T. Lippmann, and J. Haines (1993), The application of video image processing to the study of nearshore processes, *Oceanography*, *6*(3), 78–85.

Holman, R., J. Stanley, and H. Özkan Haller (2003), Applying video sensor networks to nearshore environmental monitoring, *IEEE Pervasive Computing*, *2*(4), 14–21.

Holman, R. A., and A. J. Bowen (1982), Bars, bumps and holes: Models for the generation of complex beach topography, *Journal of Geophysical Research*, *87*(C1), 457–468.

Holman, R. A., and J. Sallenger, Asbury H. (1993), Sand bar generation: A discussion of the duck experiment series, *Journal of Coastal Research*, *SI*(15), 76–92, special Issue No. 15.

Holman, R. A., G. Symonds, E. Thornton, and R. Ranashinghe (2006), Rip spacing and persistence on a pocket beach, *Journal of Geophysical Research*, *111*, C01,006.

Holthuijsen, L., N. Booij, and T. Herbers (1989), A prediction model for stationary, short-crested waves in shallow water with ambient currents, *Coastal Engineering*, *17*(23), 211–225.

Irish, J. L., and W. J. Lillycrop (1999), Scanning laser mapping of the coastal zone: the shoals system, *ISPRS Journal of Photogrammetry and Remote Sensing*, *54*(2-3), 123–129.

Keulegan, G. H. (1948), An experimental study of submarine sand bars, *Tech. rep.*, Beach Erosion Board, U.S. Army Corps of Engineers.

King, C. A. M., and W. W. Williams (1949), The formation and movement of sand bars by wave action, *Geogr. J.*, *113*, 70–85.

Komar, P. (1983), Rhythmic shoreline features and their origins, in *Mega-Geomorphology*, edited by R. Gardner and H. Scoging, pp. 92–112, Claredon Press, Oxford.

Komar, P. D. (1974), *Beach Processes and Sedimentation*, Prentice-Hall, Englewood Cliffs, N.J.

Komar, P. D., and D. L. Inman (1970), Longshore sand transport on beaches, *Journal of Geophysical Research*, *75*, 5914–27.

Lippmann, T., and R. Holman (1990), The spatial and temporal variability of sand bar morphology, *Journal of Geophysical Research*, *95*(C7), 11,575–11,590.

Lippmann, T. C., and R. A. Holman (1989), Quantification of sand bar morphology: A video technique based on wave dissipation, *Journal of Geophysical Research*, *94*(C1), 995–1011.

MacMahan, J. H. (2001), Hydrographic surveying from a personal watercraft, *Journal of Survey Engineering*, *127*(1), 12–24.

Marino-Tapia, I., P. Russell, T. O'Hare, M. Davidson, and D. Huntley (2007), Cross-shore sediment transport on natural beaches and its relation to sandbar migration patterns: 1. field observations and derivation of a transport parameterization, *Journal of Geophysical Research*, *112*(C03001), doi:10.1029/2005JC002893.

McLachlan, A., E. Jaramillo, T. Donn, and F. Wessels (1993), Sandy beach macrofauna communities and their control by the physical environment: A geographical comparison, *Journal of Coastal Research*, *15*, 27–38.

Misra, S. K., A. Kennedy, and J. Kirby (2003), An approach to determining nearshore bathymetry using remotely sense ocean surface dynamics, *Coastal Engineering*, *47*, 265–293.

Munk, W., and M. Traylor (1947), Refraction of ocean waves: a process linking underwater topography to beach erosion, *Journal of Geology*, *55*, 1–26.

Pe'eri, S., and W. Philpot (2007), Increasing the existence of very shallow-water LIDAR measurements using the red-channel waveforms, *IEEE Transactions on Geoscience and Remote Sensing*, *45*(5), 1217–1223.

Piotrowski, C., and J. Dugan (2002), Accuracy of bathymetry and current retrievals from airborne optical time-series imaging of shoaling waves., *IEEE Transactions on Geoscience and Remote Sensing*, *40*(12), 2602–2612.

Plant, N., and R. Holman (1997), Intertidal beach profile estimation using video images, *Marine Geology*, *140*, 1–24.

Plant, N., R. Holman, and M. Freilich (1999), A simple model for interannual sand bar behavior, *Journal of Geophysical Research*, *104*(C7), 15,755–15,776.

Plant, N., M. Freilich, and R. Holman (2001), The role of morphological feedback in surf zone sand bar response, *Journal of Geophysical Research*, *106*(C1), 973–989.

Plant, N., K. Holland, and R. A. Holman (2006), A dynamical attractor governs beach response to storms, *Geophysical Research Letters*, *33*, L17,607.

Plant, N., K. T. Holland, and M. Haller (2008), Ocean wavenumber estimation from wave-resolving time series imagery, *IEEE Transactions on Geoscience and Remote Sensing*, *46*, 2644–2658, doi:10.1109/TGRS.2008.919821.

Ranasinghe, R., G. Symonds, K. Black, and R. A. Holman (2004), Morphodynamics of intermediate beaches: a video imaging and numerical modeling study, *Coastal Engineering*, *51*, 629–655.

Reniers, A., G. Symonds, and E. Thornton (2001), Modeling of rip currents during RDEX, in *Coastal Dynamics '01*, edited by H. Hanson and M. Larson, pp. 493–499, ASCE, Lund, Sweden.

Reniers, A., E. Thornton, and J. Roelvink (2004), Morphodynamic modeling of an embayed beach under wave-group forcing, *Journal of Geophysical Research*, *109*(C01030).

Roelvink, J., and M. Stive (1989), Bar-generating cross-shore flow mechanisms on a beach, *Journal of Geophysical Research*, *94*(C4), 4785–4800.

Ruessink, B., K. Wijnberg, R. Holman, Y. Kuriyama, and I. van Enckevort (2003), Inter-site comparisons of interannual nearshore bar behavior, *Journal of Geophysical Research*, *108*, doi:10.1029/2002JC001,505.

Ruessink, B., Y. Kuriyama, A. Reniers, J. Roelvink, and D. Walstra (2007), Modeling cross-shore sandbar behavior on the timescale of weeks, *Journal of Geophysical Research*, *112*(F03010), doi:doi:10.1029/2006JF000730.

Sallenger, J., Asbury H., and P. A. Howd (1989), Nearshore bars and the break-point hypothesis, *Coastal Engineering*, *12*, 301–313.

Sandidge, J. C., and R. J. Holyer (1998), Coastal bathymetry from hyperspectral observations of water radiance, *Remote Sensing of Environment*, *65*, 341–352.

Seiwell, H. R. (1947), Military oceanography in World War II, *Military Engineering*, *39*(259), 202–210.

Senet, C. M., J. Seemann, S. Flampouris, and F. Ziemer (2008), Determination of bathymetric and current maps by the method DiSC based on the analysis of nautical X-band radar image sequences of the sea surface (November 2007), *IEEE Transactions on Geoscience and Remote Sensing*, *46*(8), 2267–2279.

Shepard, F. P. (1950), Longshore bars and troughs, *Tech. Memo. 15*, U.S. Army Corps Engineers, Beach Erosion Board.

Short, A., and N. Trenaman (1992), Wave climate of the sydney region, and energetic and highly variable ocean wave regime, *Australian Journal of Marine and Freshwater Research*, *43*, 765–791.

Sonu, C. J. (1973), Three-dimensional beach changes, *Journal of Geology*, *81*, 42–46.

Splinter, K., R. Holman, and N. Plant (submitted), A behavior-oriented dynamical model for sand bar migration and 2DH evolution, *Journal of Geophysical Research*.

Splinter, K. D., and R. A. Holman (2006), Bathymetric estimation based on wave refraction patterns, in *Proceedings of the 30th International Conference on Coastal Engineering*, vol. 1, edited by J. M. Smith, pp. 451–463, World Scientific Publishing Co.

Stive, M., and J. Battjes (1984), A model for offshore sediment transport, in *Proceedings of the 10th International Conference on Coastal Engineering*, pp. 1420–1436, ASCE, New York.

Stockdon, H., and R. Holman (2000), Estimation of wave phase speed and nearshore bathymetry from video imagery, *Journal of Geophysical Research*, *105*(C9), 22,015–22,033.

Svendsen, I. (1984), Mass flux and undertow in a surf zone, *Coastal Engineering*, *8*, 347–364.

Svendsen, I. A. (2006), *Introduction to Nearshore Hydrodynamics*, *Advanced Series on Ocean Engineering*, vol. 24, World Scientific Publishing Co.

Thornton, E., R. Humiston, and W. Birkemeier (1996), Bar/trough generation on a natural beach, *Journal of Geophysical Research*, *101*, 12,097–12,110.

Thornton, E. B., and R. T. Guza (1982), Energy saturation and phase speeds measured on a natural beach, *Journal of Geophysical Research*, *87*(C12), 9499–9508.

Thornton, E. B., and R. T. Guza (1983), Transformation of wave height distribution, *Journal of Geophysical Research*, *88*(C10), 5925–5938.

van Enckevort, I., and B. Ruessink (2001), Effect of hydrodynamics and bathymetry of video estimates of nearshore sand bar position, *Journal of Geophysical Research*, *106*(C8), 16,969 – 16,979.

van Enckevort, I., and B. Ruessink (2003a), Video observations of nearshore bar behaviour. part 1: alongshore uniform variability, *Continental Shelf Research*, *23*, 501–512.

van Enckevort, I., and B. Ruessink (2003b), Video observations of nearshore bar behaviour. part 2: alongshore uniform variability, *Continental Shelf Research*, *23*(513-532).

van Enckevort, I., B. Ruessink, G. Coco, K. Suzuki, I. Turner, N. Plant, and R. A. Holman (2004), Observations of nearshore crescentic sandbars, *Journal of Geophysical Research*, *109*(C6).

van Maanen, B., P. de Ruiter, G. Coco, K. Bryan, and B. Ruessink (2008), Onshore sandbar migration at tairua beach (new zealand): Numerical simulations and field measurements, *Marine Geology*, *253*(3-4), 99–106, doi:doi:10.1016/j.margeo.2008.05.007.

Walker, R. (1994), *Marine light field statistics*, Wiley series in pure and applied optics, John Wiley and Sons, Inc., New York.

Wijnberg, K., and A. Kroon (2002), Barred beaches, *Geomorphology*, *48*, 103–120.

Williams, W. W. (1946), The determination of gradients of enemy-held beaches, *Geographical Journal*, *107*, 76–93.

Wilson, G., H. Özkan Haller, and R. Holman (in review), Alongshore nonuniform dynamics in the surf zone: 1 theory, *Journal of Geophysical Research*.

Wright, L., F. Coffey, and P. Cowell (1980), Nearshore oceanography and morphodynamics of the broken bay - palm beach region, n.s.w. : implications for offshore dredging, *Tech. Rep. 80/1*, Coastal Studies Unit, Department of Geography, The University of Sydney, Sydney, Australia.

Wright, L., A. Short, J. Boon III, B. Hayden, S. Kimball, and J. List (1987), The morphodynamic effects of incident wave groupiness and tide range on an energetic beach, *Marine Geology*, *74*, 1–20.

Wright, L. D., and A. D. Short (1984), Morphodynamic variability of surf zones and beaches: A synthesis, *Marine Geology*, *56*, 93–118.

Yu, J., and D. Slinn (2003), Effects of wave-current interaction on rip currents, *Journal of Geophysical Research*, *108*(C3), 3088, doi:doi:10.1029/2001JC001105.

Zenkovich, V. (1967), *Processes of Coastal Development*, Oliver and Boyd, White Plaines, NY, USA.